Dissertation

Phase Behavior of Simple Fluids
and
their Mixtures

ausgeführt zum Zwecke der Erlangung des akademischen
Grades eines Doktors der technischen Wissenschaften
unter der Leitung von

Ao.Univ.Prof. Mag. Dipl.-Ing. Dr. Gerhard Kahl
E136
Institut für theoretische Physik

eingereicht an der technischen Universität Wien
Fakultät für technische Naturwissenschaften und Informatik
von

Dipl.-Ing. Elisabeth Schöll-Paschinger
Matr.-Nr. 9226409
Bürgerspitalgasse 29/24, 1060 Wien

Wien, am 19. Februar 2002

Zusammenfassung

Phasenübergänge in Flüssigkeiten sind vertraute Vorgänge aus unserem Alltagsleben, und ihre theoretische Beschreibung ist wesentlich für ein tieferes Verständnis dieser komplexen Phänomene. In dieser Arbeit haben wir, um die Abhängigkeit des Phasenverhaltens einer Substanz von ihren mikroskopischen Eigenschaften zu untersuchen, zur Weiterentwicklung klassischer Flüssigkeitstheorien beigetragen und diese auf einfache Flüssigkeiten sowie deren Mischungen angewandt. Einer der von uns verwendeten theoretischen Zugänge ist die *Self-Consistent Ornstein Zernike Approximation* (SCOZA), eine mikroskopische Flüssigkeitstheorie, die sehr präzise Resultate für die Koexistenzkurve liefert und sogar im kritischen Bereich des Phasendiagramms erfolgreich bleibt. Diese Theorie wurde von uns für eine Flüssigkeit von sphärischen Teilchen erweitert, deren Paarwechselwirkung sich aus einem Hartkugelanteil und einer Linearkombination von Yukawa Potentialen zusammensetzt. Diese Erweiterung erlaubt es uns, realistische Modellpotentiale durch eine geeignete Linearkombination von Yukawa- Potentialen darzustellen, und somit über einfache Hartkugel-Yukawa Potentiale hinauszugehen: das Lennard-Jones und das Girifalco Potential für Fullerene stellen Potentiale von Systemen dar, die wir im Detail untersucht haben. Wir haben zusätzlich mit der SCOZA erstmals eine *quantitative* Untersuchung des Phänomens der Doppelkritikalität durchgeführt, die u.a. in Systemen mit explizit dichteabhängigem Potential auftritt. Weiters haben wir uns mit zweikomponentigen Flüssigkeitsmischungen beschäftigt, die im Vergleich zu Einkomponentenflüssigkeiten ein wesentlich reicheres Phasenverhalten aufweisen. Wir haben die SCOZA auf eine sogenannte symmetrische binäre Flüssigkeit erweitert. Drei Typen von Phasendiagrammen, die durch den Ort charakterisiert werden, wo die λ-Linie (die kritische Linie von Entmischungübergängen) die Flüssig-Gas Koexistenzkurve schneidet, konnten identifiziert werden, und lieferten eine quantitative Ergänzung zu Untersuchungen mit einer Mean Field Theorie. Diese binäre Mischung wurde anschließend in thermisches Gleichgewicht mit einer porösen Matrix gebracht, die als erstarrte Flüssigkeit modelliert wurde. Der notwendige Formalismus zur Beschreibung dieses teilweise erstarrten Systems wurde mit einer Störungstheorie – der *Optimized Random Phase Approximation* – in Verbindung mit dem sogenannten Replica Trick hergeleitet. In Übereinstimmung mit Experimenten beobachteten wir, daß bereits eine sehr kleine Matrixdichte das Phasenverhalten der Flüssigkeit drastisch verändern kann und konnten systematisch sowohl den Einfluß der externen Systemparameter (Matrixeigenschaften und Matrix-Flüssigkeit Wechselwirkung) sowie der internen Systemparameter (Eigenschaften der Flüssigkeit) auf das Phasenverhalten untersuchen.

Abstract

Phase transitions in fluids are practically ubiquitous in our everyday lives and their theoretical description is essential for a deeper understanding of these complex phenomena. In an effort to gain more insight into the relationship between the microscopic properties of a fluid and its phase behavior we have contributed to a further development of classical liquid-state theories and have applied them to simple fluids and their mixtures. In particular, we have focused on the *Self-Consistent Ornstein Zernike Approximation* (SCOZA), a microscopic liquid-state theory that is known to give highly accurate results for the coexistence curves and that remains successful even in the critical region. We have generalized the SCOZA to a fluid of spherical particles with a pair potential given by a hard-core repulsion and a linear combination of Yukawa tails. This allows us to go beyond the one-tail Yukawa potential by approximating realistic model potentials by a suitable linear combination of Yukawa tails: Lennard-Jones and Girifalco potentials (for fullerenes $C_{n \geq 60}$) characterize systems that were studied in detail. In addition, our generalized SCOZA version allows us for the first time a *quantitative* study of the phenomenon of double-criticality, that is observed in systems with explicitly density-dependent potentials. Further work is dedicated to binary fluid mixtures: their phase behavior shows, compared to simple one-component fluids, a much richer variety of phenomena. We have extended the SCOZA to the case of a symmetric binary mixture: here the like-particle interactions are equal, while the interactions between the unlike fluid particles differ from the likes ones. Three archetypes of phase diagrams, characterized by the location where the λ-line (i.e. the critical line of demixing transitions) intersects the vapor-liquid coexistence curve were identified, supplementing thus previous mean-field type studies in a quantitative way. We have then brought this binary mixture in thermal equilibrium with a porous matrix, which is represented by a frozen configuration of equally sized particles. The necessary framework to describe such a partly quenched system has been derived using the simpler *Optimized Random Phase Approximation* in combination with the so-called replica trick. We observe – in qualitative agreement with experiments – that already a minute matrix density is able to lead to drastic changes in the phase behavior of the fluid. We systematically investigate the influence of the external system parameters (due to the matrix properties and the fluid-matrix interactions) and of the internal system parameters (due to the fluid properties) on the phase diagram.

Contents

Chapter 1

Introduction

Phase transitions are practically ubiquitous in our everyday lives, ranging from very simple, commonplace events to rather complicated and sophisticated production processes in industry where special knowledge of the phase diagrams of substances is required. Therefore, the technological aspect of investigations in phase diagrams is of importance and industrial developments and processes often rely on accurate and reliable phase diagrams.

Phase transitions belong to the most challenging and fascinating problems in physics. The complexity of these phenomena, their large diversity (such as transitions from liquid to gas, from the conducting to the superconducting phase, from a paramagnet to a ferromagnet, demixing separations in mixtures and others), and the discovery of new phases (such as quasi-crystals or superfluids) has attracted the interest of condensed matter scientists in this research field. One of the central challenging questions is: How do the microscopic properties of a system influence its phase behavior and its critical phenomena? During the past decades significant contributions to describe phase transitions have been proposed in theoretical and computational physics. Meanwhile, theoretical concepts in combinations with computational tools can be considered as complements to experimental techniques: on the one side they are able to reproduce experimental results with high accuracy and contribute thus to a deeper insight into these phenomena; on the other side they might be more economical than experiments and are able to indicate, whether it is worthwhile to push experiments in a direction where difficult experimental conditions are to be expected. They can sometimes even predict results which are barely accessible in experiment (such as matter under extreme conditions).

The discontinuities in physical behavior, which occur when a system undergoes a phase transition, have claimed the attention of scientists for many years. It was recognized already in the 19th century that the discontinuities are associated with the in-

teractions between the microscopic particles of the system. Thus it became necessary to develop a statistical mechanical treatment of phase transitions [1]. The first steps in this direction were done in the fundamental works of van der Waals and Weiss who explained phase transitions in fluid and magnetic systems with mean field theories. Further progress was achieved by Landau in his phenomenological explanations which provide insight into the detailed character of the discontinuities. In 1944 the modern era in phase transitions started when Onsager found an exact statistical mechanical solution for the two-dimensional Ising model. His solution showed that previous 'classical' theories were unreliable in their quantitative predictions and stimulated a closer investigation of the true behavior near discontinuities.

Particular interest has been focused on phenomena associated with critical points such as that of gas-liquid equilibrium, or the Curie point in ferromagnetic materials. In the critical region, anomalies in thermodynamic functions are observed which result in the divergence of such thermodynamic quantities as specific heat, compressibility, etc. These critical fluctuations are very difficult to handle theoretically and much effort has gone into this. Starting in the 1960's considerable progress towards a greater understanding of critical phenomena was made by introducing the ideas of renormalization group theory [2].

In the present work we intend to contribute to a deeper understanding of phase transitions. Various concepts were proposed over the last decades to describe these phenomena from a theoretical point of view: One of them is the above mentioned renormalization group theory which is the most successful tool to study cooperative phenomena in statistical mechanics and has lead to a deeper understanding of phase transitions and critical phenomena. However, it it not able to predict non-universal quantities (such as the location of the critical point). Computer simulations represent another access to the problem [3]. For a given interparticle potential they provide 'quasi' exact results – apart from finite size effects induced by the finite size of the simulation cell. These effects become obviously more severe in the critical regions where long-range fluctuations occur. Sophisticated techniques are meanwhile available to cope with this problem. In this work we have chosen another theoretical approach, namely microscopic liquid-state theories that are based on statistical mechanics [4]. The aim of these theories is to predict the thermodynamic and structural properties of a fluid from the presumed knowledge of the forces between the fluid particles. So once the interparticle forces are fixed, the theory should be able to determine the phase behavior (including criticality) of the system.

In this work we have focused on the phase behavior of fluids. Over the past decade much evidence was found that the fluid states, gas and liquid, possess many structural similarities and that both are quite distinct from the solid state. Hence, it is not surprising

that the same theoretical approach can be used to describe both the liquid, the gas and the supercritical fluid. In this work we will be exclusively concerned with the phase behavior of fluids and their mixtures, i.e. we restrict our investigations to that part of the entire phase diagram that includes liquid-gas transitions and liquid-liquid demixing transitions in mixtures omitting the determination of the melting line that would require in addition other theoretical approaches like e.g. classical density functional theory.

Apart from the one-component fluid we also study the properties of fluid mixtures; here new phenomena are encountered that are not present in pure substances. According to the Gibbs rule now up to four phases can be observed simultaneously and the way these phases can coexist often leads to rather complex phase diagrams. The phase behavior is mainly triggered by two mechanisms (and their interrelation): first, there is the size difference of the particles of the two components and their (partial) penetrability; second, there is the chemical influence, expressed via the set of the three interatomic potentials. Depending on the relative sizes of the particle species and the properties of the interaction forces a large variety of different types of phase behavior can be observed [5].

We shall exclusively consider simple classical liquids with interparticle potentials, that can be considered as realistic models of a fairly large number of real fluids. 'Quasi-experimental' data for these systems are available from computer simulations (either Monte Carlo or Molecular Dynamics simulations). Comparison of these data with those from sophisticated microscopic liquid-state theories has shown that these theories produce results for systems well inside the liquid-state region that are practically indistinguishable from the simulation data. However, the accuracy of these approaches begins to decrease as one leaves the liquid-state region and approaches the liquid-gas coexistence curve and/or the critical region. In particular, the shape of the coexistence curve and the location of the critical point is not reproduced correctly and the critical exponents are not the exact ones. Some theoretical approaches even fail to converge in the critical region, so that the liquid and vapor branches of the coexistence curve remain unconnected. To overcome this highly unsatisfactory situation two microscopic liquid-state theories have been developed in the past years that cope with the problems encountered in the critical region and near the phase boundaries: one is the self-consistent Ornstein Zernike approximation (SCOZA) [6], the other one is the hierarchical reference theory (HRT) [7] that merges concepts of renormalization group theory with liquid-state theories.

The first part of this work is dedicated to the SCOZA which was proposed by Stell and Høye already in the 1970s; the OZ relation is supplemented with a generalized mean spherical ansatz (GMSA), introducing in the MSA relation a density- and temperature-dependent function which is determined by enforcing consistency between the different

thermodynamic routes. Although introduced nearly thirty years ago its first numerical implementation was - due to substantial numerical problems - successfully realized only a few years ago in 1996 [8]: a reformulation of the SCOZA partial differential equation made an access to subcritical temperatures possible. Ever since, the SCOZA has been applied only to a few discrete and continuum systems restricted in the latter case to hard-core Yukawa systems. However, these results showed in an impressive way that this theory remains successful even in the critical region: it is able to predict critical temperatures within 0.6% (or even less) and to reproduce the exact value for the critical exponent β very accurately.

The obvious success of the SCOZA has motivated us to contribute to its extension: further development of the SCOZA and its application to a larger variety of systems are summarized in the first part of this work. In the case of continuum fluids the SCOZA has been solved up to now only for hard-core Yukawa systems. This restriction can be traced back to the fact that the SCOZA is based on the semi-analytic MSA solution which is available for multi-component hard-core multi-Yukawa systems. In this work we have generalized the SCOZA to one-component fluids with hard-core multi-Yukawa interactions. This modification considerably increases the variety of systems that can now be studied: several realistic interactions can be modeled by a suitable linear combination of Yukawa tails, like the Lennard-Jones (LJ) fluid modeling the interaction between rare gas atoms and the Girifalco potential being a spherical approximation of the interaction between fullerene molecules like e.g. C_{60}. In particular, the latter system has become of great interest in the last years (for an overview see [9]) because the pair potential differs significantly from the LJ one: the ratio of the width of the attractive well to the equilibrium distance is much less for the C_{60}-C_{60} intermolecular potential than for the LJ one, furthermore the repulsive wall of the C_{60}-C_{60} interaction is much stiffer. Since the phase behavior depends in a very sensitive way on the nature of the forces the phase behavior was expected to be completely different from that of rare gas atoms. It was even speculated that C_{60} might be a substance with no liquid phase at all. The SCOZA, being known to yield reliable and accurate results for the coexistence curves even in the critical regions, confirmed that C_{60} should possess a liquid phase. Comparison with previous simulation results illustrated once more that the SCOZA yields reliable predictions even in the critical region.

Using the SCOZA we have also studied another phenomenon that has become of interest in the last years: increasing experimental evidence is found that some pure substances exhibit in addition to the usual liquid-gas transition a second liquid-liquid transition [10] so that two critical points occur. This phenomenon is usually referred to as double

criticality and was observed experimentally in systems where the interaction potential is anisotropic. In a first approximation this interaction can be replaced by an effective spherically symmetric pair potential by averaging over the angular degrees of freedom, leading thus to a density-dependent pair potential. Studies with a simple van der Waals theory, more refined theories and computer simulations showed that a non-monotonic density-dependence of the interaction range leads to a second liquid-liquid transition [11]. However, discrepancies were found between computer simulation results and theoretical data. The SCOZA, giving highly accurate results for the phase diagram (even close to the critical point), represents an ideal tool to investigate *quantitatively* these phenomena. We have made a detailed study of phase diagrams for hard-core Yukawa systems introducing a density-dependent Yukawa screening length. We were able to locate the range of the system parameters were double criticality was observed, and, by carefully varying these parameters, we could shift the location of the two critical points. For selected parameters we could even merge them leading thus (as we could see from an analysis of the critical exponent) to a tricritical point.

Finally, we have generalized the SCOZA to a binary symmetric mixture: here the interaction between like particles is equal, only the interaction between the different particle species is different; phase diagrams were calculated for various system parameters. Despite its simplicity this model system shows a very rich variety of phase behavior and interesting phenomena can be observed such as a critical end point or a tricritical point that is not present in a general binary mixtures. Three different types of phase diagrams can be distinguished, classified by the location where the λ-line (the critical line of the demixing transitions) intersects the first order vapor-liquid coexistence curve. As already shown in a qualitative mean field study [12] the sequence of these types of phase diagrams is triggered by a microscopic parameter, i.e., the interaction ratio of the unlike to the like interactions. In contrast to conventional liquid-state theories we are able to obtain results even in the critical regions.

The second part of this work is dedicated to a more realistic problem: we have brought the above mentioned binary symmetric mixture in contact with a porous matrix of immobile particles, realized in our case by a frozen liquid configuration of hard-sphere particles of the same size as the fluid particles. This model is a simple representation of a scenario, which has become during the past decade of technological relevance: Fluids in contact with porous media are encountered in many technological applications such as catalysis, adsorption, enhanced oil recovery or gas purification. Therefore, investigations of fluids that are in equilibrium with a disordered matrix have become during the past years a very challenging field in liquid state physics [13]. Experimental and theoretical studies revealed

that a porous matrix (even if it occupies only a minute fraction of the volume) can have a substantial influence on the phase behavior of the liquid: ^{4}He and N_2 in high-porosity aerogel [14] are two examples where the near-critical liquid-vapor (LV) curve is narrowed drastically under the influence of a matrix. The effects become of course richer and more interesting in the case that the fluid is a binary mixture: for example, experiments on a ^{3}He-^{4}He mixture inside a highly porous silica-gel or a porous gold matrix have shown a drastic modification of the superfluid transition [15]. A deeper understanding of these obviously very complex effects is all the more desirable as it might help to predict properties of materials of technological relevance. However, in these rather complex systems the combined influence of pore structure, randomness, wetting phenomena, capillary condensation, *etc.*, on phase separation is not yet satisfactorily explained. Disentanglement of the role of these various factors can, however, be made by studying well defined model systems, amenable to either theoretical analysis or computer simulations, in which these factors can be varied in a controlled way.

Such a theoretical approach is followed in the present work for a model of a symmetric binary mixture adsorbed in a porous matrix formed by immobile particles modeled as hard spheres. From the theoretical point of view, the main problem in the description of such a system lies in the double average required for the calculation of thermodynamic and structural properties: one average is taken over the configurations of the liquid, keeping the matrix particles in fixed positions, the second average is then taken over different matrix configurations. The first steps to solve this complex problem were proposed by Madden and Glandt [16] who derived cluster expansions for the distribution functions; integral-equations for the correlation functions, that are similar to the Ornstein-Zernike equations in standard liquid state theory, have been presented. In subsequent work, Given and Stell have applied the replica method (introduced originally in the theory of spin glasses [17]) to this problem [18] and have thus provided a powerful tool on which many of the present day approaches in this field are based. The replica trick exploits a mathematical isomorphism between a partly quenched system and a limiting case of a corresponding equilibrium system which consists of the now mobile matrix particles and of s noninteracting identical copies of the liquid: the properties of the quenched system are obtained by considering the limit $s \to 0$ of the properties of the equilibrium system, which, in turn, can be treated by standard liquid state theories. Given and Stell presented in their work the (now correct) formulation of the so-called replica Ornstein-Zernike equations, the counterpart of the Ornstein-Zernike equations in standard liquid state theory: they relate the liquid-liquid, the liquid-matrix and the matrix-matrix correlation functions.

Based on the replica formalism, we have generalized a thermodynamic perturbation

theory - the Optimized Random Phase Approximation (ORPA) - to the binary case. From a detailed and systematic investigation we have found that now the transition between the different types of phase diagrams is not only triggered by the ratio of the unlike to the like interactions as this is the case for the bulk fluid. In addition, we could show, that the transition between the different types of phase diagrams can also be triggered by the parameters governing the matrix-matrix and matrix-fluid interactions. Our results are confirmed quantitatively by grand canonical Monte Carlo simulations [19].

This work is organized as follows: in the first part we summarize in sect. 2.1 briefly the statistical mechanics foundations of microscopic liquid-state theories, we define the structure functions and their relationships with thermodynamic quantities. In sect. 2.2 we give a brief overview over two classes of microscopic liquid-state theories: integral equation theories and perturbation theories and discuss especially those approximations that are related to this work: the MSA and the ORPA. In chapter 3 basic thermodynamic concepts and quantities necessary to describe phase equilibria and stability conditions are introduced and the different types of phase diagrams that occur in a binary symmetric fluid are schematically illustrated.

The second part is dedicated to the SCOZA: in sect. 4.1 we first give an overview over thermodynamically self-consistent liquid-state theories putting emphasize on the presentation of the SCOZA; In sect. 4.2 we then formulate the SCOZA for a one-component hard-core multi-Yukawa fluid and present results for the Lennard-Jones fluid, for fullerenes and for systems with explicit density-dependent potentials. The SCOZA for a binary symmetric fluid is formulated in sect. 4.3 where also results are presented.

In the third part of the work we investigate the phase behavior of a binary symmetric fluid in a disordered porous matrix. We give a brief overview over the development in this field in sect. 5.1, present our model system in sect. 5.2, and summarize the formulae of structural and thermodynamic properties in sect. 5.3. In Sect. 5.4, finally, we describe the results: comparison is made between simulation results and ORPA predictions and trends in the variation of the phase diagrams induced by the different system parameters are discussed.

Part I

Basics of Liquid-State Theory

Chapter 2

Theoretical Concepts

The aim of statistical mechanics is to provide a macroscopic description of a system based on its microscopic properties. Starting with a given interparticle law of force of a certain fluid model one should be able to derive its structural and thermodynamic properties and to determine the type of phase equilibria that will be encountered in the system.

The central quantity in liquid-state theory that provides the link between the microphysics and macrophysics of a fluid is the so called pair distribution function $g(r)$. It measures the degree of correlation between the particles separated by a distance r and thus describes the structure of a fluid. In fact, basic thermodynamic quantities as the pressure or the internal energy from which all other thermodynamic quantities, relevant for the determination of phase coexistence, can be determined, are expressible in terms of this function. On the other hand, the pair distribution function itself is a functional of the interparticle potential. However, to calculate $g(r)$ for a given interaction potential is a complex and unsolvable problem and some simplifying assumption must be made for an approximate determination of the pair distribution function and hence of the structure. These approximation schemes include on the one hand integral equation theories (IETs) where an integral equation, in which $g(r)$ is the unknown function, has to be solved. Another group of approximation schemes are the perturbation theories, which represent generalizations of the theory of van der Waals and calculate thermodynamic and structural properties as perturbation to those of the well known hard-sphere reference system.

In the following chapter we will first briefly introduce some basic definitions of the structural functions and their relationships with thermodynamic quantities; then some approximation schemes of liquid-state theory will be presented. Emphasis will be put on those concepts that are used in the present work: the mean spherical approxima-

tion (MSA) and the Lowest-Order γ-ordered Approximation (LOGA) or the equivalent Optimized Random Phase Approximation (ORPA).

2.1   Structure functions

2.1.1   Radial distribution function

We define the structure functions in the canonical ensemble. So we consider a macroscopic system of N identical particles, enclosed in a volume V at a given temperature T. The potential energy of the system is assumed to be given by $V_N(\mathbf{r}^N)$, where we use the notation $\mathbf{r}^N = \{\mathbf{r}_1, \mathbf{r}_2, \ldots, \mathbf{r}_N\}$ for the positions of the N particles.

Then the one-particle density, that is defined as the ensemble average over the local particle density

$$\rho(\mathbf{r}) = \sum_{i=1}^{N} \delta(\mathbf{r} - \mathbf{r}_i) \tag{2.1}$$

is

$$\rho_N^{(1)}(\mathbf{r}) = \left\langle \sum_{i=1}^{N} \delta(\mathbf{r} - \mathbf{r}_i) \right\rangle = \frac{N}{Q_N(V,T)} \int \ldots \int e^{-\beta V_N(\mathbf{r}, \mathbf{r}_2, \ldots, \mathbf{r}_N)} d^3 r_2 \ldots d^3 r_N, \tag{2.2}$$

where $\beta = 1/k_B T$ is the inverse temperature, k_B the Boltzmann constant, and

$$Q_N(V,T) = \int e^{-\beta V_N(\mathbf{r}^N)} d^3 r_1 \ldots d^3 r_N \tag{2.3}$$

the configurational integral. For a homogenous system it follows that $\rho^{(1)}(\mathbf{r}) = \frac{N}{V} = \rho$.

Similarly, the probability of finding any two particles in the volume elements $d^3 r_1$ and $d^3 r_2$ at $\mathbf{r}_1$ and $\mathbf{r}_2$, irrespective of the positions of the other particles, is given by [20, 4]

$$\rho_N^{(2)}(\mathbf{r}_1, \mathbf{r}_2) d^3 r_1 d^3 r_2 = \frac{N(N-1)}{Q_N(V,T)} \left[\int \ldots \int e^{-\beta V_N(\mathbf{r}^N)} d^3 r_3 \ldots d^3 r_N \right] d^3 r_1 d^3 r_2, \tag{2.4}$$

where $\rho_N^{(2)}(\mathbf{r}_1, \mathbf{r}_2)$ is called the two-particle density. The factor $N(N-1)$ takes account of the indistinguishability of the particles. For an ideal gas, $V_N(\mathbf{r}^N) = 0$, the two particle density reduces to

$$\rho_N^{(2)}(\mathbf{r}_1, \mathbf{r}_2) = \rho^2 (1 - \frac{1}{N}). \tag{2.5}$$

The (dimensionless) pair distribution function $g_N^{(2)}(\mathbf{r}_1, \mathbf{r}_2)$ is defined in terms of the two-particle density as

$$g_N^{(2)}(\mathbf{r}_1, \mathbf{r}_2) = \frac{\rho_N^{(2)}(\mathbf{r}_1, \mathbf{r}_2)}{\rho_N^{(1)}(\mathbf{r}_1) \rho_N^{(1)}(\mathbf{r}_2)}. \tag{2.6}$$

If the system is both homogeneous and isotropic then $g_N^{(2)}(\mathbf{r}_1, \mathbf{r}_2)$ is a function only of the distance $r = |\mathbf{r}_1 - \mathbf{r}_2|$ - called the radial distribution function and simply written as $g(r)$. A more illustrative interpretation of the definition (2.6) is the following: given a reference particle at the origin then $g(r)$ is the factor by which the mean number of particles, $4\pi r^2 dr \rho g(r)$, in a spherical shell of radius r and thickness dr centered around the reference particle deviates from the ideal gas value, $4\pi r^2 dr \rho$, due to interactions between the particles. If the repulsion between two particles is large at small distances, $g \to 0$ as $r \to 0$. For distances r much larger than the range of the interaction potential, the particles become uncorrelated and the pair distribution function approaches the ideal gas limit (2.5)

$$g(r) \to 1 - \frac{1}{N} \quad \text{for} \quad r \to \infty, \tag{2.7}$$

or, in the thermodynamic limit $g(r) \to 1$. In a typical simple liquid $g(r)$ is for large distances an oscillating function around 1 and shows for short and intermediate distances a series of peaks (see fig. (2.1)) which correspond to first neighbors, second neighbor shells, etc. and express the short range order that exists in a liquid.
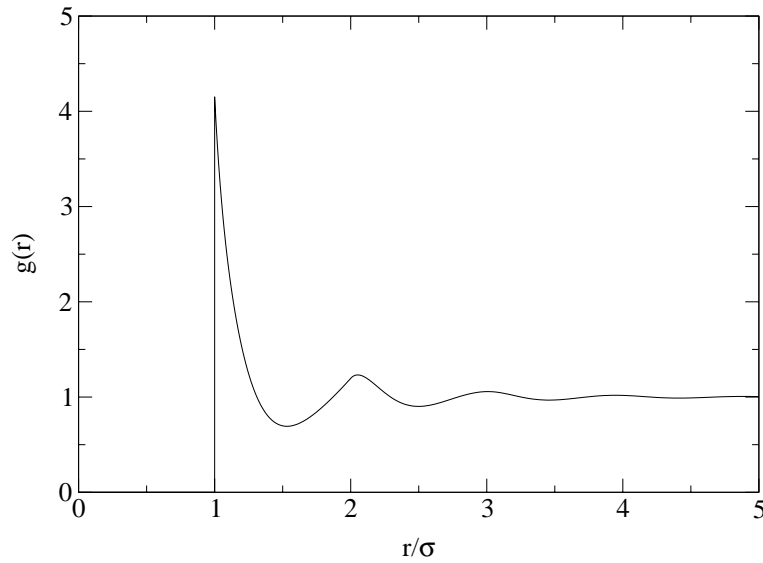
Figure 2.1: Typical pair distribution function of a hard-core system.

Let us assume in the following that the particles interact through central pair forces, thus

$$V_N(\mathbf{r}^N) = \sum_{i<j} \phi(r_{ij}), \quad r_{ij} = |\mathbf{r}_i - \mathbf{r}_j|, \quad i, j \in \{1 \ldots, N\}, \tag{2.8}$$

where $\phi(r)$ is the pair potential. Then thermodynamic properties can be expressed as integrals over $g(r)$ via three different routes [4].

One of them is the internal energy route according to which the excess (over ideal) part of the internal energy U^{ex} can be written as

$$\frac{U^{ex}}{N} = \frac{1}{N}\left\langle V_N(\mathbf{r}^N)\right\rangle = 2\pi\rho\int g(r)\phi(r)r^2 dr. \qquad (2.9)$$

In the second route the equation of state is obtained as an average over the virial

$$\begin{aligned}\frac{\beta P}{\rho} &= 1 - \frac{\beta}{3N}\left\langle\sum_i \mathbf{r}_i\nabla_i V_N(\mathbf{r}^N)\right\rangle \\ &= 1 - \frac{2}{3}\pi\beta\rho\int g(r)r^3\phi'(r)dr\end{aligned} \qquad (2.10)$$

and therefore it is known as the virial route. The third possibility can be derived in the grand canonical ensemble and reads

$$1 + \rho\int\left(g(r) - 1\right)d^3r = \frac{1}{N}\left\langle(N - \langle N\rangle)^2\right\rangle = \rho k_B T\chi_T, \qquad (2.11)$$

where

$$\chi_T = -\frac{1}{V}\left(\frac{\partial V}{\partial P}\right)_T = \left[\rho\left(\frac{\partial P}{\partial\rho}\right)_T\right]^{-1} \qquad (2.12)$$

is the isothermal compressibility of the system. Eq. (2.11) is known as the compressibility equation.

Now three routes are available to determine the equation of state $\beta P/\rho$ starting from the pair distribution function. One of them leads to the pressure directly via the virial equation (2.10). We will use the notation P_V for the pressure obtained in this way. The second possibility is given via the compressibility equation (2.11). Integrating $\frac{1}{\rho\chi_T}$ with respect to the density along an isothermal path yields the pressure. In the following, we will denote the pressure obtained in this way by P_C. The third route is based on the excess internal energy U^{ex} as given by the energy route (2.9). U^{ex} is related to the excess (over ideal) Helmholtz free energy F^{ex} by the equation

$$U^{ex} = \left(\frac{\partial\beta F^{ex}}{\partial\beta}\right)_V. \qquad (2.13)$$

Thus βF^{ex} can be obtained by integrating U^{ex} with respect to the inverse temperature along an isochore. By differentiating F^{ex} one obtains the excess (over ideal) pressure via

$$P^{ex} = -\left(\frac{\partial F^{ex}}{\partial V}\right)_T = \rho^2\left(\frac{\partial F^{ex}/N}{\partial\rho}\right)_T. \qquad (2.14)$$

We will use the notation P_E for the pressure obtained via the energy route.

If the exact $g(r)$ were known from some liquid-state theory, then the value of the pressure obtained via the virial, the compressibility and the energy equation should be the same, i.e. $P_V = P_C = P_E$. The theory is then called thermodynamically self-consistent. However, integral equation or perturbation theories only yield, as a consequence of the approximations in their concepts, an approximate $g(r)$ and thus are, more or less, thermodynamically inconsistent. So the liquid-vapor coexistence curves obtained from the different routes will not coincide, with different values of the critical point parameters. E. g., the MSA is known to be highly inconsistent [21]: the curve of diverging compressibility falls well inside the liquid-vapor coexistence curve obtained from the energy route. Liquid-state theories that enforce thermodynamic consistency will be presented in chapter 4.1.

2.1.2 Total correlation function

We introduce the so called total correlation function $h(r)$ by subtracting from the pair distribution function its ideal gas value

$$h(r) = g(r) - 1. \tag{2.15}$$

Thus $h(r) \to 0$ for $r \to \infty$.

In order to describe the correlation between density fluctuations $\delta\rho(\mathbf{r}) = \rho(\mathbf{r}) - \langle\rho(\mathbf{r})\rangle$ at $\mathbf{r}$ and $\mathbf{r}'$ we introduce the density-density correlation function

$$\Gamma(\mathbf{r}, \mathbf{r}') = \langle\delta\rho(\mathbf{r})\delta\rho(\mathbf{r}')\rangle. \tag{2.16}$$

By inserting the local particle density (2.1) it follows that

$$\Gamma(\mathbf{r}, \mathbf{r}') = \rho_N^{(2)}(\mathbf{r}, \mathbf{r}') + \rho_N^{(1)}(\mathbf{r})\delta(\mathbf{r} - \mathbf{r}') - \rho_N^{(1)}(\mathbf{r})\rho_N^{(1)}(\mathbf{r}'); \tag{2.17}$$

in the homogeneous isotropic case we obtain $\Gamma(r) = \rho^2 h(r) + \rho\delta(r)$. The Fourier transform of $\Gamma(r)$ is known as the static structure factor

$$S(\mathbf{k}) = \frac{\widetilde{\Gamma}(\mathbf{k})}{\rho} = 1 + \rho\tilde{h}(\mathbf{k}), \tag{2.18}$$

where the Fourier transform is defined as

$$\tilde{h}(\mathbf{k}) = \int h(r)e^{-i\mathbf{k}\mathbf{r}}d^3r. \tag{2.19}$$

The $k = 0$ limit of $S(\mathbf{k})$ is thus related to the isothermal compressibility (2.11)

$$S(0) = \rho k_B T \chi_T. \tag{2.20}$$

2.1.3 Ornstein-Zernike relation

The Ornstein Zernike (OZ) relation [22] defines the direct correlation function $c^{(2)}(\mathbf{r}_1, \mathbf{r}_2)$ in terms of the total correlation function $h^{(2)}(\mathbf{r}_1, \mathbf{r}_2)$

$$h^{(2)}(\mathbf{r}_1, \mathbf{r}_2) = c^{(2)}(\mathbf{r}_1, \mathbf{r}_2) + \int dr_3^3 \rho^{(1)}(\mathbf{r}_3) c^{(2)}(\mathbf{r}_1, \mathbf{r}_3) h^{(2)}(\mathbf{r}_3, \mathbf{r}_2). \tag{2.21}$$

The name direct correlation function for $c^{(2)}(\mathbf{r}_1, \mathbf{r}_2)$ can be motivated as follows: solving the OZ equation (2.21) iteratively, leads to

$$\begin{aligned} h^{(2)}(\mathbf{r}_1, \mathbf{r}_2) &= c^{(2)}(\mathbf{r}_1, \mathbf{r}_2) + \int dr_3^3 \rho^{(1)}(\mathbf{r}_3) c^{(2)}(\mathbf{r}_1, \mathbf{r}_3) c^{(2)}(\mathbf{r}_3, \mathbf{r}_2) \\ &\quad + \iint dr_3^3 dr_4^3 \rho^{(1)}(\mathbf{r}_3) \rho^{(1)}(\mathbf{r}_4) c^{(2)}(\mathbf{r}_1, \mathbf{r}_3) c^{(2)}(\mathbf{r}_3, \mathbf{r}_4) c^{(2)}(\mathbf{r}_4, \mathbf{r}_2) + \ldots \end{aligned} \tag{2.22}$$

Thus the total correlation between two particles is given by the direct correlation plus an indirect correlation mediated via an increasing number of intermediate particles.

For a homogeneous isotropic fluid the OZ relation takes the form

$$h(r) = c(r) + \rho \int dr'^3 c(r') h(|\mathbf{r} - \mathbf{r}'|), \tag{2.23}$$

which has a simpler form in Fourier space

$$1 + \rho \tilde{h}(k) = \left(1 - \rho \tilde{c}(k)\right)^{-1}. \tag{2.24}$$

So from the compressibility equation (2.11) it follows that

$$\rho \tilde{c}(0) = 1 - \frac{1}{\rho k_B T \chi_T}. \tag{2.25}$$

Thus $\tilde{c}(0)$ is finite and hence $c(r)$ is a short ranged function even at the critical point where the correlation length of density fluctuations and the isothermal compressibility diverges.

2.1.4 Extension to mixtures

The definitions and relations presented in the previous subsection for a one-component fluid can be generalized in a straightforward way to multi-component fluids. Since we will also be concerned with the thermodynamics and the phase behavior of binary mixtures we will briefly summarize these basic relations.

We consider a homogeneous isotropic fluid consisting of m components and particle numbers N_i, $i = 1, \ldots, m$. $\rho_i = \frac{N_i}{N}$ denotes the partial number density of the ith species,

$\rho = \sum_i \rho_i$ the total number density and $x_i = \frac{\rho_i}{\rho}$ is the mole fraction (or number concentration) of the ith component in the mixture. Thus $\sum_i x_i = 1$ The structure of the fluid is described by the set of $\frac{1}{2}m(m-1)$ radial distribution functions $\{g_{ij}(r)\}$, which satisfy the symmetry relations $g_{ij}(r) = g_{ji}(r)$. These functions have the following meaning: given a particle of species i at the origin then $4\pi r^2 dr g_{ij}(r)\rho_j$ is the mean number of particles of species j found in a distance r apart. The radial distribution functions satisfy the symmetry relations $g_{ij}(r) = g_{ji}(r)$. Similarly to eq. (2.18) one can define the partial structure factors as

$$S_{ij}(k) = \sqrt{x_i x_j}\delta_{ij} + x_i x_j \rho \tilde{h}_{ij}(k), \tag{2.26}$$

where $h_{ij}(r) = g_{ij}(r) - 1$. The multicomponent OZ equations read

$$h_{ij}(r) = c_{ij}(r) + \sum_{k=1}^{m} \rho_k \int d^3 r' c_{ik}(|\mathbf{r} - \mathbf{r}'|)h_{kj}(r'), \tag{2.27}$$

where the $c_{ij}(r)$ are the direct correlation functions between particles of species i and j. Hence,

$$\sqrt{x_i x_j}\delta_{ij} - \rho x_i x_j \tilde{c}_{ij}(k) = \left(\mathsf{S}^{-1}\right)_{ij}, \tag{2.28}$$

where the matrix notation $\mathsf{S} = (S_{ij})$ was introduced.

The generalization to mixtures of the internal energy route reads

$$\frac{U^{ex}}{V} = 2\pi \sum_i \sum_j \rho_i \rho_j \int g_{ij}(r)\phi_{ij}(r)r^2 dr \tag{2.29}$$

and of the compressibility route

$$\frac{1}{\rho k_B T \chi_T} = 1 - \frac{1}{\rho} \sum_{ij} \rho_i \rho_j \tilde{c}_{ij}(0). \tag{2.30}$$

Equivalent results for the partial direct correlation functions are

$$-\sqrt{\rho_i \rho_j}\left(\frac{\partial \beta \mu_i}{\partial \rho_j}\right)_{V,T,\rho_{i \neq j}} = \delta_{ij} - \rho \tilde{c}_{ij}(0), \tag{2.31}$$

where μ_i is the chemical potential of species i.

Appropriate linear combinations of the structure factors S_{ij} that correspond to the correlations between fluctuations in the density and concentration have been introduced in [23] and will be presented in the following. We will restrict the considerations to the simpler binary mixture where the number concentrations of the two components are $x_1 \equiv x$ and $x_2 = 1 - x$.

We define the fluctuations of the total density as

$$\delta\rho(\mathbf{r}) = \delta\rho_1(\mathbf{r}) + \delta\rho_2(\mathbf{r}), \tag{2.32}$$

where $\delta\rho_i(\mathbf{r}) = \rho_i(\mathbf{r}) - \rho_i$ is the fluctuation of the local density of particle species i around its average value ρ_i. Similarly, we define the concentration fluctuation

$$\delta c(\mathbf{r}) = \frac{x_2\delta\rho_1(\mathbf{r}) - x_1\delta\rho_2(\mathbf{r})}{\rho}. \tag{2.33}$$

Then the following structure factors express the correlations between total density fluctuations, concentration fluctuations and the cross correlations between density and concentration fluctuations:

$$
\begin{aligned}
S_{NN}(k) &= \frac{1}{\rho}\mathcal{FT}\left[\langle\delta\rho\cdot\delta\rho\rangle\left(|\mathbf{r}-\mathbf{r}'|\right)\right] = S_{11}(k) + S_{22}(k) + 2S_{12}(k) \\
S_{CC}(k) &= \rho\mathcal{FT}\left[\langle\delta c\cdot\delta c\rangle\left(|\mathbf{r}-\mathbf{r}'|\right)\right] = x_2^2 S_{11}(k) + x_1^2 S_{22}(k) - 2x_1 x_2 S_{12}(k) \\
S_{NC}(k) &= \mathcal{FT}\left[\langle\delta c\cdot\delta\rho\rangle\left(|\mathbf{r}-\mathbf{r}'|\right)\right] = x_2 S_{11}(k) - x_1 S_{22}(k) + (x_2 - x_1)S_{12}(k),
\end{aligned}
\tag{2.34}
$$

where $\mathcal{FT}\left[\cdot\right]$ denotes the Fourier transform of the expression in the brackets. The generalization of eq. (2.20) to the binary mixture case are the following relationships between the long-wavelength limits of the structure factors defined in (2.34) and thermodynamic properties [23]

$$
\begin{aligned}
S_{CC}(0) &= NkT/\left(\frac{\partial^2 G}{\partial x^2}\right)_{T,P,\rho} \tag{2.35} \\
S_{NN}(0) &= \rho k_B T\chi_T + \delta^2 S_{CC}(0) \tag{2.36} \\
S_{NC}(0) &= -\delta S_{CC}(0), \tag{2.37}
\end{aligned}
$$

where G is the Gibbs free energy, and $\delta = \rho(v_1 - v_2)$. $v_i = \left(\frac{\partial V}{\partial N_i}\right)_{P,T,N_{j\neq i}}$ is the partial molar volume of species i.

2.2 Liquid-State Techniques

We have shown in the preceeding subsection that the pair distribution function $g(r)$ plays a central role in liquid-state theories since once this function is known thermodynamic quantities can be calculated. In order to determine $g(r)$ for a system with a given interatomic pair potential some approximation must be made. In this section we will present those liquid-state approximations that are relevant for our work, the MSA and the LOGA/ORPA. They represent examples of two different approximate schemes,

namely integral equation theories (IETs) and perturbation theories (PTs). In the following we will briefly introduce the basic ideas of these two groups of liquid-state theories, a more detailed description (including the derivation of those relations) can, f. i., be found in [4].

2.2.1 Integral Equation Theories

From a cluster expansion of $g(r)$ [4] it follows that

$$g(r) = e^{-\beta\phi(r)+h(r)-c(r)+E(r)}, \tag{2.38}$$

introducing the so-called brigde function $E(r)$. Eq. (2.38) can be considered as an exact closure relation to the OZ equation if the exact $E(r)$ were known. Then we have a set of two equations in the two unknowns $c(r)$ and $h(r)$ for a given pair potential $\phi(r)$. An approximate closure relation is obtained by introducing either an approximation for $E(r)$ or, instead of assuming an approximation for $E(r)$, one could also derive an approximate closure relation to the OZ equation from exact relations of statistical mechanics, introducing simplifying assumptions; this leads to a functional relation between $h(r)$ and $c(r)$, including the pair potential $\phi(r)$, i.e.

$$F(c(r), h(r), \phi(r)) = 0. \tag{2.39}$$

So $h(r)$ and $c(r)$ are then determined by solving the OZ integral equation (2.23) supplemented by some closure relation (2.39).

Various closure relations have been derived by using diagrammatic expansions or functional Taylor expansions [4], like e.g. the well known Percus-Yevick (PY) closure relation which assumes that

$$c(r) = \left(1 - e^{\beta\phi(r)}\right) g(r). \tag{2.40}$$

For a hard-sphere (HS) fluid with interaction potential

$$\phi(r) = \begin{cases} \infty & r < \sigma \\ 0 & r > \sigma \end{cases}, \tag{2.41}$$

where σ is the HS diameter it follows from (2.40), (2.41) and (2.38) that

$$\begin{aligned} c(r) &= 0 & r > \sigma \\ g(r) &= 0 & r < \sigma. \end{aligned} \tag{2.42}$$

The second relation, the so called core condition is exact and expresses the fact that the HSs are not allowed to overlap. The OZ equation (2.23) with the closure relation (2.42) is analytically solvable (see e.g. [4]).

Another approximation, that is very frequently used due to its semi-analytic solubility for pair potentials like the HS Yukawa potential [24], charged HSs [25], dipolar HSs [26], sticky HSs [27] and a generalized HS Yukawa potential [28] is the mean spherical approximation (MSA). The conventional MSA is only applicable to systems where the pair potential consists of a hard-core (HC). So, let us assume in the following a HC potential with HC diameter σ and some tail

$$\phi(r) = \begin{cases} \infty & r < \sigma \\ w(r) & r > \sigma \end{cases}. \qquad (2.43)$$

From cluster expansion [4] it follows that the asymptotic behavior of the direct correlation function is given by

$$c(r) \rightarrow -\beta\phi(r) \quad \text{for} \quad r \rightarrow \infty. \qquad (2.44)$$

Thus $c(r)$ behaves at long range as the interparticle potential. The approximation in the MSA scheme is the assumption that the relation (2.44) is valid also for short distances. So the MSA reads

$$\begin{aligned} c(r) &= -\beta w(r) \quad r > \sigma \\ g(r) &= 0 \quad r < \sigma. \end{aligned} \qquad (2.45)$$

In the case of a pure HS interaction the MSA reduces to the PY approximation.

2.2.2 Perturbation Theories, LOGA/ORPA

The basic idea of PTs is a separation of the pair potential into a harsh, short-ranged repulsion and a smoothly varying long-ranged attraction. It is known that the repulsive part mainly determines the structure of a fluid while the attractive part plays a minor role and can therefore be treated as a perturbation of the repulsive reference system leading to (small) corrections of the thermodynamic and structural properties [29]. Furthermore, it is rather convenient to approximate the repulsion by the infinitely steep repulsion of the HS potential, since the HS fluid represents a reference system whose structural and thermodynamic properties are known with great accuracy.

Thus in the spirit of a perturbation theory one can regard - in the simplest approximation - a fluid as a system of HSs that move in a uniform attractive background. In this approximation one arrives at the famous van der Waals equation. Higher order approximations can be obtained by expanding the Helmholtz free energy either in powers of the strength of the perturbation (λ-expansion) or in powers of the interaction range (γ-expansion) [4].

The perturbation theory which is used in the present work, the LOGA/ORPA [30, 31, 32], is applicable to fluids (and their mixtures) where the interactions between particles are pairwise additive. It assumes that the pair potential ϕ_{ij} between particles of species i and j is split up into

$$\phi_{ij}(r) = \phi_{r;ij}(r) + \phi_{p;ij}(r), \tag{2.46}$$

where $\phi_{r;ij}(r)$ is the pair potential of the reference system and $\phi_{p;ij}(r)$ is the attractive perturbation. Since in the present work we consider exclusively HC interactions it is most obvious that the $\phi_{r;ij}(r)$ are represented by HS potentials characterized by HS diameters σ_{ij}. This defines the $\phi_{p;ij}(r)$ apart from finite variations inside the core. In the case where $\phi_{r;ij}(r)$ is not a HS potential, the softness of the potential can be taken into account via the Weeks-Chandler-Andersen 'blip'-function expansion [33].

The separation of the potential leads naturally to the decomposition of all the correlation functions

$$h_{ij}(r) = h_{r;ij}(r) + h_{p;ij}(r) \tag{2.47}$$

and

$$c_{ij}(r) = c_{r,ij}(r) + c_{p;ij}(r), \tag{2.48}$$

where $h_{r;ij}(r)$ and $c_{r;ij}(r)$ are the correlation functions of the reference fluid and $h_{p;ij}(r)$ and $c_{p;ij}(r)$ are the corrections to the correlation functions of the reference system due to the attractive interaction. For convenience we define the matrices $\mathsf{C}_p = \left(\sqrt{\rho_i \rho_j} c_{p;ij} \right)$ and $\mathsf{C}_r = \left(\sqrt{\rho_i \rho_j} c_{r;ij} \right)$.

In the random phase approximation (RPA) one assumes that

$$c_{p;ij}(r) = -\beta \phi_{p;ij}(r). \tag{2.49}$$

However, this approximation does not guarantee that $g_{ij}(r)$ vanishes inside the HC as it should in an exact theory. This means that geometrical exclusion effects are not treated correctly. On the other hand, in this framework, there is a flexibility in the choice of $\phi_{p;ij}(r)$ that can usefully be exploited: It is clear that eq. (2.46) does not define the perturbation uniquely for $r < \sigma_{ij}$. For this physically inaccessible region, the perturbation can be

chosen to have any finite functional form. Thus the perturbing potential $\phi_{p;ij}(r)$ inside the hard core ($r < \sigma_{ij}$) can be varied to obtain the so called optimized potential. We thus obtain the LOGA/ORPA which is formulated via the two relations:

$$c_{p;ij}(r) = -\beta \phi_{p;ij}(r) \quad \text{for} \quad r > \sigma_{ij} \tag{2.50}$$

and the perturbation potential inside the core is chosen so that

$$g_{p;ij}(r) = h_{p;ij}(r) = 0 \quad \text{for} \quad r < \sigma_{ij}. \tag{2.51}$$

It can be shown that the excess (over the ideal gas) free energy of the system is given in the RPA by

$$A^{\star} = -\frac{\beta A^{ex}}{V} = \mathcal{A}^{RPA} = A_r^{\star} + \mathcal{A}_{HTA} + \mathcal{A}_{ring}, \tag{2.52}$$

where $A_r^{\star}$ is the excess free energy density of the reference system, $\mathcal{A}_{HTA}$ is the so called high temperature approximation

$$\mathcal{A}_{HTA} = \frac{1}{2} \sum_{ij} \rho_i \rho_j \int d^3 r \, g_{r;ij}(r) c_{p;ij}(r). \tag{2.53}$$

and $\mathcal{A}_{ring} = \mathcal{A}_{ring}[\mathsf{C_p}]$ is a functional being the sum of composite ring diagrams [29] which is found to be given by

$$\mathcal{A}_{ring}\left[\widetilde{\mathsf{C_p}}\right] = -\frac{1}{2(2\pi)^3} \int d^3 k \left(\text{tr}\left(\widetilde{\mathsf{C_p}}(\mathsf{I} - \widetilde{\mathsf{C_r}})^{-1} \right) + \ln \det\left((\mathsf{I} - \widetilde{\mathsf{C}})(\mathsf{I} - \widetilde{\mathsf{C_r}})^{-1} \right) \right), \tag{2.54}$$

where 'tr' and 'det' denote the trace and determinant of a matrix and the matrix I is the unit matrix.

Using the RPA expression for the free energy, $\mathcal{A}_{RPA} = \mathcal{A}_{RPA}[\mathsf{C_p}]$, that is a functional of the perturbation part of the direct correlation functions $c_{p;ij}(r)$ one can show that [34]

$$\frac{\delta \mathcal{A}^{RPA}}{\delta c_{p;ij}(r)} = \frac{2 - \delta_{ij}}{2} \rho_i \rho_j \left[g_{r;ij}(r) + h_{p;ij}(r) \right]. \tag{2.55}$$

In particular, $\frac{\delta \mathcal{A}^{RPA}}{\delta c_{p;ij}(r)} = 0$ for $r < \sigma_{ij}$ if the core condition is fulfilled. This relation points out that the solution of the OZ equations along with the LOGA/ORPA closure relation (2.50) and the core condition (2.51) is equivalent to a minimization of the functional with respect to variations of the $c_{p;ij}(r)$ inside the core region.

As shown in [35] the expression for the free energy (2.52) can be rewritten with the help of the OZ equations (2.27) and Parseval's theorem as follows:

$$\mathcal{A}^{RPA} = \mathcal{A}_r + \frac{1}{2} \sum_{i,j} \rho_i \rho_j \tilde{c}_{p;ij}(k) \Big|_{k=0} - \frac{1}{2} \sum_i \rho_i c_{p;ii}(r) \Big|_{r=0}$$

$$-\frac{1}{2(2\pi)^3} \int d^3k \left(\ln \det \left(\mathsf{I} - \widetilde{\mathsf{C}} \right) - \ln \det \left(\mathsf{I} - \widetilde{\mathsf{C}}_r \right) \right). \tag{2.56}$$

From the integral equation point of view, the solution of the LOGA/ORPA may also be viewed as a solution of the OZ equation with the closure relation (2.50) and the core condition (2.51). It is therefore similar to the MSA, the only difference is the exact treatment of the hard-sphere reference system in the LOGA/ORPA.

Chapter 3

Phase Coexistence

3.1 Phase Behavior and Stability Conditions

3.1.1 One-component System

A typical phase diagram of a one-component substance in the P-T and T-ρ plane is shown in fig. (3.1). The liquid phase exists only in the small part of the entire P-ρ-T space that is bounded above by a critical point where coexisting vapor and liquid become identical and below by a triple point. Above the critical point there exists only a single fluid phase and there is a continuous path from the gas via the fluid to the liquid phase as indicated in the figure. This is not the case for the transition from liquid to solid that does not end at a critical point. Consider moving along the gas-liquid coexistence line in the direction of increasing temperature, then the difference in density between the gas and the liquid decreases continously to zero and becomes zero at the critical point. The density difference $\Delta\rho = \rho_l - \rho_v$ between the coexisting liquid and gas phase, which is nonzero below the critical temperature, is called the order parameter of the gas-liquid coexistence transition.

In general, the conditions for coexistence of two phases in contact with each other [36, 37] are

$$T = T', \quad P = P', \quad \mu = \mu', \tag{3.1}$$

where the primed and unprimed quantities T, P, μ are the temperature, pressure and chemical potential of the two phases. The first condition expresses thermal equilibrium, the second mechanical equilibrium and the third material equilibrium between two phases. From the Gibbs rule it follows that a one-component system cannot have more than three
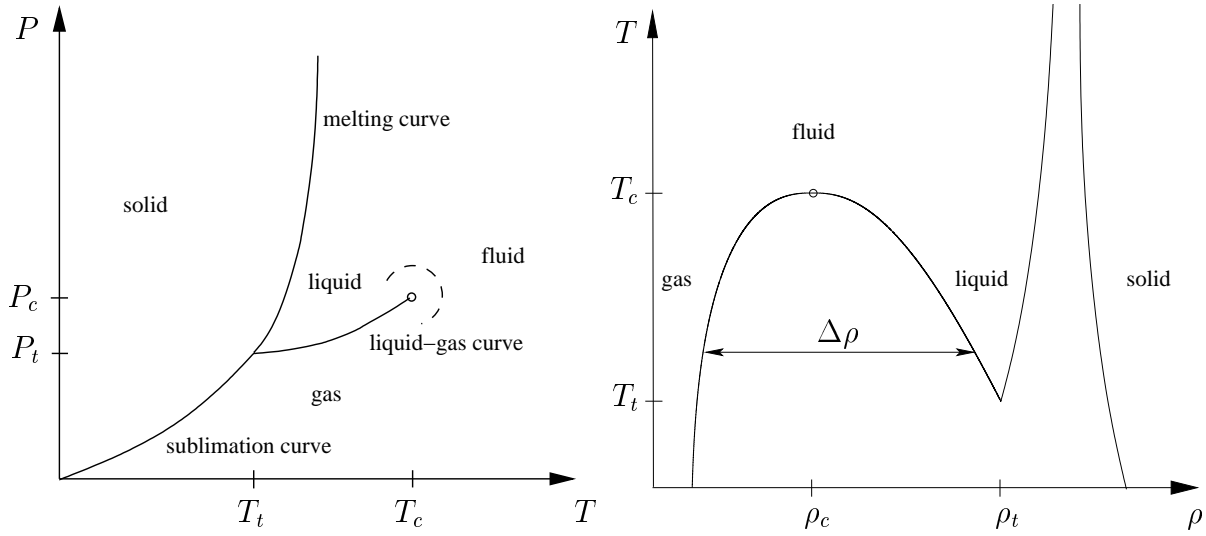
Figure 3.1: Left: Phase diagram of a one-component system in the P-T plane. The indices 't' and 'c' indicate the triple and critical point. The gas-liquid coexistence curve ends at a critical point. So there is a continuous path from the gas to the liquid phase as indicated by the dashed line. Right: Gas-liquid coexistence curve for a one-component substance in the T-ρ plane. The indices 't' and 'c' indicate the triple and critical point. The order parameter of the gas-liquid transition, $\Delta\rho = \rho_l - \rho_v$, vanishes at the critical point.

coexisting phases and that the coexistence of three phases can only appear at a single point, the triple point.

The coexistence curves in the $T - \rho$ plane can be determined by expressing the chemical potential and the pressure as functions of the density at fixed temperature T and solving the coupled set of equations

$$\mu(\rho, T) = \mu(\rho', T) \tag{3.2}$$

$$P(\rho, T) = P(\rho', T) \tag{3.3}$$

for ρ and ρ'. This route was chosen in the present work. Equivalent routes are the well-known Maxwell construction see fig. (3.2) and the common tangent construction for the Helmholtz free energy per volume F/V as a function of the density.

The condition of phase stability for a one-component system is

$$\left(\frac{\partial^2 F}{\partial V^2}\right)_{T,N} = -\left(\frac{\partial P}{\partial V}\right)_{T,N} = \frac{1}{V\chi_T} > 0, \tag{3.4}$$

meaning that the pressure cannot decrease with increasing density. The points where χ_T diverges define the so-called spinodal line that separates the stable from the unstable
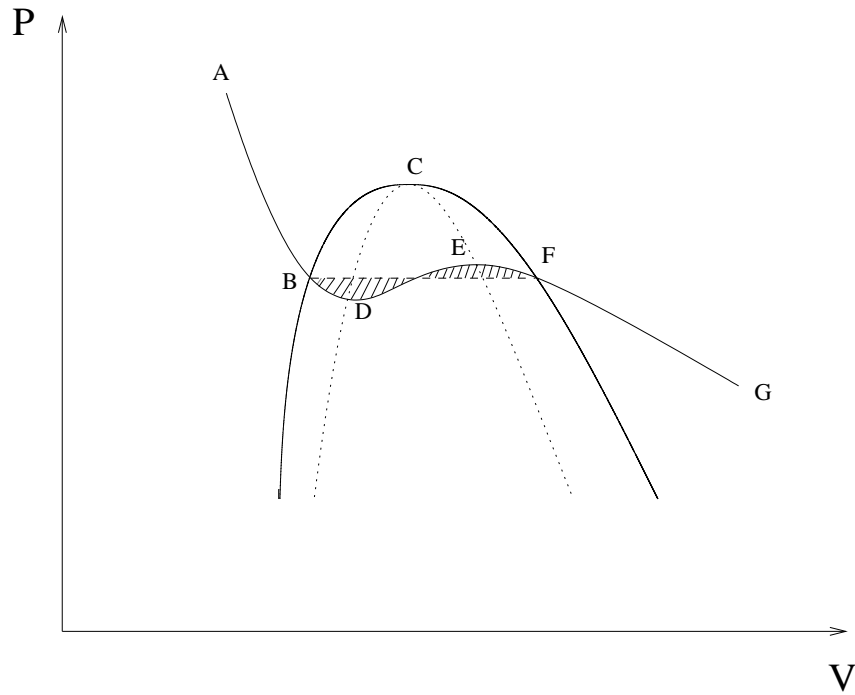
Figure 3.2: Van der Waals construction to determine phase equilibria along an isotherm (ABDEFG). The shaded areas enclosed by the curve linking BDEF and the dashed line are equal and indicate the Maxwell construction. B and F are points of the liquid-vapor coexistence curve (binodal) - full line, D and E points of the spinodal line, where $\chi_T = \infty$ corresponding to a local maximum and minimum of the isotherms - dotted line. The binodal and spinodal curve touch each other at the critical point C. Along the curves BD and EF the system is metastable ($\chi_T > 0$), while it is mechanically unstable along the curve DE ($\chi_T < 0$).

region. In the stable region, where $\chi_T > 0$, the system can exist in a single phase while inside the other region the free energy can be lowered by phase separation into two phases with different density. Thus the single phase gets unstable and phase separation occurs.

3.1.2 Binary Mixtures

The phase behavior of binary mixtures is of course much richer than that of a simple one-component substance. Depending on the relative sizes of the two particle species and the strength of their interactions one observes a large variety of different phase diagrams [5]. A systematic study of the different phase diagram topologies was performed by Konynenburg and Scott by using the van der Waals equation of state [38]. Even for the simple case of

equally sized particles they identified not less than 12 different types of phase diagrams distinguished by the presence and absence of three-phase lines and azeotrope lines, by the number of critical lines and by the way the critical lines terminate.

The conditions for phase equilibrium generalize to the case of a two-component system with concentrations $x_1 \equiv x$ and $x_2 = 1 - x$ by requiring that

$$T = T', \quad P = P', \quad \mu_1 = \mu_1', \quad \mu_2 = \mu_2'. \tag{3.5}$$

At an azeotropic point two phases with the same composition are in equilibrium, hence additionally to the usual coexistence conditions the condition $x = x'$ must be fulfilled. According to the Gibbs rule up to four phases can coexist in a binary mixture; four phases coexist in a point and three phases can coexist along a line (triple line).

The conditions of phase coexistence and phase stability are expressible in terms of the Gibbs free energy G. Similarly to the common tangent construction for the Helmholtz free energy F in the one-component case, the concentrations x and x' of two coexisting phases at a given temperature T and pressure P can be obtained via a common tangent construction of the Gibbs free energy as a function of x. The concentration of two coexisting phases at fixed pressure P can be reported in a $T - x$ diagram. Various types of diagrams are distinguishable depending on the number and loci of the critical points [5].

For a given composition, density and temperature, a fluid mixture can be present in a single homogeneous phase only if thermodynamic stability is satisfied. In contrast to a one-component system where only mechanical stability, expressed via $\chi_T > 0$, must be satisfied, a fluid mixture must have both mechanical (or liquid-vapor) stability and material (or liquid-liquid) stability. The latter is expressed via

$$\left(\frac{\partial^2 G}{\partial x^2} \right)_{T,P,\rho} \geq 0. \tag{3.6}$$

If this condition is not satisfied then the Gibbs free energy can be decreased - while keeping temperature and pressure constant - by phase separation into two phases of different compositions: this phase separation is called demixing transition.

While the first kind of instability where χ_T diverges and which forces the fluid to phase separate into two phases of different densities is associated with a divergence of $S_{NN}(0)$ (see (2.36)), the material instability corresponds to a divergence of the correlation length of concentration fluctuations and thus $S_{CC}(0)$ (see eq. (2.35)). The spinodal line of a mixture is thus located at those points where either $S_{CC}(0)$ or $S_{NN}(0)$ or both diverge. In the case in which a mixture is mechanically unstable, but materially stable,

i.e. at an azeotropic instability, $S_{CC}(0)$ remains finite and $S_{NN}(0)$ diverges leading to a separation into two phases of different densities but equal compositions. So it follows from (2.26) and (2.34) that at an azeotropic instability $\tilde{h}_{12}(0) = \frac{1}{2}\left(\tilde{h}_{11}(0) + \tilde{h}_{22}(0)\right)$ and $S_{CC}(0) = x_1 x_2$. Furthermore, from eq. (2.37) it follows that $v_1 - v_2 = \frac{1}{2}\left(\tilde{h}_{11}(0) - \tilde{h}_{22}(0)\right)$. From eqs. (2.35– 2.37) one sees that a divergence of $S_{CC}(0)$ also causes a divergence of the other structure factors, so it is not straightforward to distinguish in the general case of a binary mixture the two kinds of instability. The situation is different in the case of a so-called binary symmetric mixture (see section 4.3.4).

In the following we will restrict our investigations to this simpler model system.

3.1.3   Binary Symmetric Fluid

In the binary symmetric mixture the like-particle interactions are identical ($\phi_{11}(r) = \phi_{22}(r) \quad \forall r$), while the unlike interactions are different from the like ones ($\phi_{12}(r) \neq \phi_{ii}(r), i = 1, 2$). We further assume that the functional form of the like and unlike interactions is equal. Only the strength is different, i.e.,

$$\phi_{11}(r) = \phi_{22}(r) \tag{3.7}$$

$$\phi_{12}(r) = \alpha\phi_{11}(r), \tag{3.8}$$

where α is the relative strength of interactions between particles of dissimilar and similar species.

Due to the symmetry of the potentials one obtains symmetry relations for the structural and thermodynamic properties, like for instance

$$h_{11}(r; T, \rho, x) = h_{22}(r; T, \rho, 1 - x)$$

$$h_{12}(r; T, \rho, x) = h_{12}(r; T, \rho, 1 - x)$$

$$\mu_1(T, \rho, x) = \mu_2(T, \rho, 1 - x) \tag{3.9}$$

$$P(T, \rho, x) = P(T, \rho, 1 - x) \quad \text{etc.} \tag{3.10}$$

Although such a model system seems rather artifical and does not allow the description of an experimentally observed phase behavior [1] it shows already a rather rich variety of phase behavior and offers insight into the link between the microscopic description of a system and its phase behavior. The advantage of this simple model is the fact that its

---

[1] An example for a realistic system with such a symmetry are mixtures of d,l-optical isomers. However, liquid-liquid separations in these systems have not been reported so far (see page 524 of [38]).

interactions are characterized by only a few parameters, namely the interaction strength ratio α and the parameters of the pair potential ϕ_{11}: they trigger the phase behavior of the system, so that a systematic investigation of their influence is still within reach. On the other hand - despite the simplicity of the model - the phase diagrams show nevertheless a much richer variety than those of a one-component system and interesting phenomena, like the existence of triple points, critical lines, critical end points and tricritical points.

From the different possibilities to present phase diagrams, we have chosen in this work presentations in the $T - \rho - x$ space, their projections onto the $T - \rho$ plane and their isothermal slices leading to phase diagrams in the $\rho - x$ plane.

In the work we restrict ourselves to the determination of those coexisting phases where the number of species 1 and species 2 particles is equal, i.e. we consider only those phase equilibria where $x' = 1 - x$. In that case four different types of phase diagrams can be observed that belong to two classes.

1. The first class, where the similar species interaction is favorable, i.e. $\alpha < 1$, is characterized by the presence of a critical line of demixing transitions (the so called λ-line). For a given density there is a critical point of the demixing transition (critical consolute point) at some finite temperature T_c. The symmetry of our system implies that this critical point is located at $x = 1/2$. Above this temperature one observes a homogeneous mixture of 1 and 2 particles ($x = x' = 1/2$) - the so called mixed fluid (MF) - while below T_c the liquid separates into a 1-rich phase with concentration x and a 2-rich phase whose concentration is $x' = 1 - x$ - the so called demixed fluid (DF).

2. The second class, where $\alpha \geq 1$, is characterized by the absence of a critical line and the absence of demixing transitions.

A system of the first class exhibits in addition to these demixing transitions also liquid-vapor transitions as a one-component fluid. Depending on the interplay of these two types of phase transitions one can distinguish three types of phase diagrams that will be presented in the following. One of them is shown in fig. (3.3).

In the following we will use a simpler two-dimensional representation of the phase diagram which is obtained by the projection of the two high-density branches of the three-phase line along the x direction onto the $x = 1/2$ plane and omitting the demixing curves. Only the critical line of the demixing transitions (λ-line) will be shown. Owing to the symmetry of the system, the coexisting phases of the two high density branches of
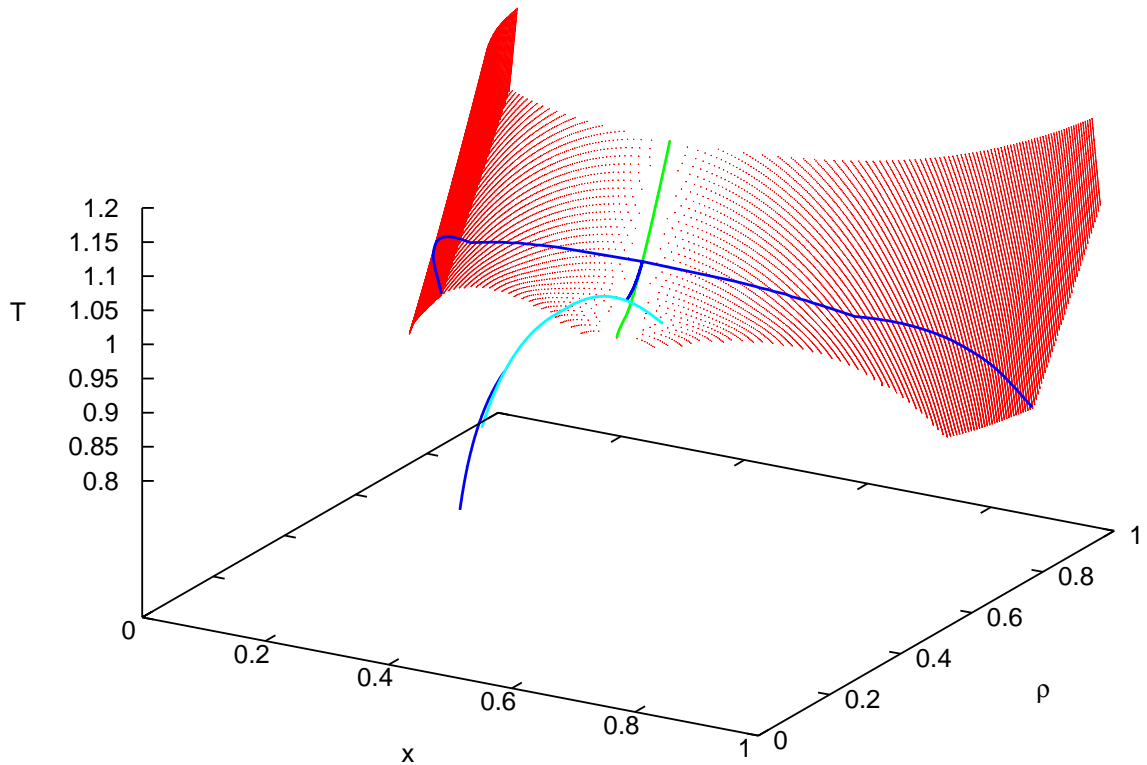
Figure 3.3: Phase diagram of type II (see text) of a binary symmetric fluid in the $T - \rho - x$ space. The phase diagram is symmetric with respect to the $x = 1/2$-plane. Red curves: demixing transitions. Green curve: λ-line. Light blue curve: VMF transition. Dark blue curve: VDF/MFDF transitions.

the three phase line have the same density and thus their projections yield only one line. Using this representation, fig. (3.4) shows a schematic drawing of the three different types of phase diagrams of class 1. The three types differ in the way the second order transition associated with demixing merges into the first order liquid-vapor (LV) transition:

Type I: Fig. (3.4a) shows the situation when the λ-line approaches the LV coexistence curve well below the critical point. In that case the λ-line intersects the first order LV curve at a critical end point (CEP). At the CEP, a critical liquid coexists with a noncritical vapor. Above the CEP temperature a vapor and a homogeneous liquid of intermediate density coexist becoming identical at the LV critical point. At higher

densities, as one crosses the λ-line, the fluid demixes. The full line below the CEP temperature is a triple line where a gas, a 1-rich and a 2-rich liquid coexist.

Type III: In fig. (3.4c) the λ-line intersects the LV line at the LV critical point. In that case the first order transition between the vapor and the mixed liquid is absent and the λ-line ends at a tricritical point where three phases become critical at the same time: a vapor, a 1-rich liquid and a 2-rich liquid. So two order parameters, namely $\Delta\rho = \rho_l - \rho_v$, where ρ_l and ρ_v are the coexisting liquid and vapor densities, and $\Delta x = x - x' = 2x - 1$ vanish at the same time. The tricriticality is a specific feature of the symmetric model. In a general binary fluid tricriticality does not occur (see [38]).

Type II: The intermediate situation is shown in fig. (3.4b) where the λ-line approaches the LV coexistence curve slightly below the LV critical point. As in type I one finds a LV critical point and as in type III a tricritical point. Additionally this type is characterized by a triple point where – to be correct - four phases coexist: a vapor, a mixed liquid at intermediate density, a 1-rich and a 2-rich liquid at higher density.

In a mean field study [12] it was shown that the transition between the different types of phase diagrams is triggered by the parameter α.

Another type of phase diagram has been observed in grand canonical Monte Carlo (GCMC) simulations of a binary symmetric fluid inside a porous matrix ($\rho_0 = 0.05, \alpha = 0.7, y = 3.5$ - see chapter 5 for the definitions of these parameters) [39], in which the λ-line intersects the LV critical line at a CEP on the vapor side (see fig. (3.5)). So above the CEP temperature one finds a four-phase line, where 1- and 2-rich phases of lower density coexist with 1- and 2-rich phases of higher densities. In the simulations the constraint of equal particle numbers was replaced by imposing equal chemical potentials for both species. So the demixed fluid phase that is observed comprises either a homogeneous 1-rich or 2-rich phase, which are - due to the symmetry - indistinguishable. Thus if the coexisting 1- and 2-rich phases are regarded as a single liquid phase (the demixed fluid) the 'four-phase' line would not violate the Gibbs rule.

Similar archetypes of phase diagrams (and sequences of these) are encountered in systems with completely different interatomic potentials: as examples we list here the *Heisenberg* fluid [40] (a fluid where the particles interact via hard-core and a *Heisenberg*-type interaction of their dipolar moments) and the *Stockmayer* fluid [41] (a fluid where the particles carry dipolar moments and interact - in addition - via Lennard-Jones potentials).
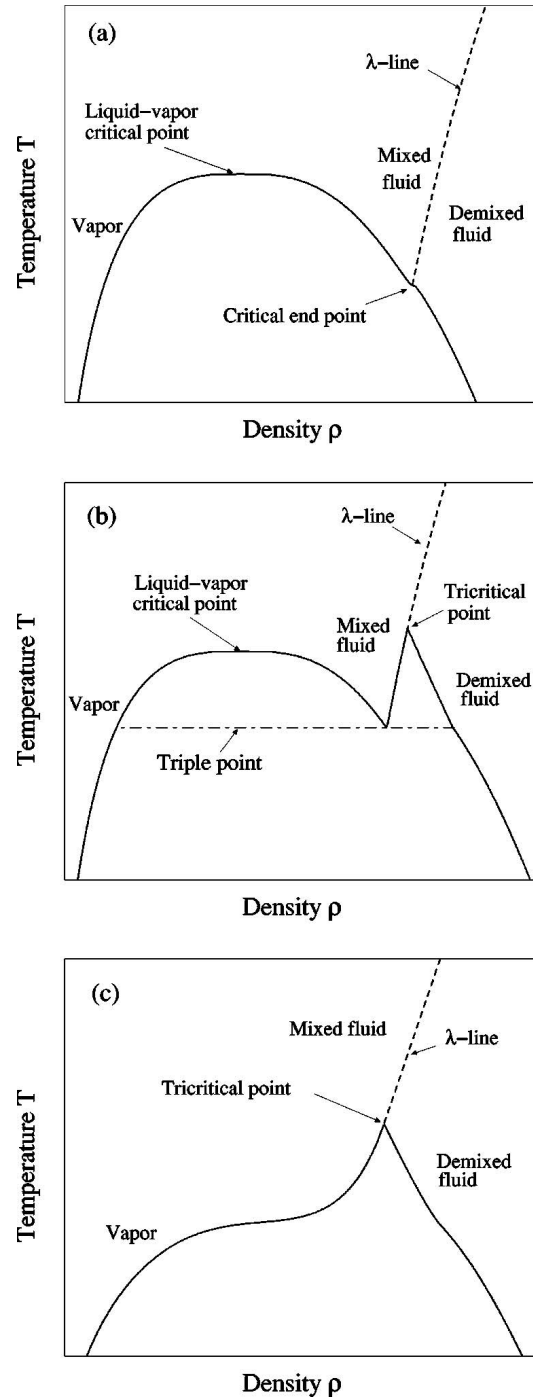
Figure 3.4: Schematic representation of the three types of phase diagrams of class 1 introduced in the text (from [12]). The phase diagrams are projections of the three-dimensional $T - \rho - x$ phase diagrams onto the $x = 1/2$-plane. The full curve is the liquid-vapor boundary. The dashed curve is the λ-line.
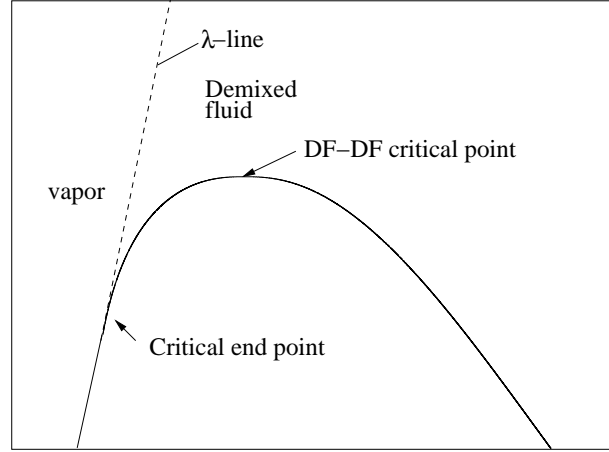
Figure 3.5: Schematic representation of the fourth type of phase diagram of class 1, that was observed in the GCMC studies of a binary symmetric fluid inside a porous matrix [39]. The full curve is the liquid-vapor boundary. The dashed curve is the λ-line.

Both, in the case of a binary mixture in the bulk and confined in a disordered porous matrix we have calculated the phase diagrams by equating, at a given temperature T, the pressure, P, and the chemical potentials, μ_i, of the coexisting phases. The general equilibrium conditions read

$$
\begin{aligned}
\mu_i(\rho, x, T) &= \mu_i(\rho', x', T) \qquad i = 1, 2 & (3.11) \\
P(\rho, x, T) &= P(\rho', x', T), & (3.12)
\end{aligned}
$$

where the thermodynamic states of the coexisting phases are given by (ρ, x) and (ρ', x'). In the following we use the symmetry relations expressed in eqs. (3.9) and (3.10).

First the azeotrope line [2] is obtained by solving the set of equations

$$
\begin{aligned}
\mu_i(\rho, x = 1/2, T) &\equiv \mu(\rho, x = 1/2, T) = \mu(\rho', x = 1/2, T) \\
P(\rho, x = 1/2, T) &= P(\rho', x = 1/2, T). & (3.13)
\end{aligned}
$$

For the V-MF and the MF-DF transitions we proceed in two steps. First we determine the phase diagram of the demixing transition, i.e. we search for two coexisting states with concentrations x and $x' = 1 - x$. Due to the symmetry eq. (3.10) $\rho' = \rho$ and due to eq. (3.9) equations (3.11) reduce to solving at a given temperature T and density ρ the equation

$$
\mu_1(\rho, x, T) = \mu_2(\rho, x, T), \tag{3.14}
$$

---

[2]It follows from the van der Waals study of [38] (see eq. (21) of this reference) that an azeotropic behavior in a binary symmetric mixture can only appear at $x = \frac{1}{2}$.

which defines the line $x(\rho)$ of the second order demixing transition - if it exists. Along this line the chemical potentials of the two species are equal by construction and denoted by $\mu(\rho, x(\rho), T)$. In a second step the solution of the two equations,

$$\mu(\rho, x = 1/2, T) \;=\; \mu(\rho', x(\rho'), T) \tag{3.15}$$

$$P(\rho, x = 1/2, T) \;=\; P(\rho', x(\rho'), T) \tag{3.16}$$

gives the density of the V or MF, ρ, and that of the DF, ρ', with concentrations $x(\rho')$ and $1 - x(\rho')$, in equilibrium.

Part II

Bulk Fluids

Chapter 4

Self Consistent Liquid-State Methods

4.1 Introduction

As was pointed out already in Chapter 2.1.1 integral equation and perturbation theories suffer from a lack of thermodynamic consistency: that is, different routes to thermodynamics yield different results. Thus several integral equation theories have been modified in such a way that consistency between different routes is enforced.

One of these approaches is the generalized mean spherical approximation (GMSA) which is an extension of the MSA. It was introduced by Waisman [42] to improve the PY solution of hard spheres. He modified the PY ansatz $c(r) = 0$ for $r > \sigma$, by assuming a form of a Yukawa tail for $c(r)$ outside the HC, i.e.

$$c(r) = \frac{K}{r} e^{-z(r-\sigma)} \quad \text{for} \quad r > \sigma. \tag{4.1}$$

Waisman derived an analytic solution of the OZ equation supplemented by the exact core condition and the closure relation (4.1). Based on this analytic solution he chose the parameters K and z in order to fit the thermodynamics of this model to computer simulation data, parameterized in terms of the Carnahan Starling (CS) equation of state [43]. The radial distribution function so obtained considerably improved the PY one. Waisman's analytic solution was extended by Høye and Stell [44] to the case when the direct correlation function is a linear combination of two Yukawa tails.

$$c(r) = \frac{A_1}{r} e^{-z_1(r-\sigma)} + \frac{A_2}{r} e^{-z_2(r-\sigma)} \quad \text{for} \quad r > \sigma. \tag{4.2}$$

If one interprets the first Yukawa term as corresponding to the MSA closure relation for $c(r)$ outside the core for a system with the pair potential $\beta\phi(r) = -\frac{A_1}{r}e^{-z_1(r-\sigma)}$ then the second term can be viewed as a correction term as in the Waisman parameterization of $c(r)$ for hard spheres. Again there are two parameters A_2 and z_2 available either to fit thermodynamically consistent quantities, as given by computer simulation, or to satisfy the thermodynamic self-consistency relation without any further thermodynamic input. So this is a possibility to improve the MSA whose main deficiency is the substantial lack of thermodynamic consistency while retaining its great advantage of analytic solubility for hard-core Yukawa (HCY) systems.

A similar GMSA scheme was developed by Stell *et al.* for ionic and dipolar fluids [45]: There it was called a self-consistent Ornstein Zernike approximation (SCOZA) since self-consistency among the three thermodynamic routes (i.e. virial, energy and compressibility route) was enforced. However, in contrast to the SCOZA in its present version that we will introduce below, thermodynamic consistency was achieved by fitting the available GMSA parameters to some external set of data either given by a prescribed equation of state or obtained from computer simulations. In contrast, in the SCOZA with which we will be concerned below no supplementary thermodynamic or other input is necessary. Thus this scheme is entirely self-contained.

The thermodynamic consistency relations can be expressed in the form

$$\frac{\beta P_V}{\rho} = \frac{\beta P_C}{\rho} \tag{4.3}$$

$$\frac{\beta P_V}{\rho} = \frac{\beta P_E}{\rho}. \tag{4.4}$$

However, in most applications of liquid-state theories the first consistency relation is rather expressed as

$$\left(\frac{\beta \partial P_V}{\partial \rho}\right)_T = \frac{1}{\rho k_B T \chi_T}, \tag{4.5}$$

where χ_T is the isothermal compressibility obtained from the compressibility route. This is done in thermodynamically self-consistent integral equation approaches, like e.g. the modified hypernetted-chain (MHNC) theory [46]. In this approach the OZ relation is solved with the closure relation

$$g(r) = e^{-\beta\phi(r)+h(r)-c(r)+E(r)}, \tag{4.6}$$

where the bridge function $E(r)$ is approximated by that of a suitably chosen HS reference system assuming the universality hypothesis of the bridge functions [46]. The $E(r)$ are either obtained from the Verlet-Weis parameterization of the pair distribution function or,

alternatively, by the PY bridge function. The HS diameter is chosen to enforce equality of the compressibility via the virial and the compressibility route (4.5).

Other thermodynamic self-consistent closure relations use so called 'mixed closure' relations, i.e. they interpolate in a functional form between two different conventional closure relations. In this interpolation scheme a mixing function $f_\alpha(r)$ with an adjustable parameter α is introduced that is chosen so that consistency is enforced. One of these approaches is the Rogers Young (RY) approximation [47] that interpolates between the PY and the HNC approximation. Its closure is given by

$$g(r) = e^{-\beta\phi(r)} \left(1 + \frac{e^{f_\alpha(r)[h(r)-c(r)]} - 1}{f_\alpha(r)} \right). \tag{4.7}$$

An appropriate form for f_α would be e.g. $f_\alpha(r) = 1 - e^{-\alpha r}$, i.e. for $r = 0$ the PY solution is obtained that is more appropriate for short-ranged forces, while in the limit $r \to \infty$ one obtains the HNC closure that is accurate for long-ranged potentials and uses the approximation that $E(r) = 0$. The RY approximation yields excellent results for purely repulsive systems.

Another self-consistent 'mixed closure' integral equation theory is the HMSA [48], that interpolates between the HNC and the SMSA and is more suitable for systems with attractive potential than the RY approximation. Its closure is given by

$$g(r) = e^{-\beta\phi_R(r)} \left(1 + \frac{e^{f_\alpha(r)[h(r)-c(r)-\phi_A(r)]} - 1}{f_\alpha(r)} \right), \tag{4.8}$$

where

$$\phi_R(r) = \begin{cases} \phi(r) - \phi(r_m) & r \leq r_m \\ 0 & r > r_m \end{cases} \tag{4.9}$$

is the repulsive part of the potential and

$$\phi_A(r) = \begin{cases} \phi(r_m) & r \leq r_m \\ \phi(r) & r > r_m \end{cases} \tag{4.10}$$

the attractive one; r_m denotes a suitably chosen separation distance, in general it is the position of the minimum of the potential. For the mixing function $f_\alpha(r)$ one can assume a function as the one used above. In both approaches the parameter α is varied until eq. (4.5) is satisfied.

The MHNC, GMSA, and HMSA yield accurate thermodynamics and predict accurately the liquid and vapor branches of the coexistence curves [9, 49], but they fail to converge close to the critical point, leaving the two branches unconnected [50] and estimates for the critical point parameters can only be obtained by extrapolation.

The two probably most promising approaches at the moment that circumvent these problems are the hierarchical reference theory (HRT) [7] and the thermodynamically self-consistent Ornstein Zernike approach (SCOZA) both of them providing very accurate predictions for the thermodynamics, the phase diagrams and the critical behavior. Especially in the critical region, where the accuracy of integral equation theories and perturbation theories decreases dramatically (they do not succeed in reproducing the shape of the coexistence curve and the location of the critical points correctly) or their solution fails, both theories remain highly accurate and successful.

The SCOZA was proposed already some time ago by Høye and Stell [51, 52], but it was only recently that it could be solved numerically for a model system and results of remarkable accuracy were obtained [8].

The theory has been formulated in different versions, all of them building directly upon the MSA closure and combining it with the requirement of thermodynamic consistency [6] thus removing the main deficiency of the MSA. In the different versions one or more state dependent functions are introduced in the MSA relation between $c(r)$ and $-\beta\phi(r)$; and this (or these) function(s) is (are) determined in such a way that thermodynamic consistency via different thermodynamic routes is ensured, thus leading to (a) partial differential equation(s) (PDE) for this (these) parameter(s). The various versions of the SCOZA differ in the choice of these adjustable parameters.

The most comprehensive concept of this theory proposed in [51, 52] ensures self-consistency between the virial, the energy as well as the compressibility route. Due to the complexity its numerical solution was implemented for a hard-core one-Yukawa fluid (HC1Y) only recently by Caccamo *et al.* [49]. (In their contribution this version of the SCOZA is actually called GMSA[1], while the designation SCOZA therein refers to another version of the SCOZA.) In this contribution the closure relation to the OZ equation is

$$
\begin{aligned}
g(r) &= 0 && \text{for} \quad r < \sigma \\
c(r) &= -\beta\phi(r) + K\frac{e^{-z(r-\sigma)}}{r} && \text{for} \quad r > \sigma,
\end{aligned}
\tag{4.11}
$$

where σ is again the HC diameter and K and z are adjustable state-dependent parameters to ensure thermodynamic consistency. The numerical solution of this approximation was not obtained by solving a PDE but through an iterative procedure.

The version of the SCOZA with which we will be concerned in the following contains only one state dependent function $A(\rho,\beta)$ which appears as a proportionality factor

---

[1]The term GMSA comprises a family of approximations, all of which have the common feature of supplementing the $-\beta\phi(r)$ term in the direct correlation function with additional Yukawa terms. The amplitudes and ranges of these Yukawa terms are adjusted to yield thermodynamic self-consistency.

between $\phi(r)$ and the direct correlation function $c(r)$ outside the core, and enforces consistency only between the compressibility and the energy route. This closure relation amounts to setting

$$
\begin{aligned}
g(r) &= 0 &&\text{for} \quad r < \sigma \\
c(r) &= A(\rho, \beta)\phi(r) &&\text{for} \quad r > \sigma,
\end{aligned} \tag{4.12}
$$

where $A(\rho, \beta)$ is a function of the thermodynamic state (ρ, β). The condition on $g(r)$, the so-called core condition, is exact, while the expression for $c(r)$ is an approximation and implies that $c(r)$ has the same range as the potential - an ansatz that is usually referred to as the OZ approximation, thus the name self-consistent Ornstein Zernike approximation. In contrast to the MSA, where $A(\rho, \beta) = -\beta$, here $A(\rho, \beta)$ is not fixed a priori but is instead determined so that thermodynamic consistency is ensured between the compressibility and the energy route. The advantage of this simple recipe is that the solution of the OZ equation together with the closure relation (4.12) is the same as for the MSA problem.

This scheme of the SCOZA was already proposed in [52] where equations for solving the self-consistency problem were derived. Preliminary results for a three dimensional lattice gas for supercritical temperatures indicated that SCOZA could produce accurate results [53]. However, results were limited to supercritical temperatures since the numerical solution of the SCOZA PDE of [52] was found to be unstable when proceeding to temperatures below the critical point.

The first numerical results below T_c were obtained by Dickman and Stell for a three-dimensional nearest neighbor lattice gas [8]. In contrast to the original (numerically unstable) PDE used in [52], where the Helmholtz free energy was used as the quantity to solve for, these authors have used the following PDE as basis for the SCOZA equation: assuming that the thermodynamics stems from a unique Helmholtz free energy the consistency condition can be expressed as

$$
\frac{\partial}{\partial \beta}\left(\frac{1}{\chi^{red}}\right) = \rho \frac{\partial^2 u}{\partial \rho^2}, \tag{4.13}
$$

where $\chi^{red} = \rho k_B T \chi_T$ is the reduced isothermal compressibility given by the fluctuation theorem and $u = \frac{U^{ex}}{V}$ is the excess (over ideal) internal energy per volume given by the energy equation. Eq. (4.13) supplemented by the closure relation eq. (4.12) and the OZ relation yields a PDE for $A(\rho, \beta)$. Using the analytic structure of the solution of the OZ equation with the closure relation (4.12) for the system they investigated, Dickman and Stell were able to express $1/\chi^{red}$ in closed form in terms of u and to derive a PDE of diffusion type for $1/\chi^{red}$. The numerical solution procedure of this PDE was refined

in subsequent work by Pini *et al.* [54]. Pini developed an unconditionally, accurate and efficient solution algorithm, using his experience from previous work on the HRT: although this theory, that is based on renormalization group, is conceptually different from the SCOZA(for an overview see [7]), it also results in the numerical problem of solving a non-linear PDE of diffusion type.

In [8] Dickman and Stell considered the lattice gas (or the equivalent Ising model) in three dimensions with nearest neighbor interactions on various cubic lattices. The predictions were remarkably accurate, e.g. the values of T_c were obtained within 0.2% of best estimates and other critical properties agreed within 1-2% of the best numerical estimates. Also the various effective critical exponents, that are defined as the slopes of curves of logarithmic plots, e.g.

$$\gamma^{\text{eff}} = \frac{d \log \chi_T^{-1}}{d \log t},$$ (4.14)

where $t = \frac{T-T_c}{T_c}$, were investigated, and it was found that they were close to the estimated exact form unless very close to the critical point. Further numerical results for the three-dimensional lattice gas by Borge and Høye [55] and Pini *et al.* [54] confirmed this picture: above the critical temperature the theory yields the same critical exponents as the spherical model but this regime is very narrow, so that thermodynamics and effective exponents are in good agreement with the true critical behavior until the temperature differs from its critical value by less than 1%. On the coexistence curve (i.e. below T_c), on the other hand, the exponents are neither spherical nor classical and turn out to be very accurate: e.g. the curvature of the coexistence curve is described by $\beta = 0.35$ which is near to the exact value of $\beta \sim 0.326$ [56]. Borge and Høye [55] also investigated the influence of the interaction range and they found that the effective critical exponents away from the critical point vary with this range.

An analytic study of the SCOZA critical exponents and the scaling behavior in three dimensions was given by Høye *et al.* [57]. It was seen that standard scaling is not fulfilled, but rather a generalized form of scaling. In this study the SCOZA subcritical exponents for a three-dimensional system were determined to be

$$\beta = 7/20, \gamma = 7/5, \alpha = -1/10,$$ (4.15)

which are in remarkable agreement with the exact values $\beta \sim 0.326, \gamma \sim 1.24, \alpha \sim 0.11$ [56], despite the fact that SCOZA does not incorporate renormalization group ideas. On the other hand, the supercritical exponents are spherical ones

$$\gamma = 2, \delta = 5, \alpha = 0,$$ (4.16)

so the indices above do not fulfill the standard scaling relations. Thus, SCOZA fails in a very narrow regime of $|t| < 10^{-3}$ in the vicinity of the critical point which is also the error in T_c for the Ising model. However, outside this region results turn out to be very accurate.

After the first applications of the SCOZA to lattice systems, it was extended subsequently to continuum systems, too [58, 59, 60, 61]. In particular, in the case when u in eq. (4.13) can be written in closed form as a function of χ^{red} within the closure relation (4.12) the numerical solution of the SCOZA is substantially simplified leading to a PDE for u. This is actually the case for the HCY fluid, where one can make use of the extensive semi-analytic MSA studies available. So it is not surprising that the SCOZA for continuum fluids has been solved numerically up to now only for the hard-core 1-Yukawa (HC1Y) [58, 59] and hard-core 2-Yukawa (HC2Y) fluid [60, 61]. The general case has to be solved fully numerically.

In [58] the accuracy of the SCOZA approach remained somewhat unclear due to the uncertainty of the available simulation results. But it was already seen that the top of the coexistence curve was flattening, having a shape that is similar to the one of real fluids. In this paper the closure relation of eq. (4.12) was used, implying that the HS contribution to $c(r)$ vanishes outside the core, so that the treatment of the HS reference system coincides with the Percus-Yevick approximation. Alternatively, these authors also incorporated a more accurate HS theory by using a Yukawa tail that is non zero at $\beta = 0$ to reproduce the CS equation of state.

In subsequent work [59] the treatment of the HS reference part was improved by adding to $c(r)$ in (4.12) a non-vanishing contribution $c_{\mathrm{HS}}(r)$ outside the core. However, the Verlet-Weis parameterization [62] of $c_{\mathrm{HS}}(r)$, which is the most popular parameterization for the HS structure functions reproducing with high accuracy simulation data, is not convenient for the formulation of the analytic part of the SCOZA. Instead the Waisman parameterization was used, where the function $c_{\mathrm{HS}}(r)$ outside the core is assumed to have a one-Yukawa form

$$\begin{aligned} g(r) &= 0 && \text{for} \quad r < \sigma \\ c(r) &= A(\rho, \beta)\phi(r) + K_{\mathrm{HS}}\frac{e^{-z_{\mathrm{HS}}(r-\sigma)}}{r} && \text{for} \quad r > \sigma; \end{aligned} \qquad (4.17)$$

the amplitude K_{HS} and range z_{HS} are determined in such a way to reproduce CS thermodynamics. The reason why one chooses the Waisman parameterization for the HS part of the direct correlation function is a purely technical one: the mathematical formulation of the SCOZA for a $c(r)$ of 2-Yukawa form is still convenient since analytic studies for the case when $c(r)$ is a linear combination of two Yukawas [44, 63, 52] are available.

These two approaches for the HS part - the two Yukawa $c(r)$ and the one Yukawa $c(r)$ that reproduces CS behavior at $\beta = 0$ - were found to make little difference. In [59] also a new set of simulations was performed to check the SCOZA results and again the accuracy of the thermodynamics, the critical data and the coexistence curve was remarkable: the critical temperature and density predicted by SCOZA agreed with simulation results to about 0.6 %. Another application of the 2-Yukawa version of the SCOZA is to take both Yukawa terms to represent the interaction. This was actually done in order to parameterize a Lennard Jones (LJ) fluid mimicked by a hard-core two Yukawa interaction [60] and, furthermore, to investigate the effect of competing interactions on the liquid-vapor transition [61]. In the latter study the 2-Yukawa tail was assumed to be attractive at short distance and repulsive at long distance.

Since results for the three-dimensional lattice gas and the HC Yukawa fluid have confirmed that the SCOZA remains highly accurate even in the critical region, it was of interest to develop the SCOZA for other fluid and lattice gas systems and to test its general accuracy more precisely in various situations. Work in this direction has been done: the formulation of the SCOZA has been generalized to D-dimensional and continuous spins [64]. However, so far numerical results are not available. As a further test of its accuracy the SCOZA was compared with exact results for the Ising model in one and two dimension [65, 66]. In the latter case comparison with the exact Onsager solution in zero magnetic field with nearest neighbor interaction was made. A special feature in this case is that SCOZA as the MSA does not give a true phase transition in two dimensions, i.e. the singularities are smeared out. This deficiency of the SCOZA is due to the Ornstein Zernike ansatz which does not include a long-range part of the direct correlation function that would be necessary in the critical region. According to this approximation the critical exponent η is found to be 0 instead of the exact value of $\eta \sim 0.006$ in three dimensions; thus the behavior of the total correlation function is distorted which decays as $h(r) \sim f(r/\xi)/r^{d-2+\eta}$ for $r \gg 1$, where d is the dimension and ξ the correlation length. However this deficiency is only crucial in the vicinity of the critical point, where $f(r/\xi)$ is constant rather than exponentially decaying. Despite this deficiency, also in the two-dimensional case numerical results were again convincing. The temperature where the specific heat has a maximum was found almost precisely at the exact critical point temperature.

Good results have also been obtained when generalizing the SCOZA to a disordered system like the site diluted random field Ising model [67], and it has recently been applied to the spin-1 model [68] and the q-state Potts model [69]. Furthermore a binary mixture model has been studied within the SCOZA by A. Dickman and Stell [70]: the decorated

model, that is isomorphic to the lattice gas model.

The purpose of the work presented in this chapter is to extend the SCOZA to a larger class of continuum fluids. First, we have generalized the SCOZA to a one-component fluid with hard-core multi-Yukawa interaction. The theoretical formulation is given in section 4.2.1. The advantage of this generalization is the opportunity that several realistic interactions can be approximated very accurately by a linear combination of Yukawa tails, like the LJ potential or the short ranged Girifalco potential that describes the interaction between C_{60} molecules. Results for the LJ fluid are presented in section 4.2.2 and for fullerenes in section 4.2.3. We have further discovered the existence of two critical points in a hard-core Yukawa fluid whose interaction range is density-dependent; these results are summarized in section 4.2.4. Further the SCOZA was generalized to the binary symmetric mixture.

4.2 SCOZA for a One-Component Fluid

In our investigations we have chosen the version of the SCOZA proposed recently by Pini *et al.* [59] given by the closure relation eq. (4.17). For the interaction between the particles these authors have chosen a hard-core Yukawa (HCY) pair potential which has been of interest in the last years [9, 49] due to several reasons: *first*, for this simple model one has available semi-analytic theories [42, 71, 44, 63, 52, 24]. Thus the formulation of the MSA, the GMSA and the SCOZA is particularly simplified for the HCY fluid. This is not the case for other pair potentials like the square well fluid where the solution has to be obtained fully numerically. *Second*, this simple potential comprises the two key features that mimic a more realistic potential: a highly repulsive core and an attractive tail. The latter is required to observe first order liquid-gas phase transitions and liquid-gas criticality. *Third*, the potential parameters can be chosen so as to provide more realistic potentials like a solvent-averaged interaction potential between poly-electric or colloidal particles. Furthermore, the HCY potential comprises as special limiting cases the adhesive HS system [27] (when the Yukawa tail is infinitely deep and the screening length infinitely large) and charged HSs (when the screening length z is set to 0).

However, the HCY potential fails to mimic realistic interactions, the strength of the attractive tail being largest at the infinitely high hard-core repulsion. The LJ interaction on the other hand represents a smoother, more realistic potential, but is less convenient for the study by the SCOZA than is the HCY fluid. Nevertheless one can retain the mathematical conveniences of the HCY fluid while studying a more realistic interaction

by making use of the fact that the LJ tail may be very well approximated by a linear combination of two (or more) Yukawa tails [72]. If the hard-sphere reference system is treated in the Waisman approximation by an additional Yukawa tail as in eq. (4.17) this requires the solution of the OZ equation with a direct correlation function $c(r)$ of a three (or more) Yukawa form outside the core.

The OZ equation along with the MSA closure (i.e., the core condition for the pair distribution function and a direct correlation function that is of Yukawa form outside the core) has been solved semi-analytically via two different approaches. Waisman [42] has used the so called Laplace transform technique [73]. His solution for a one-Yukawa form of $c(r)$ was simplified in subsequent work [71] and generalized to the case when $c(r)$ is a linear combination of two Yukawas by Høye and Stell [44, 63, 52]. The other approach was introduced by Høye and Blum [24]. It applies a method of Baxter [74] which is based on the Wiener-Hopf factorization of the Fourier transforms of the direct correlation functions by introducing so called factor functions. In this approach the generalization of the solution from a one-Yukawa tail to the multi-Yukawa form of the direct correlation function is straightforward and considerably easier than for the Laplace transform route.

While the formulation of the SCOZA for a one-Yukawa fluid presented in [58, 59] is based on the first approach, we found it more convenient to use the latter approach for the case when the interaction potential is a linear combination of three or more Yukawa tails. In their analysis Høye and Blum reformulated the problem as a system of nonlinear equations for the coefficients of the factor functions. For the most general case of multi-component, multi-Yukawa fluid mixtures Arrieta *et al.* [75] have cast these equations into a form suitable and more convenient for numerical calculations and provided a general, direct solution algorithm. We refer to the expressions presented in their contribution (omitting in the subsect. 4.2.1 the latin indices in the formulas which denote the components of a multi-component mixture); at the beginning we briefly summarize analytic results relevant for our formulation of the SCOZA.

4.2.1 Formulation of the Theory

Following Baxter's factorization method it can be shown that under certain conditions [76] the OZ relation is equivalent to the equations

$$2\pi r c(r) = -Q'(r) + \rho \int_0^\infty Q(t)Q'(r+t)dt \qquad (4.18)$$

$$2\pi r h(r) = -Q'(r) + 2\pi\rho \int_0^\infty (r-t)h(|r-t|)Q(t)dt,$$

where the factor function $Q(r)$ has been introduced. From eqs. (4.18) and from the closure relation

$$
\begin{aligned}
h(r) &= -1 & r < \sigma \\
c(r) &= \sum_{\nu=1}^{n} \widetilde{K}_{\nu} \frac{e^{-z_{\nu}(r-\sigma)}}{r} & r > \sigma,
\end{aligned}
\tag{4.19}
$$

it follows that $Q(r)$ must have the form

$$
Q(r) = Q^0(r) + \sum_{\nu=1}^{n} \frac{1}{z_{\nu}} D_{\nu} e^{-z_{\nu}(r-\sigma)},
\tag{4.20}
$$

where

$$
Q^0(r) = \begin{cases} \frac{a}{2}(r-\sigma)^2 + b(r-\sigma) + \sum_{\nu=1}^{n} \frac{1}{z_{\nu}} C_{\nu} \left(e^{-z_{\nu}(r-\sigma)} - 1 \right) & 0 < r < \sigma \\ 0 & \sigma < r \end{cases},
\tag{4.21}
$$

with yet undetermined coefficients a, b, C_{ν} and D_{ν}.

One further introduces the quantities

$$
G_{\nu} = z_{\nu} \hat{g}(z_{\nu}) e^{z_{\nu}\sigma} = z_{\nu} \int_{\sigma}^{\infty} r e^{-z_{\nu}(r-\sigma)} g(r) dr,
\tag{4.22}
$$

where $\hat{g}(z)$ denotes the Laplace transform of $rg(r)$. Inserting the form of $Q(r)$ in eqs. (4.18) and using the closure relation (4.19) permits to express the unknown variables a, b, C_{ν} as functions of D_{ν} and G_{ν} and to derive a system of $2n$ nonlinear equations for the $2n$ unknowns G_{ν} and D_{ν}

$$
\sum_{\tau=1}^{n} A_{\tau\nu}^{(1)} G_{\tau} D_{\tau} D_{\nu} + \sum_{\tau=1}^{n} A_{\tau\nu}^{(2)} D_{\tau} D_{\nu} + A_{\nu}^{(3)} D_{\nu} + A_{\nu}^{(4)} = 0 \quad \nu = 1, \ldots, n
\tag{4.23}
$$

$$
\sum_{\tau=1}^{n} B_{\tau\nu}^{(1)} G_{\tau} D_{\tau} G_{\nu} + \sum_{\tau=1}^{n} B_{\tau\nu}^{(2)} G_{\tau} D_{\tau}
$$

$$
+ \sum_{\tau=1}^{n} B_{\tau\nu}^{(3)} D_{\tau} G_{\nu} + \sum_{\tau=1}^{n} B_{\tau\nu}^{(4)} D_{\tau} + B_{\nu}^{(5)} G_{\nu} + B_{\nu}^{(6)} = 0 \quad \nu = 1, \ldots, n,
\tag{4.24}
$$

where

$$
A_{\nu}^{(4)} = 2\pi \widetilde{K}_{\nu},
\tag{4.25}
$$

while the remaining coefficients $A^{(\gamma)}$ and $B^{(\gamma)}$ are temperature independent. Their explicit expressions are given in Appendix A of [75]. They are calculated from the system parameters ρ, z_{ν}, and σ.

The inverse reduced isothermal compressibility calculated via the fluctuation theorem is found to be

$$
\frac{1}{\chi^{red}} = 1 - \rho \tilde{c}(k=0) = \left(\frac{a}{2\pi} \right)^2,
\tag{4.26}
$$

where $\tilde{c}(k)$ denotes the Fourier transform of $c(r)$. The expression for a in terms of the quantities G_ν and D_ν is obtained from

$$a = A^0(1 + M) - \frac{4}{\sigma^2}B^0 N \tag{4.27}$$

with

$$
\begin{aligned}
M &= -\sum_{\tau=1}^{n} \frac{1}{z_\tau^2}\rho \left\{ M_\tau^{(a)} D_\tau + (1 - M_\tau^{(a)} e^{-z_\tau \sigma}) f_\tau \right\} \\
N &= \sum_{\tau=1}^{n} \frac{1}{z_\tau^3}\rho \left\{ L_\tau^{(a)} D_\tau + (1 - L_\tau^{(a)} e^{-z_\tau \sigma}) f_\tau \right\} \\
f_\tau &= \frac{2\pi}{z_\tau^2}\rho G_\tau D_\tau,
\end{aligned}
\tag{4.28}
$$

where the quantities $M_\tau^{(a)}, L_\tau^{(a)}, A^0$ and B^0 are again calculated from ρ, z_ν and σ and are compiled in Appendix A of [75].

The second system of equations (4.24) is linear in $\mathbf{D} = (D_1, \ldots, D_n)$ for given $\mathbf{G} = (G_1, \ldots, G_n)$ and can be rewritten as

$$\sum_{\tau=1}^{n} O_{\nu\tau} D_\tau = Q_\nu \tag{4.29}$$

with

$$O_{\nu\tau}(\rho, \mathbf{G}) = B_{\tau\nu}^{(1)} G_\tau G_\nu + B_{\tau\nu}^{(2)} G_\tau + B_{\tau\nu}^{(3)} G_\nu + B_{\tau\nu}^{(4)} \tag{4.30}$$

and

$$Q_\nu(\rho, \mathbf{G}) = -B_\nu^{(5)} G_\nu - B_\nu^{(6)}. \tag{4.31}$$

Solution of this system of n linear equations yields $\mathbf{D}(\rho, \mathbf{G})$. This result can then be inserted into (4.23) which becomes a set of n coupled nonlinear equations in the $\mathbf{G}$.

We now consider a fluid of particles interacting via a spherically symmetric pair potential $\phi(r)$ given by

$$\phi(r) = \begin{cases} +\infty & r < 1 \\ w(r) & r > 1 \end{cases}, \tag{4.32}$$

where the hard-sphere diameter σ has been set to unity and the attractive tail $w(r) < 0$ is given by a linear combination of Yukawa tails

$$w(r) = -\epsilon \sum_{\nu=2}^{n} c_\nu \frac{e^{-z_\nu(r-1)}}{r}. \tag{4.33}$$

We enforce consistency between the compressibility and energy route to the thermodynamic properties. The reduced isothermal compressibility via the compressibility route is

given by (4.26). On the other hand the excess (over ideal) internal energy per unit volume calculated via the internal energy route is found to be

$$\frac{U^{ex}}{V} = u = 2\pi\rho^2 \int_1^\infty dr\, r^2 w(r) g(r) \tag{4.34}$$

$$= -2\pi\rho^2 \epsilon \sum_{\nu=2}^n c_\nu \frac{G_\nu}{z_\nu}.$$

Both χ^{red} and u are related to the Helmholtz free energy density $\frac{F}{V} = f = f^{id} + f^{ex}$, where f^{id} and f^{ex} are the ideal and excess parts of the free energy density. Thus

$$\rho \frac{\partial^2 u}{\partial \rho^2} = \rho \frac{\partial^2}{\partial \rho^2} \frac{\partial \beta f^{ex}}{\partial \beta} = \frac{\partial}{\partial \beta}\left(\rho \frac{\partial \beta \mu^{ex}}{\partial \rho}\right) = \frac{\partial}{\partial \beta}\left(\frac{1}{\chi^{red}}\right), \tag{4.35}$$

where $\mu^{ex} = \frac{\partial f^{ex}}{\partial \rho}$ is the excess chemical potential. In general eq. (4.35) is not fulfilled for approximate $g(r)$ as obtained, for instance, by conventional integral equation and perturbation theories [4]. In the approach considered here this consistency is enforced.

The OZ equation together with the thermodynamic consistency relation eq. (4.35) is supplemented with the following closure relation

$$\begin{aligned} g(r) &= 0 & \text{for} \quad r < 1 \\ c(r) &= c_{\text{HS}}(r) + K(\rho, \beta) w(r) & \text{for} \quad r > 1, \end{aligned} \tag{4.36}$$

where $K(\rho, \beta)$ is a function of the thermodynamic state. The closure resembles to the one used in the LOGA/ORPA where $K(\rho, \beta) = -\beta$ is fixed. Here, $K(\rho, \beta)$ is not given a priori but is determined so that thermodynamic self-consistency is obtained between the compressibility and the energy route. Using the semi-analytic formalism (outlined above) this consistency requirement leads to a PDE for u. This will be shown in the following.

For mathematical conveniences we choose the Waisman parameterization for $c_{\text{HS}}(r)$ [42, 71] which ensures a highly self-consistent description of the thermodynamic properties of the HS part. It assumes a Yukawa form for $c_{\text{HS}}(r)$ outside the hard-core

$$c_{\text{HS}}(r) = K_1(\rho) \frac{e^{-z_1(\rho)(r-1)}}{r} \quad \text{for} \quad r > 1 \tag{4.37}$$

where $K_1(\rho)$ and $z_1(\rho)$ are known functions of the density (see Appendix A of [59]). These expressions guarantee that both compressibility and virial route yield the CS equation of state [43] for HS. Using eqs. (4.33, 4.37), eq. (4.36) becomes

$$\begin{aligned} g(r) &= 0 & \text{for} \quad r < 1 \\ c(r) &= K_1(\rho)\frac{e^{-z_1(\rho)(r-1)}}{r} - K(\rho, \beta)\epsilon \sum_{\nu=2}^n c_\nu \frac{e^{-z_\nu(r-1)}}{r} & \text{for} \quad r > 1. \end{aligned} \tag{4.38}$$

We use now the analytic results presented above to derive a relation between χ^{red} and u, leading to a PDE for u. Using eq. (4.26), eq. (4.35) yields

$$2\frac{a}{(2\pi)^2}\frac{\partial a}{\partial u}\frac{\partial u}{\partial \beta} = \rho\frac{\partial^2 u}{\partial \rho^2}. \tag{4.39}$$

a is given by eqs. (4.27, 4.28) as a function of $\mathbf{D}$ and $\mathbf{G}$; inserting the solution $\mathbf{D}(\rho, \mathbf{G})$ of the linear system eq. (4.29) yields $a(\rho, \mathbf{G})$ and thus

$$2\frac{a}{(2\pi)^2}\left(\sum_{\nu=1}^{n}\frac{\partial a}{\partial G_\nu}\frac{\partial G_\nu}{\partial u}\right)\frac{\partial u}{\partial \beta} = \rho\frac{\partial^2 u}{\partial \rho^2} \tag{4.40}$$

or

$$B(\rho, u)\frac{\partial u}{\partial \beta} = C(\rho)\frac{\partial^2 u}{\partial \rho^2}, \tag{4.41}$$

once that a, $\frac{\partial a}{\partial G_\nu}$ and $\frac{\partial G_\nu}{\partial u}$ have been determined as functions of ρ and u (see below). B and C are given by

$$\begin{aligned} B(\rho, u) &= 2\frac{a}{(2\pi)^2}\sum_{\nu=1}^{n}\frac{\partial a}{\partial G_\nu}\frac{\partial G_\nu}{\partial u} \\ C(\rho) &= \rho. \end{aligned} \tag{4.42}$$

Thus we now have derived a PDE for $u(\rho, \beta)$.

What remains is to determine a, $\frac{\partial a}{\partial G_\nu}$ and $\frac{\partial G_\nu}{\partial u}$ as functions of ρ and u. First of all we introduce n nonlinear equations $F_i(\rho, u, \mathbf{G}) = 0$. Their solution gives $G_\nu(\rho, u)$. The first equation is linear and is the energy equation (4.34)

$$u + 2\pi\rho^2\epsilon\sum_{\nu=2}^{n}c_\nu\frac{G_\nu}{z_\nu} = 0 \tag{4.43}$$

or formally written as

$$F_1(\rho, u, G_2, \ldots, G_n) = 0. \tag{4.44}$$

To establish the remaining $n-1$ nonlinear equations we make use of eqs. (4.23 – 4.25). Expressions for the $\widetilde{K}_\nu$ in eq. (4.25) are obtained by comparison of eq. (4.19) with the closure relation (4.38)

$$\begin{aligned} \widetilde{K}_1 &= K_1(\rho) \\ \widetilde{K}_\nu &= -K(\rho, \beta)\epsilon c_\nu \quad \text{for} \quad \nu = 2, \ldots, n \end{aligned} \tag{4.45}$$

and thus

$$\begin{aligned} A_1^{(4)} &= 2\pi K_1(\rho) \tag{4.46} \\ A_\nu^{(4)}c_\mu &= A_\mu^{(4)}c_\nu \quad \text{for} \quad \nu, \mu = 2, \ldots, n. \tag{4.47} \end{aligned}$$

The second nonlinear equation is relation (4.23) for $\nu = 1$ with the solution $\mathbf{D}(\rho, \mathbf{G})$ of eq. (4.29), inserting relation (4.46)

$$\sum_{\tau=1}^{n} A_{\tau 1}^{(1)} G_\tau D_\tau(\rho, \mathbf{G}) D_1(\rho, \mathbf{G}) + \sum_{\tau=1}^{n} A_{\tau 1}^{(2)} D_\tau(\rho, \mathbf{G}) D_1(\rho, \mathbf{G})$$
$$+ A_1^{(3)} D_1(\rho, \mathbf{G}) + 2\pi K_1(\rho) = 0, \tag{4.48}$$

or, formally written as

$$F_2(\rho, \mathbf{G}) = 0. \tag{4.49}$$

Further equations are obtained from eq. (4.23) for $\nu > 1$, inserting $\mathbf{D}(\rho, \mathbf{G})$, the solution of eq. (4.29) and eliminating the unknown function $K(\rho, \beta)$ in the coefficients $A_\nu^{(4)}$ via the relations (4.47) (for $\nu = 2, \mu > 2$) i.e.,

$$\left\{ \sum_{\tau=1}^{n} A_{\tau 2}^{(1)} G_\tau D_\tau(\rho, \mathbf{G}) D_2(\rho, \mathbf{G}) + \sum_{\tau=1}^{n} A_{\tau 2}^{(2)} D_\tau(\rho, \mathbf{G}) D_2(\rho, \mathbf{G}) \right.$$
$$\left. + A_2^{(3)} D_2(\rho, \mathbf{G}) \right\} c_\mu -$$
$$\left\{ \sum_{\tau=1}^{n} A_{\tau \mu}^{(1)} G_\tau D_\tau(\rho, \mathbf{G}) D_\mu(\rho, \mathbf{G}) + \sum_{\tau=1}^{n} A_{\tau \mu}^{(2)} D_\tau(\rho, \mathbf{G}) D_\mu(\rho, \mathbf{G}) \right.$$
$$\left. + A_\mu^{(3)} D_\mu(\rho, \mathbf{G}) \right\} c_2 = 0$$
$$\text{for} \quad \mu = 3, \dots, n \tag{4.50}$$

or formally written as

$$F_3(\rho, \mathbf{G}) = 0$$
$$\vdots$$
$$F_n(\rho, \mathbf{G}) = 0. \tag{4.51}$$

For given ρ and u the $\mathbf{G}$ are determined in the following way: the coupled set of nonlinear equations (4.44, 4.49, 4.51) is solved numerically via a Newton-Raphson technique using explicit expressions for the Jacobian matrix $J = \left(\frac{\partial F_\mu}{\partial G_\nu} \right)$. In each step of the iteration the $\mathbf{D}$ are obtained by numerical solution of the linear system (4.24).

The analytic Jacobian matrix J is given by

$$J = \begin{pmatrix} 0 & 2\pi\rho^2 \frac{c_2}{z_2} & \dots & 2\pi\rho^2 \frac{c_n}{z_n} \\ \frac{\partial F_2}{\partial G_1} & \frac{\partial F_2}{\partial G_2} & \dots & \frac{\partial F_2}{\partial G_n} \\ \vdots & \vdots & & \vdots \\ \frac{\partial F_n}{\partial G_1} & \frac{\partial F_n}{\partial G_2} & \dots & \frac{\partial F_n}{\partial G_n} \end{pmatrix}, \tag{4.52}$$

where

$$
\begin{aligned}
\frac{\partial F_2}{\partial G_\mu}(\rho, \mathbf{G}) \;=\; & A_{\mu 1}^{(1)} D_\mu D_1 + \sum_{\tau=1}^{n} A_{\tau 1}^{(1)} G_\tau \left(\frac{\partial D_\tau}{\partial G_\mu} D_1 + D_\tau \frac{\partial D_1}{\partial G_\mu} \right) + \\
& \sum_{\tau=1}^{n} A_{\tau 1}^{(2)} \left(\frac{\partial D_\tau}{\partial G_\mu} D_1 + D_\tau \frac{\partial D_1}{\partial G_\mu} \right) + A_1^{(3)} \frac{\partial D_1}{\partial G_\mu}
\end{aligned}
\tag{4.53}
$$

and similar relations for the partial derivatives of the other nonlinear functions $F_3, \ldots, F_n$.

The partial derivatives $\frac{\partial D_\tau}{\partial G_\mu}(\rho, \mathbf{G})$ required in (4.53) are obtained by implicit differentiation of eq. (4.29)

$$
\begin{aligned}
\sum_{\tau=1}^{n} O_{\nu\tau} \frac{\partial D_\tau}{\partial G_\mu}(\rho, \mathbf{G}) \;=\; & \frac{\partial Q_\nu}{\partial G_\mu} - \sum_{\tau=1}^{n} \frac{\partial O_{\nu\tau}}{\partial G_\mu} D_\tau \tag{4.54} \\
\;=\; & -\left(B_{\mu\nu}^{(1)} G_\nu + B_{\mu\nu}^{(2)} \right) D_\mu(\rho, \mathbf{G}) \tag{4.55} \\
& -\left\{ \sum_{\tau=1}^{n} \left(B_{\tau\nu}^{(1)} G_\tau + B_{\tau\nu}^{(3)} \right) D_\tau(\rho, \mathbf{G}) + B_\nu^{(5)} \right\} \delta_{\mu\nu}.
\end{aligned}
$$

$\delta_{\mu\nu}$ denotes the Kronecker delta given by

$$
\delta_{\mu\nu} = \begin{cases} 1 & \text{for} \quad \mu = \nu \\ 0 & \text{otherwise} \end{cases}.
\tag{4.56}
$$

Solution of the nonlinear equations via the procedure described above yields the $\mathbf{G}$ as functions of ρ and u. We now calculate the derivatives $\frac{\partial G_\nu}{\partial u}(\rho, u)$ required in the coefficient $B(\rho, u)$ in eq. (4.42). They are determined by implicitly differentiating equations $F_1 = 0, \ldots, F_n = 0$ with respect to u

$$
\begin{pmatrix} \frac{\partial G_1}{\partial u} \\ \frac{\partial G_2}{\partial u} \\ \vdots \\ \frac{\partial G_n}{\partial u} \end{pmatrix} = J\left(\rho, \mathbf{G}(\rho, u) \right)^{-1} \cdot \begin{pmatrix} -1 \\ 0 \\ \vdots \\ 0 \end{pmatrix}.
\tag{4.57}
$$

Finally, the $\frac{\partial a}{\partial G_\nu}(\rho, u)$ are obtained from (4.27),

$$
\frac{\partial a}{\partial G_\nu} = A^0 \frac{\partial M}{\partial G_\nu} - 4B^0 \frac{\partial N}{\partial G_\nu},
\tag{4.58}
$$

where

$$
\begin{aligned}
\frac{\partial M}{\partial G_\nu} \;=\; & -\sum_{\tau=1}^{n} \frac{1}{z_\tau^2} \rho \left\{ M_\tau^{(a)} \frac{\partial D_\tau}{\partial G_\mu} + (1 - M_\tau^{(a)} e^{-z_\tau}) \frac{\partial f_\tau}{\partial G_\mu} \right\} \\
\frac{\partial N}{\partial G_\nu} \;=\; & \sum_{\tau=1}^{n} \frac{1}{z_\tau^3} \rho \left\{ L_\tau^{(a)} \frac{\partial D_\tau}{\partial G_\mu} + (1 - L_\tau^{(a)} e^{-z_\tau}) \frac{\partial f_\tau}{\partial G_\mu} \right\} \\
\frac{\partial f_\tau}{\partial G_\mu} \;=\; & \frac{2\pi}{z_\tau^2} \rho \left(\delta_{\mu\tau} D_\tau + G_\tau \frac{\partial D_\tau}{\partial G_\mu} \right)
\end{aligned}
\tag{4.59}
$$

with $\mathbf{D} = \mathbf{D}(\rho, \mathbf{G}(\rho, u))$ and $\{\frac{\partial D_\mu}{\partial G_\nu}(\rho, \mathbf{G}(\rho, u))\}$.

The PDE (4.41) is a quasilinear diffusion equation that has been solved numerically by an implicit finite-difference algorithm [77] described in detail in [54] in the region $(\beta, \rho) \in [0, \beta_f] \times [0, \rho_0]$. The integration with respect to β starts at $\beta = 0$ and goes down to lower temperatures. At each temperature the set of nonlinear equations (4.44, 4.49, 4.51) is solved giving $\{G_\nu(\rho, u)\}$: to ensure rapid convergence the values of the $\{G_\nu(\rho, u)\}$ obtained at the previous temperature step in the solution algorithm of the PDE are taken as initial guess for the solution of the system of nonlinear equations. In the next step $\{D_\nu(\rho, u)\}$, $a(\rho, u)$, $\{\frac{\partial D_\mu}{\partial G_\nu}(\rho, u)\}$, $\{\frac{\partial a}{\partial G_\nu}(\rho, u)\}$ and $\{\frac{\partial G_\nu}{\partial u}(\rho, u)\}$ are determined to calculate the coefficient $B(\rho, u)$. The boundary conditions are the same as in [59]: for $\rho = 0$ one obtains from eq. (4.34)

$$u(\rho = 0, \beta) = 0 \quad \forall \beta. \tag{4.60}$$

For the boundary condition at high density ρ_0 (we have set $\rho_0 = 1$ in the calculations) we make use of the so-called high temperature approximation (HTA) [4] according to which the excess Helmholtz free energy per unit volume is given by

$$f_{\mathrm{HTA}}^{ex}(\rho, \beta) = 2\pi\rho^2 \int w(r) g_{\mathrm{HS}}(r) r^2 dr \quad \forall \beta. \tag{4.61}$$

This approximation becomes more accurate for high densities so that for a sufficiently large value of the density ρ_0 a boundary condition based on the HTA should be reasonable. If we use the HTA at $\rho = \rho_0$ one obtains for the reduced compressibility

$$\frac{\partial^2 u}{\partial \rho^2}(\rho_0, \beta) = \frac{\partial^2 u}{\partial \rho^2}(\rho_0, \beta = 0) \quad \forall \beta. \tag{4.62}$$

The initial condition $u(\rho, \beta = 0)$ can be determined by taking into account that for $\beta = 0$ the direct correlation function $c(r)$ coincides with that of the HS gas. Thus $\widetilde{K}_\nu = 0$ for $\nu = 2, \ldots, n$, yielding $D_\nu(\rho, \beta = 0) = 0$ for $\nu = 2, \ldots, n$. Hence, eq. (4.29) reduces to

$$O_{\nu 1} D_1 = Q_\nu \quad \text{for} \quad \nu = 1, \ldots, n. \tag{4.63}$$

For $\nu = 1$ this leads to

$$D_1(\rho, \beta = 0) = \frac{Q_1(G_1(\rho, \beta = 0))}{O_{11}(G_1(\rho, \beta = 0))}, \tag{4.64}$$

where $G_1(\rho, \beta = 0)$ is obtained from the known quantity $\gamma_1(\rho, \beta = 0)$ that was introduced in the Laplace transform technique (see Appendix A of [59]) via

$$G_1(\rho, \beta = 0) = \frac{z_1}{4\pi\rho} \frac{A - 1}{A\sigma_1 - \tau_1}, \tag{4.65}$$

where

$$A = (2 - \sqrt{q} - \gamma_1(\rho, \beta = 0)) \frac{2(2 + z_1)}{4 + 2z_1 - z_1^2}$$

$$\sigma_1 = \frac{1}{2z_1} \left(\frac{z_1 - 2}{z_1 + 2} + e^{-z_1} \right)$$

$$\tau_1 = \frac{1}{2z_1} \left(\frac{z_1^2 + 2z_1 - 4}{4 + 2z_1 - z_1^2} + e^{-z_1} \right)$$

$$q = \frac{(1 + 2\eta)^2}{(1 - \eta)^2} \tag{4.66}$$

with $\eta = \frac{\pi}{6}\rho$ being the packing fraction. From eq. (4.63) for $\nu \neq 1$ one obtains

$$G_\nu(\rho, \beta = 0) = -\frac{D_1(\rho, \beta = 0) \left(B_{1\nu}^{(2)} G_1(\rho, \beta = 0) + B_{1\nu}^{(4)} \right) + B_\nu^{(6)}}{D_1(\rho, \beta = 0) \left(B_{1\nu}^{(1)} G_1(\rho, \beta = 0) + B_{1\nu}^{(3)} \right) + B_\nu^{(5)}} \tag{4.67}$$

and thus

$$u(\rho, \beta = 0) = -2\pi\rho^2\epsilon \sum_{\nu=2}^{n} c_\nu \frac{G_\nu(\rho, \beta = 0)}{z_\nu}. \tag{4.68}$$

The unphysical region inside the spinodal curve is determined by checking the sign of a given in (4.27): in the forbidden region a becomes negative. The boundary conditions on the spinodal used here are the same as those in [59]

$$u(\rho_{S_i}, \beta) = u_S(\rho_{S_i}) \quad i = 1, 2, \tag{4.69}$$

where $\rho_{S_i}(i = 1, 2)$ are approximates for the spinodal densities on the discrete density grid at a given temperature. Their values are determined by locating the change of sign of a. $u_S(\rho)$ is the value of the excess internal energy per unit volume where $\frac{1}{\chi^{red}} = 0$. This value is determined by solving the set of equations

$$a(\rho, G_1, \ldots, G_n) = 0$$
$$F_2(\rho, G_1, \ldots, G_n) = 0$$
$$\vdots$$
$$F_n(\rho, G_1, \ldots, G_n) = 0 \tag{4.70}$$

with respect to $G_1, \ldots, G_n$ providing again the analytic Jacobian matrix of this nonlinear system. Inserting the solutions $G_1(\rho), \ldots, G_n(\rho)$ in the energy equation (4.34) yields $u_S(\rho)$.

Once $u(\rho, \beta)$ has been determined by solving the PDE (4.41) the pressure P and the chemical potential μ are obtained by integrating $\frac{\partial \beta P}{\partial \beta}$ and $\frac{\partial \beta \mu}{\partial \beta}$ with respect to β from

$$\frac{\partial \beta P}{\partial \beta} = -u + \rho \frac{\partial u}{\partial \rho} \tag{4.71}$$

and

$$\frac{\partial \beta \mu}{\partial \beta} = \frac{\partial u}{\partial \rho},\tag{4.72}$$

where we have taken as integration constants at $\beta = 0$ the CS values for βP and $\beta \mu$

$$\beta P(\rho, \beta = 0) = \rho \frac{1 + \eta + \eta^2 - \eta^3}{(1 - \eta)^3}$$

$$\beta \mu(\rho, \beta = 0) = \ln \rho + \frac{8\eta - 9\eta^2 - 3\eta^3}{(1 - \eta)^3}.\tag{4.73}$$

Alternatively, βP and $\beta \mu$ can be obtained by integrating, respectively, $\frac{1}{\chi^{red}}$ and $\frac{1}{\rho \chi^{red}}$ with respect to the density from

$$\left(\frac{\partial \beta P}{\partial \rho}\right)_T = \frac{1}{\chi^{red}}$$

$$\left(\frac{\partial \beta \mu}{\partial \rho}\right)_T = \frac{1}{\rho \chi^{red}}.\tag{4.74}$$

Both paths lead to the same thermodynamics due to the thermodynamic consistency enforced by eq. (4.35). However, the latter route has a serious drawback: in order to reach the high density branch of the subcritical isotherms, that is separated from the low-density branch by the spinodal, one has to circumvent the forbidden region via a path 'around' the coexistence curve.

4.2.2 Lennard-Jones fluid

The 12-6 Lennard Jones interaction describes surprisingly good the interaction between rare gas atoms. The attractive r^{-6} term represents a dipole-induced dipole interaction between the rare gas atoms, while the r^{-12} term is an approximation for the harsh repulsion at short range that has its origin in the overlap of the outer electron shells. Structural and thermodynamic properties of this model system have been extensively studied in the last decades using both computer simulations and theoretical approaches. For an overview over these results see e.g. [4, 9].

Using the formalism developed in the preceeding section we are now able to study, within the framework of the SCOZA, the liquid-gas phase behavior of a LJ fluid that is modeled by a hard-core multi-Yukawa fluid. This system has already been investigated by Pini *et al.* [60] using a simpler version of the SCOZA. In an effort to enable a direct comparison of their results we will first use their fit to the LJ potential. In their study the LJ potential was approximated by a hard-core two-Yukawa potential

$$w(r) = \frac{A_1 \epsilon}{r} e^{-z_1(r-\sigma)} - \frac{A_2 \epsilon}{r} e^{-z_2(r-\sigma)}.\tag{4.75}$$

Here σ is the zero and ϵ the well-depth at the minimum of the LJ potential

$$\phi^{\mathrm{LJ}}(r) = 4\epsilon \left(\left(\frac{\sigma}{r} \right)^{12} - \left(\frac{\sigma}{r} \right)^{6} \right). \tag{4.76}$$

The parameters $A_1 = 1.6438\sigma$, $z_1 = 14.7\sigma^{-1}$, $A_2 = 2.03\sigma$ and $z_2 = 2.69\sigma^{-1}$ are chosen to fit the LJ potential (see fig. (4.2)).

In contrast to the route chosen in [60] where the HS contribution to the direct correlation function is treated in an approximate way to avoid the introduction of a third Yukawa tail we use here the closure relation (4.36) where the HS direct correlation function is given in the Waisman parameterization by an additional Yukawa term. So we deal here with a direct correlation function of a three-Yukawa form outside the core.
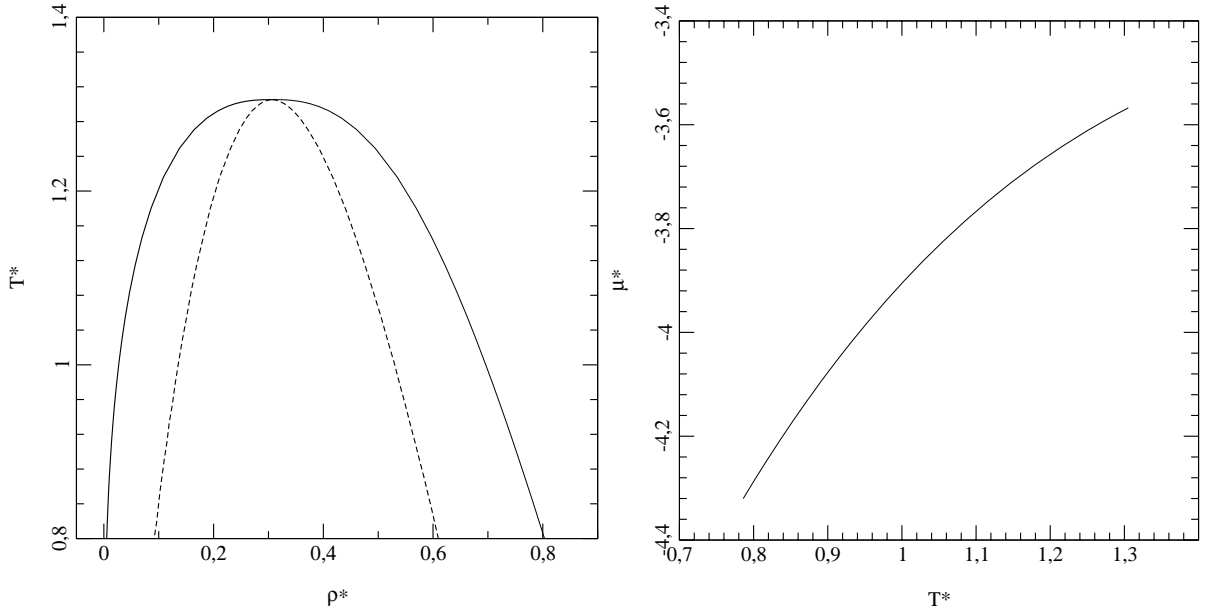

Figure 4.1: Coexistence curve of the hard-core two-Yukawa fluid mimicking a LJ-fluid (see text). Right: coexistence curve in the density-temperature plane. Solid line: binodal curve, dashed line: spinodal curve. Left: Coexistence curve in the chemical potential-temperature plane. All quantities are in reduced units ($\mu^\star = \sigma\mu/\epsilon$).

The numerical solution of the PDE (4.41) with the initial condition and the boundary conditions has been performed on a density grid with $\Delta\rho^\star = 10^{-3}$ and a temperature grid $\Delta\beta^\star = 10^{-5}$. In order to locate the critical point accurately $\Delta\beta^\star$ is decreased when approaching the critical point and afterwards increased back to the initial value. The critical point $(\rho_c^\star, T_c^\star)$ is located by the vanishing of the inverse compressibility $\frac{1}{\chi^{red}}$. At

subcritical temperatures the region enclosed by the spinodal is excluded. The coexistence curve is determined by equating the chemical potential and the pressure

$$\mu(\rho_g^\star, T^\star) = \mu(\rho_l^\star, T^\star)$$
$$P(\rho_g^\star, T^\star) = P(\rho_l^\star, T^\star), \tag{4.77}$$

where $\rho_g^\star$ and $\rho_l^\star$ are the densities of the coexisting gas and liquid. The values for the critical density and temperature obtained in the different approaches are compared in Tab. (4.1) with the predictions of the versions of the SCOZA of [60] and the MC simulation results present therein. The coexistence curve in the temperature-density plane and chemical potential-temperature plane is given in figs. (4.1). The curves are hardly distinguishable from the ones of the version of the SCOZA reported in [60] where the HS part of $c(r)$ is treated by a Yukawa form whose range coincides with that of the repulsive contribution to the tail potential.

	MC	SCOZA	SCOZA*	SCOZA$^\diamond$
$\rho_c^\star$	0.310(1)	0.306	0.307	0.304
$T_c^\star$	1.295(1)	1.305	1.304	1.293

Table 4.1: Critical density and temperature for the hard-core two-Yukawa fluid mimicking a LJ-fluid (see text). MC simulation from [60]. SCOZA results for three-Yukawa c(r). $\star$: SCOZA results using 2-Yukawa c(r) of eq. (2.17) of [60]. $\diamond$: SCOZA results using 2-Yukawa c(r) of eq. (2.1) of [60].

As a further application of the formalism developed in the preceding section we have fitted a three-Yukawa interaction by means of a point by point, least squares procedure

$$\phi(r) = \begin{cases} \infty & r < \sigma \\ c_1\epsilon\left(\frac{e^{-z_2(r-\sigma)}}{r} - c_2\frac{e^{-z_3(r-\sigma)}}{r} - (1-c_2)\frac{e^{-z_4(r-\sigma)}}{r}\right) & r > \sigma \end{cases}, \tag{4.78}$$

to a HC LJ potential

$$\phi^{LJ}(r) = \begin{cases} \infty & r < \sigma \\ 4\epsilon\left(\left(\frac{\sigma}{r}\right)^{12} - \left(\frac{\sigma}{r}\right)^6\right) & r > \sigma \end{cases}, \tag{4.79}$$

see fig. (4.2). The difference between the HC LJ-potential and the fitted potential is not distinguishable on the scale of the figure. For the fitting we have chosen 1000 points starting at $r = 1$ and spaced proportional to r^2, all of the points were equally weighted; so we have provided more fitting points at lower values of r. The parameters were found to be $z_2\sigma = 13.446, z_3\sigma = 3.482, z_4\sigma = 1.317$ and $c_1\sigma^{-1} = 2.351, c_2 = 0.910$.

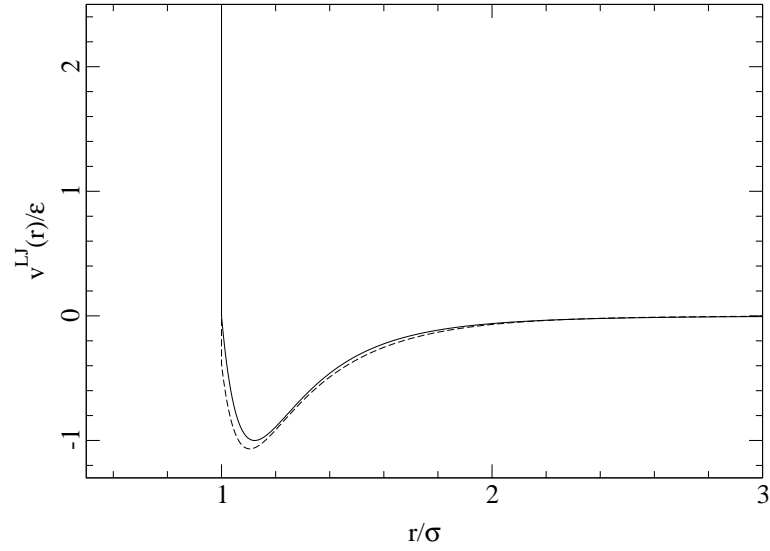The coexistence curve for this model potential is given in fig. (4.3).

Figure 4.2: Full line: Hard-core three-Yukawa interaction potential. The parameters - specified in the text - are chosen to fit a hard-core Lennard Jones potential. Dashed line: HC2Y fit of Pini *et al.* [60] to the LJ potential.
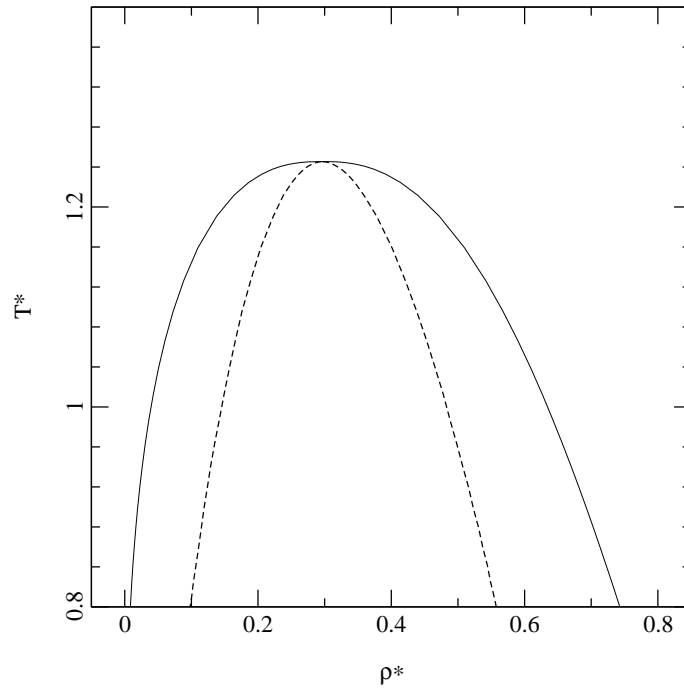

Figure 4.3: Coexistence curve for the hard-core three-Yukawa interaction fluid that mimics a hard-core LJ fluid in the temperature-density plane. Solid line: binodal curve; dashed line: spinodal curve. Critical point at $(\rho_c^\star, T_c^\star) = (0.296, 1.245)$.

4.2.3 Fullerenes

The most studied case among the fullerenes is the C_{60} molecule which consists of 60 carbon atoms held together by covalent bonds on the surface of a truncated icosahedron. The molecules themselves interact with each other by van der Waals forces. Up to now, most studies have focused on the solid phase (see [78] and references therein). At low temperature C_{60} crystallizes in an FCC lattice with orientationally ordered molecules. This orientationally ordered phase is known to be only stable below 250 K, while at room temperature the molecules undergo hindered rotations.

The LV phase transitions and the critical point of C_{60} fall into a temperature regime that is much higher, where the C_{60} molecules can be considered to rotate freely. Thus in this temperature region - in which we are interested in this study - one can ignore the internal structure of the C_{60} molecules and treat each molecule as if it were a sphere with a uniform surface density. This rigid sphere approximation was assumed by Girifalco [79] in order to derive a central analytic pair potential between the C_{60} molecules. As interaction between pairs of carbon atoms on different molecules he assumed a LJ-like potential

$$\phi(r) = -\frac{A}{r^6} + \frac{B}{r^{12}}, \tag{4.80}$$

where the values of A and B are known from studies on graphite ($A = 32{\cdot}10^{-60}\text{ergcm}^6, B = 55.77 \cdot 10^{-105}\text{ergcm}^{12}$). In the smeared out spherical approximation, Girifalco [79] has shown that the interaction between two fullerene molecules with N carbon atoms can be integrated over the two interacting spheres and leads to an analytic effective interaction potential of the form

$$\phi(r) = -\alpha \left[\frac{1}{s(s-1)^3} + \frac{1}{s(s+1)^3} - \frac{2}{s^4} \right] + \beta \left[\frac{1}{s(s-1)^9} + \frac{1}{s(s+1)^9} - \frac{2}{s^{10}} \right]. \tag{4.81}$$

Here $s = \frac{r}{R}, \alpha = \frac{N^2 A}{12R^6}, \beta = \frac{N^2 B}{90R^{12}}$, N and R are the number of carbon atoms (N=60 for C_{60}) and the diameter, respectively, of the fullerene molecules.

Molecular dynamic (MD) simulations [78] have been carried out both for the sphericalized Girifalco potential with only one interaction site and the full 60-site model where the interaction between two C_{60} molecules is represented as the sum over the interactions between all of the carbon atoms on one molecule with those of the other, the interaction between pairs of carbon atoms on different molecules being described by eq. (4.80). In this study it was confirmed that the center-of mass pair distribution function $g(r)$ for the full 60-site model is nearly identical with that obtained from the Girifalco potential. Thus the use of the central pair potential - which represents an enormous simplification - was justified for subsequent studies.
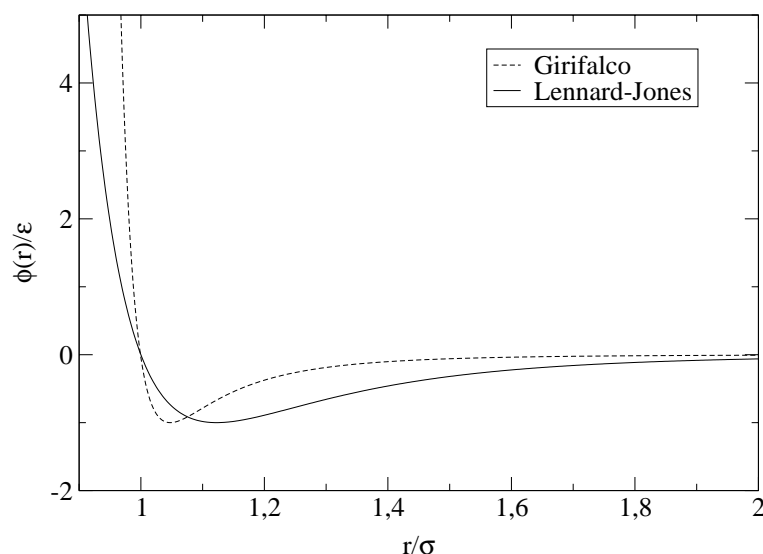
Figure 4.4: A comparison of the 12-6 LJ potential (solid line) and the Girifalco potential for C_{60} (dashed line). The potential energy is expressed in units of the well depth, the range in units of the zero of the potential.

As can be seen in fig. (4.4), the Girifalco pair potential differs significantly from the LJ one. In the figure both potentials are drawn in reduced units to enable a comparison of the shape. From this figure the following differences become evident: the ratio of the width of the attractive well to the equilibrium distance is much less for the C_{60}-C_{60} intermolecular potential than for the LJ one. This is immediately clear, since the interaction range is determined by the C-C interaction range, while the diameter of the repulsive core is fixed by the size of the C_{60} molecule. Furthermore we see that the repulsive wall of the C_{60}-C_{60} interaction is much stiffer. In fact the well depth of the intermolecular interaction (at 3218 K) is two orders of magnitude larger than that of the interatomic C-C interaction.

Since the C_{60} pair potential differs in many respects from that of smaller molecules the liquid-vapor phase behavior of C_{60} was expected to differ qualitatively from that of a simple fluid like argon. Further, since the liquid range expressed by T_c/T_t (where T_c is the critical point temperature and T_t the triple point temperature) depends in a very sensitive way on the nature of the intermolecular forces [4] it was even speculated that C_{60} might be a substance with no liquid phase at all [80, 81]. A similar situation occurs in a very short ranged HCY fluid where it has been seen that the liquid phase disappears for large values of the decay length [82, 83].

Up to now, several attempts have been made to clarify this situation. Phase diagrams have been determined both with theoretical calculations and simulations, but the first

results were rather controversial [84, 80, 81]. While MD simulations combined with the thermodynamic self-consistent HMSA and the entropic freezing criterion (see below) [84] predicted the existence of a liquid phase in a narrow temperature range of approximately 200 K (from $\sim$ 1800 K to 2000 K), in other simulation studies [80], based on the Gibbs ensemble Monte Carlo technique, the freezing line was found to pass slightly above the (metastable) critical point of the LV binodal, thus implying that the C_{60} does not exist in a stable liquid phase and that direct sublimation occurs from the solid to the vapor.

Since both studies have been made for exactly the same system, namely the Girifalco potential, these controversial results were rather puzzling and stimulated a series of other theoretical and computer simulation investigations. Further theoretical studies for the Girifalco potential were based on density functional theory (DFT) [85], on the MHNC theory [86], the HRT [87]; computer simulation investigations were based both on the Girifalco potential [88, 89] and on a more refined *ab initio* potential [90]. All these studies have confirmed that C_{60} should possess a stable liquid phase and that this liquid phase is confined to a rather small temperature range compared to the value of the estimated critical temperature (the latter feature being a consequence of the very short ranged interaction potential between the C_{60} molecules). It should be noted here, that it is still an unsettled question whether this liquid phase exists experimentally: in this high temperature range the C_{60} molecules might not be stable.

Recently, also the phase behavior of $C_{n \geq 70}$ fullerenes was studied [91] theoretically, and it was found that C_{70} also possesses a stable liquid phase and that the temperature range where this phase exists is wider and the critical point occurs at higher temperatures than in the case of C_{60}.

Since the SCOZA is known to remain highly accurate in the critical region, it is of interest to apply this theory to the calculation of the phase behavior of the $C_{n \geq 60}$ fullerenes using the central Girifalco potential and to compare the results with those of previous studies. The parameters of the potential eq. (4.81) for the different fullerenes are taken from [91] and are given in table (4.2). Fig. (4.5) shows the fullerene potentials in reduced units. It becomes visible that the interaction range decreases for the higher order fullerenes. So one might speculate that the liquid range of the higher order fullerenes is even smaller and this is exactly the behavior that we found when using the SCOZA; this result is in contrast to previous results presented in [91].

In an effort to apply our SCOZA scheme to the Girifalco potential, we have approximated the harsh repulsion of this interaction by a HS interaction $\phi(r) = \infty$ for $r < R_0$, where R_0 is the equilibrium distance between two fullerene molecules; the attractive tails

	R	R_0	ϵ/k_B	α	β
C_{60}	0.71	0.9599	3218	74.94	135.95
C_{70}	0.762	1.011	3653	66.7	79.23
C_{76}	0.7991	1.048	3808	59.2	52.87
C_{84}	0.8401	1.0890	4081	53.56	35.42
C_{96}	$0.8981^{(a)}$	$1.1468^{(a)}$	$4467^{(a)}$	$46.83^{(a,b)}$	20.74

Table 4.2: Parameters for the Girifalco potential for different fullerenes C_n, n = 60, 70, 76, 84 and 96. R is the diameter of the fullerenes, R_0 is the point of zero potential, ϵ is the depth of the potential α, β are given in the text; distances are expressed in nm, temperatures in K, and α and β in units of 10^{-15} and 10^{-18} erg, respectively. (a): values taken from [92] and correcting the values from [91]. (b): correcting a misprint of [92].

were fitted by a linear combination of 3 Yukawas. Thus we are dealing again with a pair potential of HC3Y form

$$\phi(r) = \begin{cases} \infty & r < R_0 \\ c_1\epsilon \left(\frac{e^{-z_2(r-R_0)}}{r} - c_2\frac{e^{-z_3(r-R_0)}}{r} - (1-c_2)\frac{e^{-z_4(r-R_0)}}{r} \right) & r > R_0 \end{cases} . \qquad (4.82)$$

The values of the fit parameters c_1, c_2, z_2, z_3 and z_4 are summarized in table (4.3) for the

	c_1/R_0	c_2	$z_2 R_0$	$z_3 R_0$	$z_4 R_0$
C_{60}	1.7458	0.9209	45.1889	7.4129	2.1648
C_{70}	1.8906	0.8322	42.7205	9.0618	3.1977
C_{76}	1.8817	0.8347	44.4324	9.3274	3.2635
C_{84}	1.8444	0.8521	47.0927	9.3752	3.1930
C_{96}	1.8503	0.8438	49.2079	9.9826	3.4078

Table 4.3: Parameters of the fitted HC3Y potential for the different fullerenes. See text and equation (4.82).

different fullerenes. We have then solved the SCOZA and have thus determined the phase diagram and the critical data. The critical point parameters for C_{60} are summarized in table (4.4) together with other theoretical results and simulation results. It should be noted that only the SCOZA and the HRT are able to access the critical region, whereas the other theories are not able to approach the critical point: thus in these cases the critical point parameters have been obtained by extrapolation. Our value for the critical point temperature T_c is in good agreement with the simulation results of [84, 88, 89] and the value of the critical density agrees with the simulation results of [80, 88, 89].
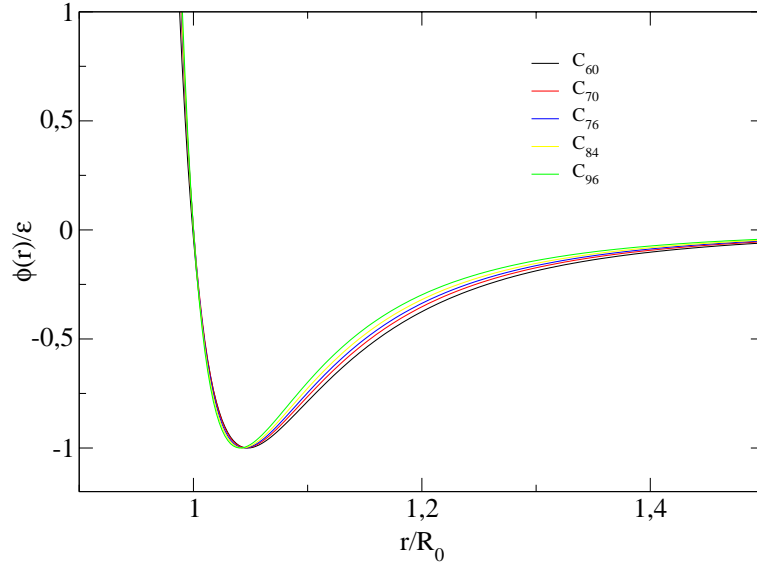
Figure 4.5: The Girifalco potential for the different fullerenes in reduced units.

In order to give an estimate for the location of the freezing line we have used the residual multi-particle excess entropy freezing criterion [93] according to which freezing takes place when

$$\Delta s = s_{ex} - s_2 = 0, \tag{4.83}$$

where the partial entropy resulting from the correlation between a pair of particles is

$$s_2 = -2\pi\rho \int_0^\infty r^2 \left(g(r) \ln g(r) - g(r) + 1 \right) dr \tag{4.84}$$

and s_{ex} is the excess entropy per particle in units of the Boltzmann constant

$$s_{ex} = \frac{\beta}{\rho} \left(u - f^{ex} \right). \tag{4.85}$$

The pair distribution function $g(r)$ required in the integral (4.84) has been calculated according to a stepwise algorithm based on Perram's procedure proposed originally for HSs [94]. Explicit formulae for its generalization to the HCY case can be found in the Appendix D of [75]. Care has to be taken when the screening lengths of the Yukawa tails are of different orders of magnitude as it is the case in our systems (see table (4.3)). For implementing a numerically stable algorithm we had to reorder the summation over the Yukawa tails occurring in these expressions. For the discretized pair distribution function $g(r)$ a grid space of 0.005σ was chosen and we have evaluated the integrand in eq. (4.84) up to 20σ. We have checked that the extension of the integrand to higher values of r does not change the value of the integral. The integral (4.84) was evaluated via the Simpson rule.

	SCOZA	HMSA	MHNC	HRT
$T_c(\text{K})$	1957	$\sim$2050	$\sim$1920	2138
$\rho_c[\text{nm}^{-3}]$	0.432	$\sim$0.56		0.50
	MD	MC	GEMC	NVT MC
$T_c(\text{K})$	1900$\pm$100	1798$\pm$10	1920-1940	1980
$\rho_c[\text{nm}^{-3}]$	0.56$\pm$0.06	0.42	0.4-0.45	0.44

Table 4.4: Critical parameters of the Girifalco potential for C_{60} as predicted by SCOZA, HMSA [84], MHNC [86], HRT [87], DFT [85], MD [84], MC [80], Gibbs ensemble Monte Carlo (GEMC) [88] simulations and NVT Monte Carlo simulations (NVT MC) [89]. In the MC study of [80] the critical point is a metastable one.

The coexistence curve, the spinodal line and the freezing line given by the SCOZA are plotted in fig. (4.6). The triple point parameters, that are obtained by intersection of the liquid branch with the freezing line, are given in table (4.5) together with other results. While our value of the triple point density is reasonable when compared to the other results, our triple point temperature is much lower than in the simulation studies.

	SCOZA	HMSA	MHNC	HRT
$T_t[K]$	1388	1774	1620	1979
$\rho_t[\text{nm}^{-3}]$	1.03	0.944	1.00	0.848
	MD	MC	GEMC	NVT MC
$T_t[K]$	1800	–	1500-1700	1880
$\rho_t[\text{nm}^{-3}]$	$\sim$1	–	0.91-1	0.74

Table 4.5: Triple point parameters of the Girifalco potential for C_{60} predicted by the SCOZA, HMSA [84], MHNC [86], HRT [87], DFT [85], MD [84], MC [80], GEMC [88] simulations and NVT MC simulations [89]. In the MC study of [80] no liquid phase and thus no triple point was found.

The phase diagrams of the other fullerenes are shown in figs. (4.7) and (4.8); the critical point and triple point parameters are compared with the results of Abramo *et al.* [91] in table (4.6). Their results for C_{70} have been obtained by the MHNC theory and by GEMC simulations, while those for the other fullerenes were approximated by assuming a law of 'corresponding states'. The corresponding state behavior was motivated in the following way: by introducing reduced units $\phi/\epsilon, r/\sigma, T^\star = kT/\epsilon$ and $\rho^\star = \rho R_0^3$ the C_{60} and C_{70} interaction potentials look very similar and the critical point parameters differ by less
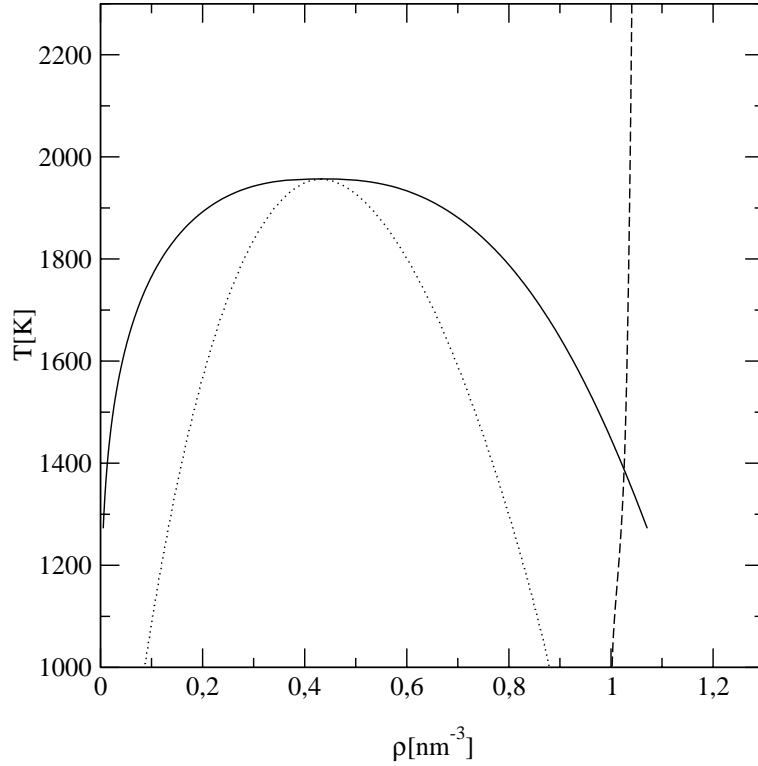
Figure 4.6: $T - \rho$ phase diagram for C_{60} determined by SCOZA. Liquid-vapor coexistence (solid line), spinodal (dotted line), freezing line (dashed line). Critical point at (ρ_c, T_c)=(0.432nm^{-3},1957K), triple point at (ρ_t, T_t)=(1.03nm^{-3},1388K).

than 1%. So the authors assumed that the critical point and triple point parameters expressed in these reduced units should be the same also for the higher order fullerenes. Table (4.6) summarizes the triple and critical point parameters for C_{70},C_{76},C_{84} and C_{96} that have been obtained by applying this 'corresponding state' rule to these fullerenes.

The SCOZA values for the critical point temperature parameters of C_{70} are in good agreement with the GEMC results, while the discrepancy with 'corresponding state' estimates is steadily increasing from C_{70} to C_{96}. This tendency is in agreement with the final remark in [91] where the authors conclude that the corresponding state rule tends to overestimate the critical point parameters. In the SCOZA the critical point temperature increases from 1957K for C_{60} to 2405K for C_{96} - since the depth of the potential increases - and the critical point density decreases from 0.432nm^{-3} to 0.264nm^{-3}. The temperature range of the liquid phase expressed by T_c/T_t decreases from 1.41 for C_{60}, 1.38 for C_{70}, 1.36 for C_{76}, 1.33 for C_{84} to 1.30 for C_{96} while it is constant by definition for the 'corresponding states' results.
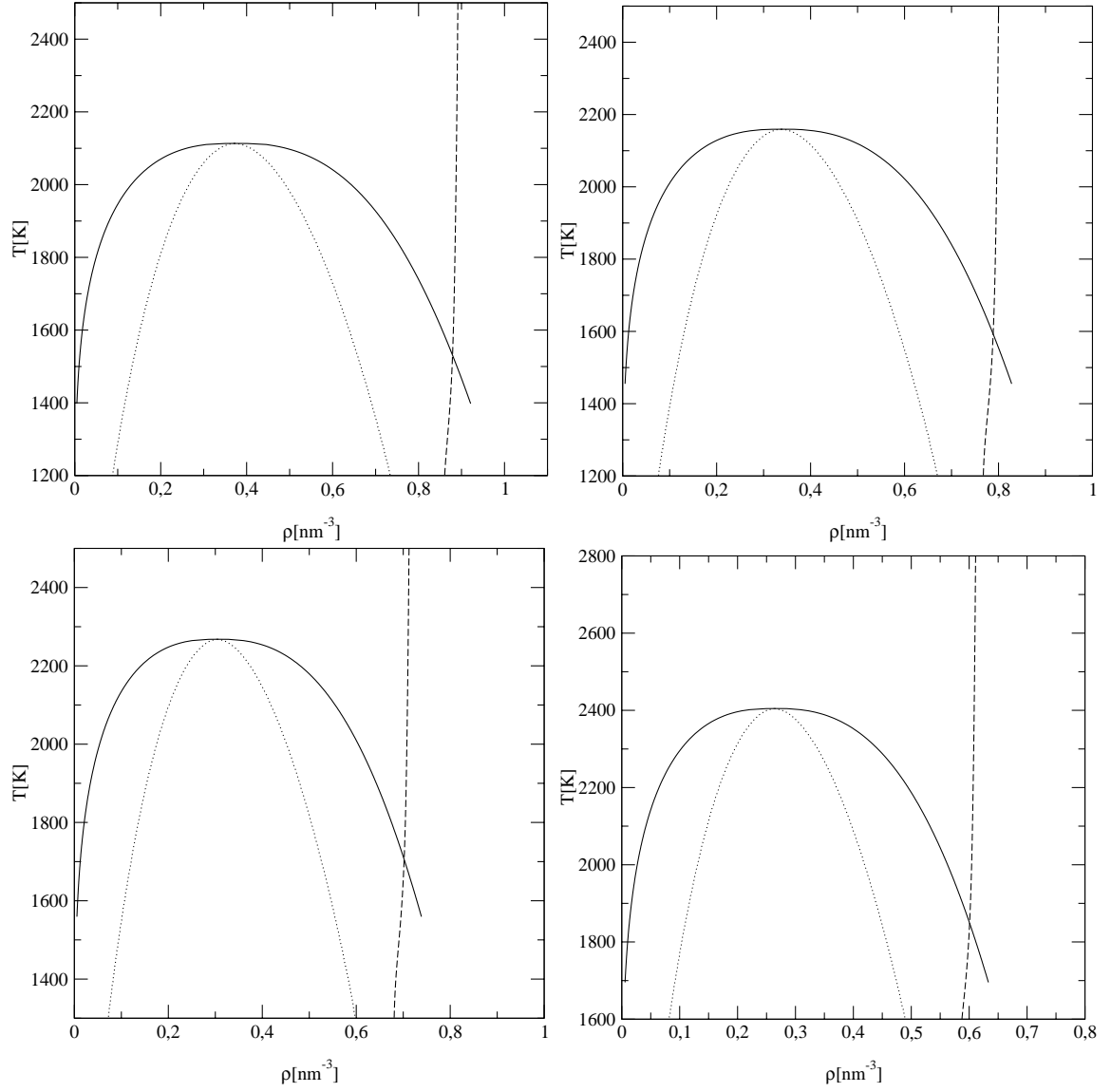
Figure 4.7: $T - \rho$ phase diagrams for C_{70}, C_{76}, C_{84}, C_{96} determined by SCOZA. The freezing line (dashed line), liquid-vapor coexistence line (solid line), spinodal (dotted line).
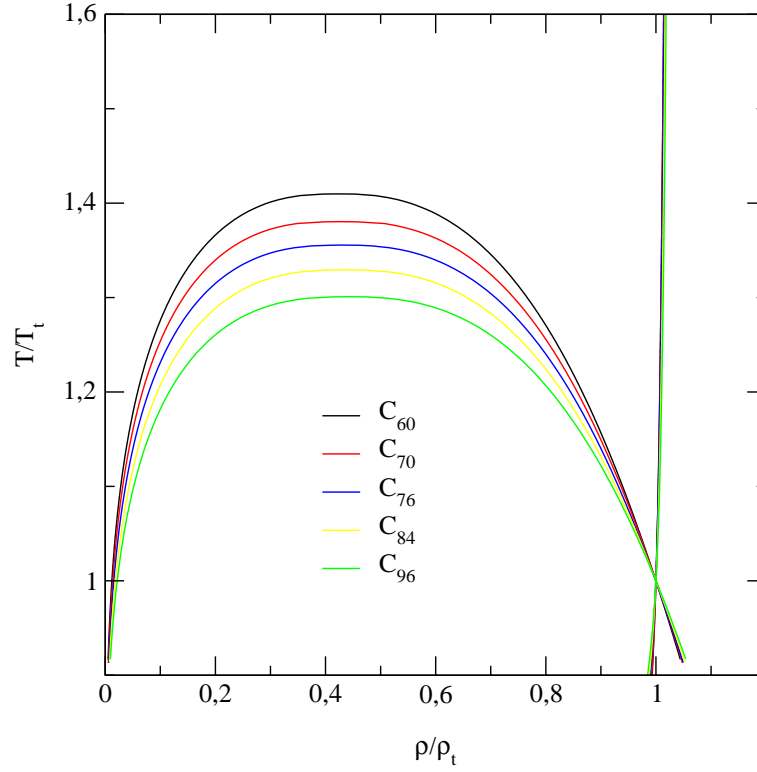
Figure 4.8: $T - \rho$ phase diagrams of the fullerenes $C_{60}, C_{70}, C_{76}, C_{84}, C_{96}$ obtained from SCOZA. Temperature and densities have been scaled with their respective triplet point values. The range of the liquid phase is decreasing with the number of carbon atoms.

	$\rho_c[\mathrm{nm}^{-3}]$	$T_c[K]$	$\rho_t[\mathrm{nm}^{-3}]$	$T_t[K]$	$\rho_c[\mathrm{nm}^{-3}]$	$T_c[K]$	$\rho_t[\mathrm{nm}^{-3}]$	$T_t[K]$
	SCOZA				GEMC			
C_{70}	0.372	2113	0.879	1531	0.376	2140	0.88	1650
	SCOZA				'Corresponding state' estimates			
C_{70}	0.372	2113	0.879	1531	0.36	2190	0.85	1703
C_{76}	0.338	2159	0.789	1593	0.32	2284	0.77	1775
C_{84}	0.304	2268	0.702	1706	0.29	2448	0.68	1902
C_{96}	0.264	2405	0.601	1849	0.24	2505	0.58	1947

Table 4.6: Critical- and triple point parameters for different fullerenes. Values for the critical point and triple point parameters from GEMC simulation and by assuming the law of 'corresponding states' are taken from [91].

4.2.4   Double Criticality

Although the Gibbs rule does not exclude the possibility of the existence of more than two fluid phases in a one-component substance, one usually finds at most two of them: one at low density (the vapor) and a second one at higher density (the liquid), the two phases becoming identical at a LV critical point. So an additional disordered phase and an additional liquid-liquid transition that is common for mixtures, is unexpected for pure substances. However, in recent experimental studies [10] evidence was found that in addition to the usual vapor-liquid transition a second liquid-liquid transition might exist in the supercooled region of certain fluids; this phenomenon is commonly referred to as double criticality.

This phenomenon has been analyzed within a simple van der Waals model by Tejero and Baus [95] and their results were confirmed qualitatively in a subsequent study by Almarza *et al.* [11] by means of computer simulation, a perturbation theory and an integral equation theory - the reference hypernetted chain (RHNC) theory.

In both studies a density-dependent inverse power interaction was considered, whose exponent has a non-monotonic density-dependence. The proposed functional form was

$$\phi(r;\rho) = \begin{cases} +\infty & r < \sigma \\ -\epsilon \left(\frac{\sigma}{r}\right)^{n(\rho)} & r > \sigma \end{cases} , , \tag{4.86}$$

where the potential index is given by

$$n(\rho) = 3 + \frac{n(0) - 3}{1 - \frac{2}{3}\alpha\rho + \frac{1}{6}\alpha^2\rho^2}. \tag{4.87}$$

By tuning $n(0)$ and α different types of critical behavior were obtained. In particular phase diagrams with two critical points were found, one corresponding to a stable or metastable (with respect to the liquid-solid transition) vapor-liquid transition and another one corresponding to a stable or metastable liquid-liquid separation. The metastable liquid-liquid critical point was found to lead to a shoulder in the liquid-solid coexistence curve [95].

Due to the discrepancies that were found in [11] between computer simulation results and theoretical results a more refined study of the phenomenon of double criticality with a reliable theory is of course desirable. Since the SCOZA is known to be a highly accurate theory even in the critical region it should be able to give quantitative predictions for the phase diagram of a system with density-dependent pair potential.

The HCY potential is the most comfortable potential for a study with the SCOZA. So we consider here a system with density-dependent pair interaction of the form

$$\phi(r;\rho) = \begin{cases} +\infty & r < \sigma \\ -\frac{\epsilon}{r}e^{-z(\rho)(r-\sigma)} & r > \sigma \end{cases}, \tag{4.88}$$

where the density-dependent screening length is assumed to be given by

$$z(\rho)\sigma = 1.6 + \frac{z_0\sigma - 1.6}{1 - \frac{2}{3}\alpha\rho + \frac{1}{6}\alpha^2\rho^2}. \tag{4.89}$$

This density-dependence was motivated by eq. (4.87). So – if $z_0\sigma \neq 1.6$ – $z(\rho)$ is a non-monotonic function of ρ which increases for $z_0\sigma > 1.6$ from the zero-density limit $z_0\sigma$ to a maximum of $(3z_0\sigma - 3.2)$ at $\rho = \frac{2}{\alpha}$ and then decreases as shown in the fig. (4.9). For $z_0\sigma < 1.6$ the curve has a minimum at $\rho = 2/\alpha$.
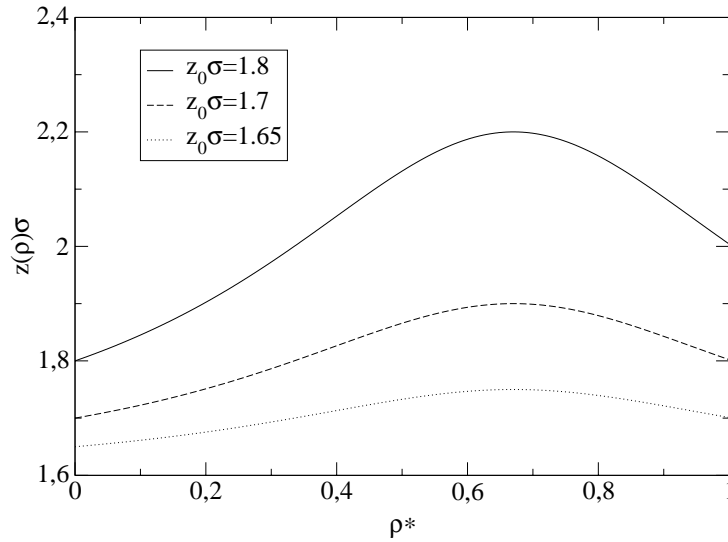
Figure 4.9: Density-dependence of the screening length $z(\rho)$ of the HCY potential of eq. (4.88) as given by eq. (4.89) with $\alpha = 5.7v_0$, where $v_0 = \frac{\pi\sigma^3}{6}$ is the HS volume for different z_0 values. Note the pronounced maximum in $z(\rho)\sigma$ for larger $z_0\sigma$ values.

Since the compressibility equation (2.11) remains valid for density-dependent pair potentials (see [96], page 342), the SCOZA scheme presented in section 4.2.1 can be applied for such a system too. We only have to take account of the fact that due to two critical points two nonphysical regions, where $1/\chi^{red} < 0$, have to be excluded from the solution of the PDE. The two different kinds of instability regions in the interval $[0, \rho_0]$ for given value of T are shown in fig. (4.10).
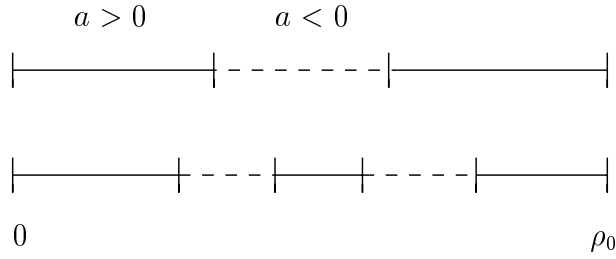
Figure 4.10: The different cases of the instability region where $a < 0$ (4.26) in the interval $[0, \rho_0]$ for a given value of T for a density-dependent HC1Y fluid. The full lines denote the stable regions where $a > 0$, while the dashed lines represent the unstable regions that are excluded from the integration of the PDE.

A series of phase diagrams with varying α values has been generated for different values of z_0; it is shown in figs. (4.11) to (4.19). In the case $z_0\sigma = 1.6$ the potential is density-independent, i.e. $z(\rho)\sigma \equiv 1.6$ and the phase diagram is shown in fig. (4.11). For $z_0\sigma > 1.6$ a non-monotonic behavior occurs that becomes more pronounced as z_0 increases.

A series of phase diagrams for $z_0 = 1.8\sigma$ is shown in figs. (4.12) and (4.13). The value
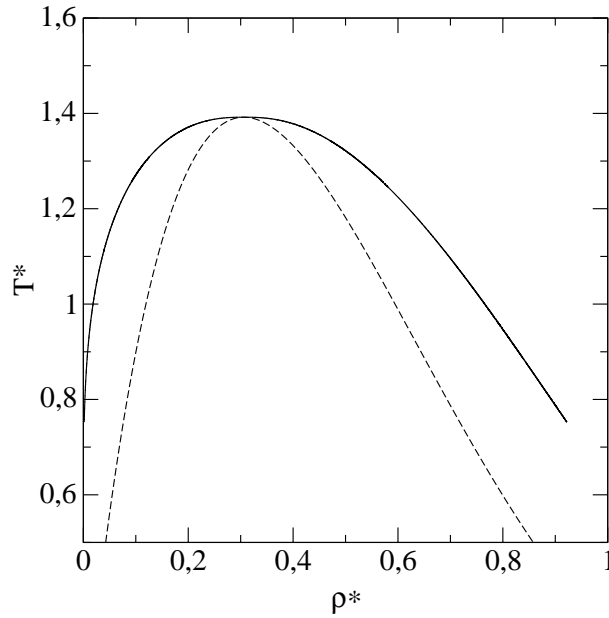
Figure 4.11: Phase diagram of a fluid with a density-dependent pair potential given by eqs. (4.88) and (4.89) for $z_0\sigma = 1.6$. Solid line: binodal curve; dashed line: spinodal curve.
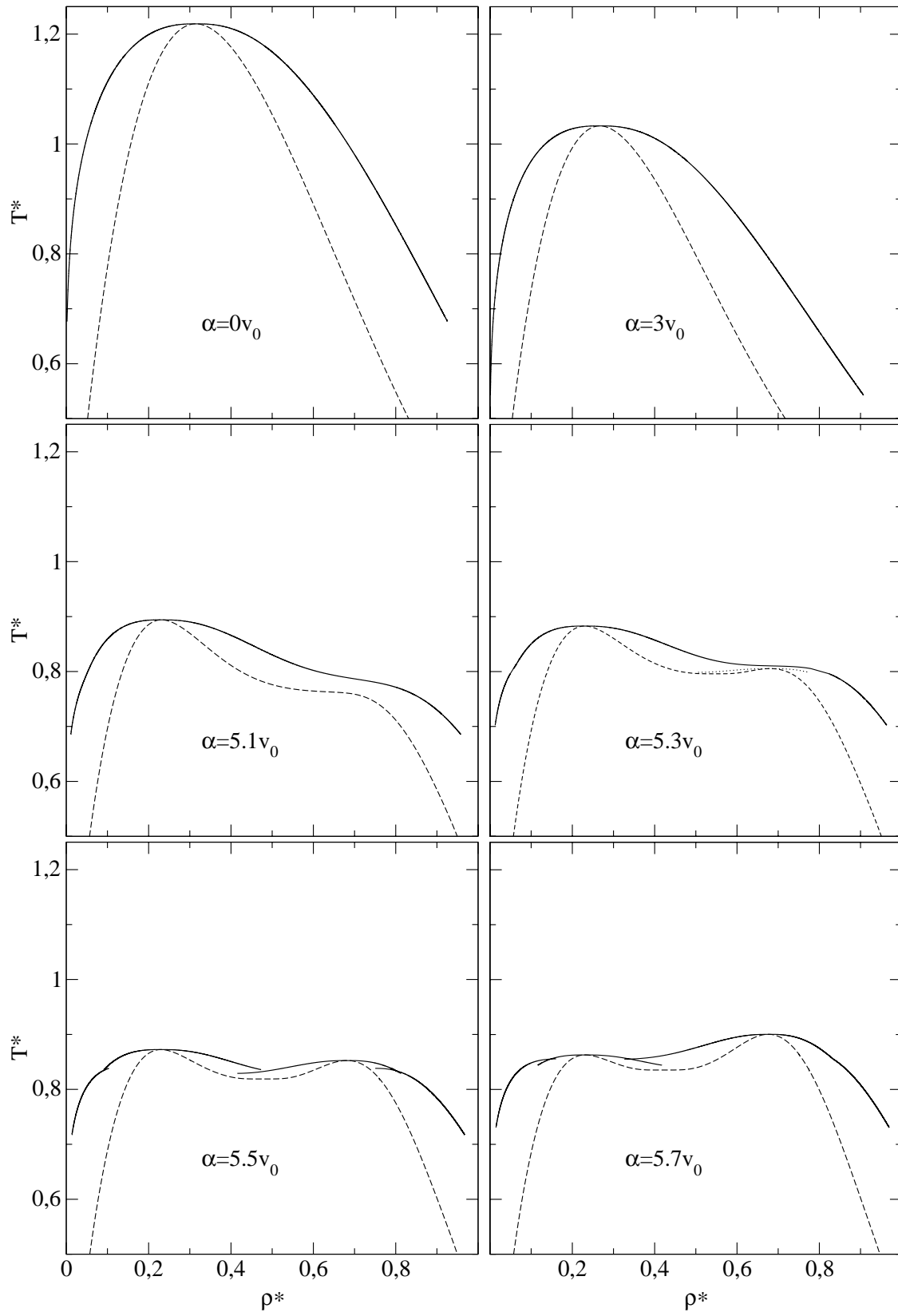
Figure 4.12: The same as in fig. (4.11) for $z_0\sigma = 1.8$. Dotted line: metastable coexistence curve.
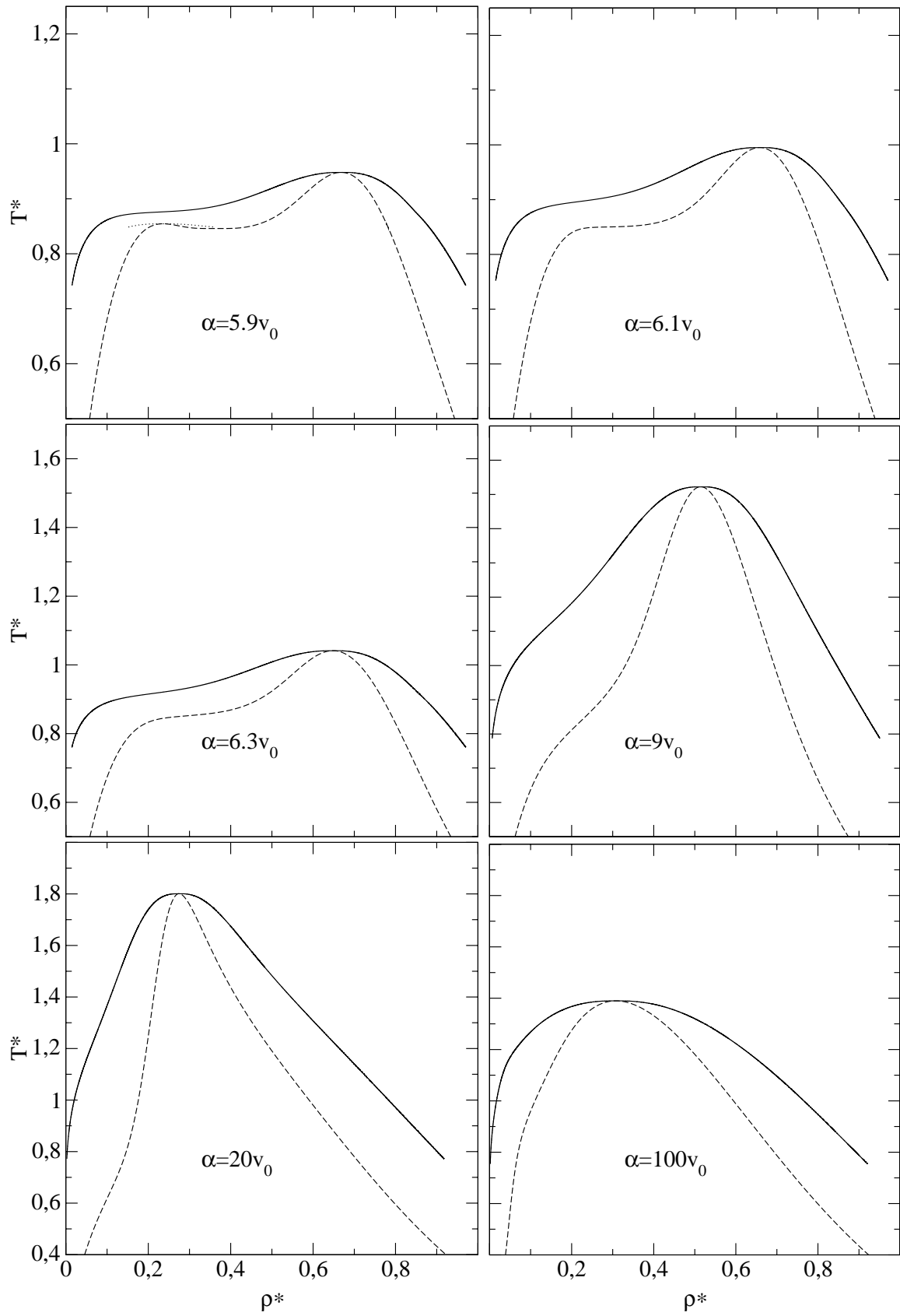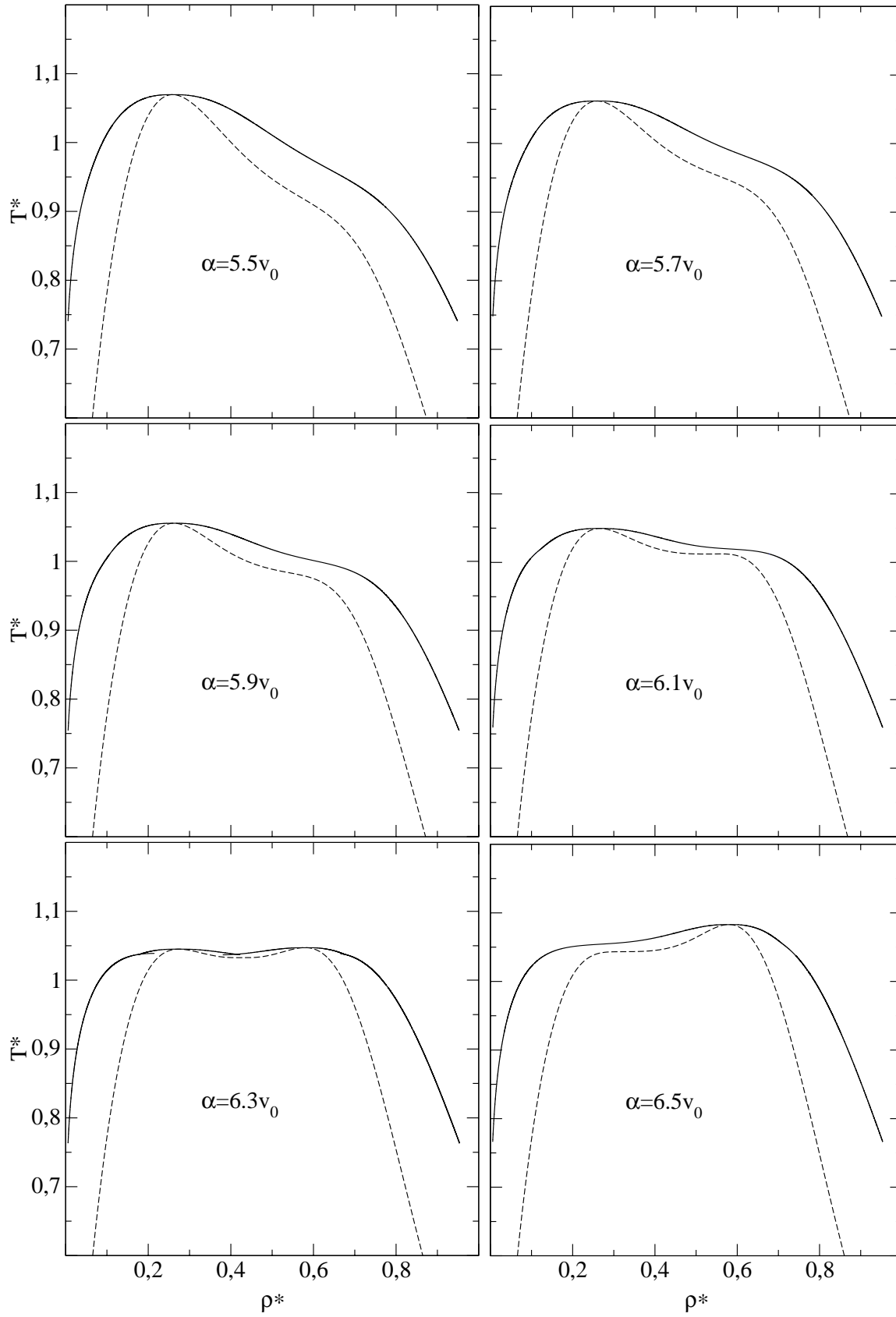
Figure 4.13: The same as in fig. (4.12) for $z_0\sigma = 1.8$.

Figure 4.14: The same as in fig. (4.12) for $z_0\sigma = 1.7$.
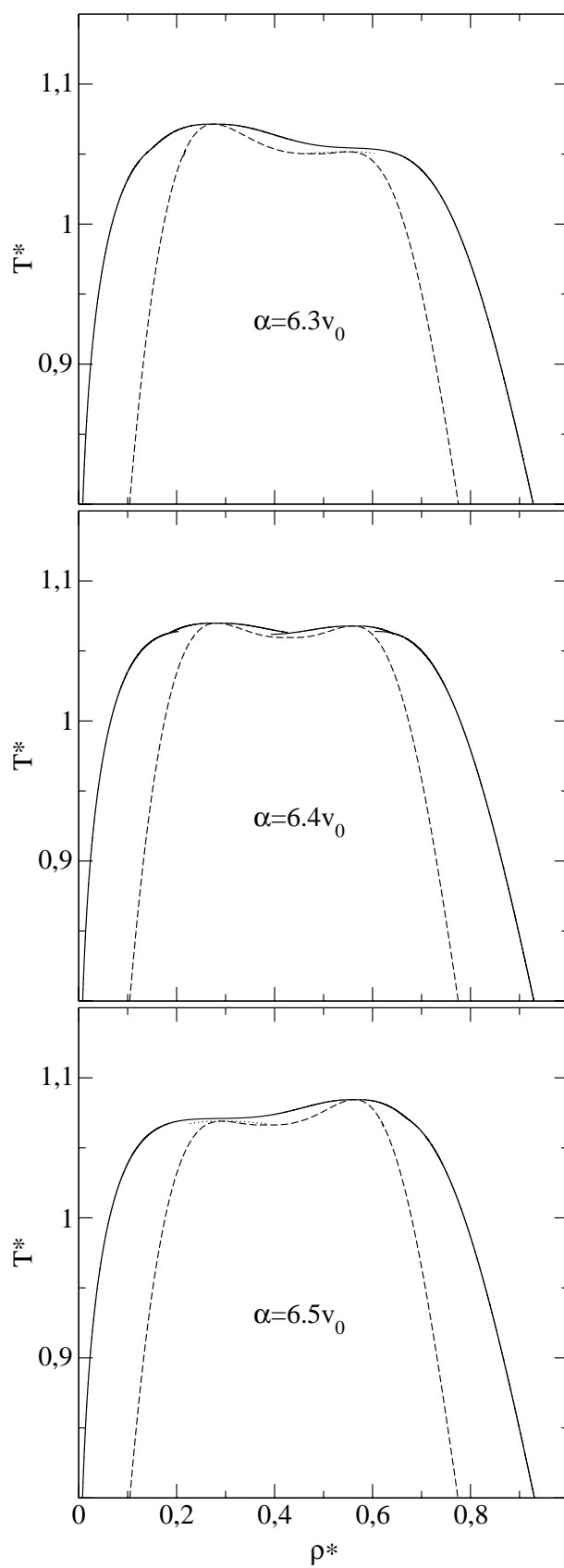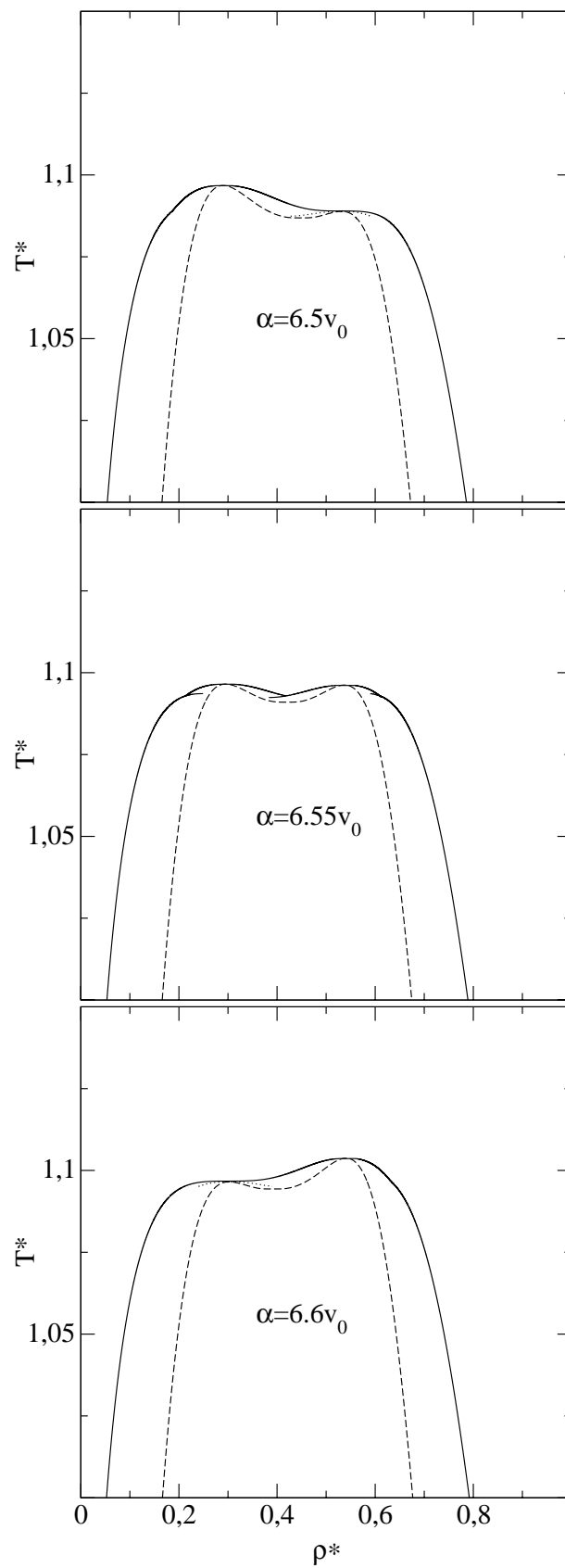
Figure 4.15: The same as in fig. (4.12) for $z_0\sigma = 1.69$.

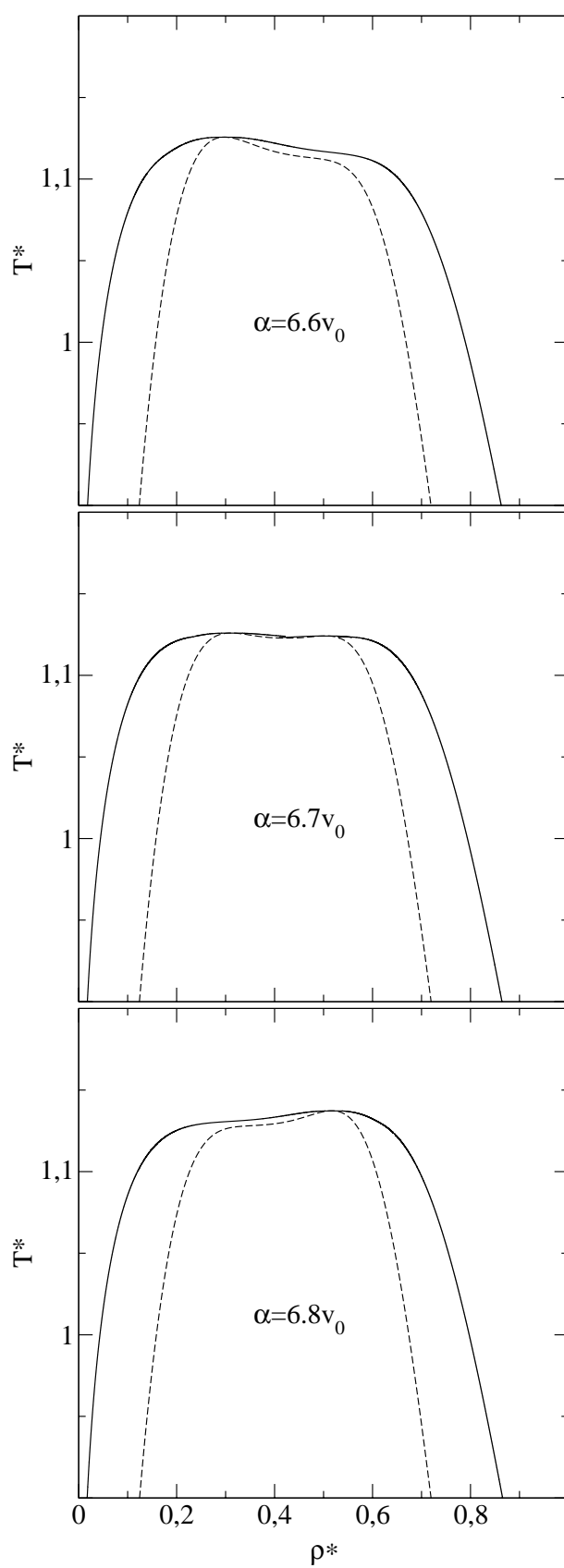Figure 4.16: The same as in fig. (4.12) for $z_0\sigma = 1.68$.

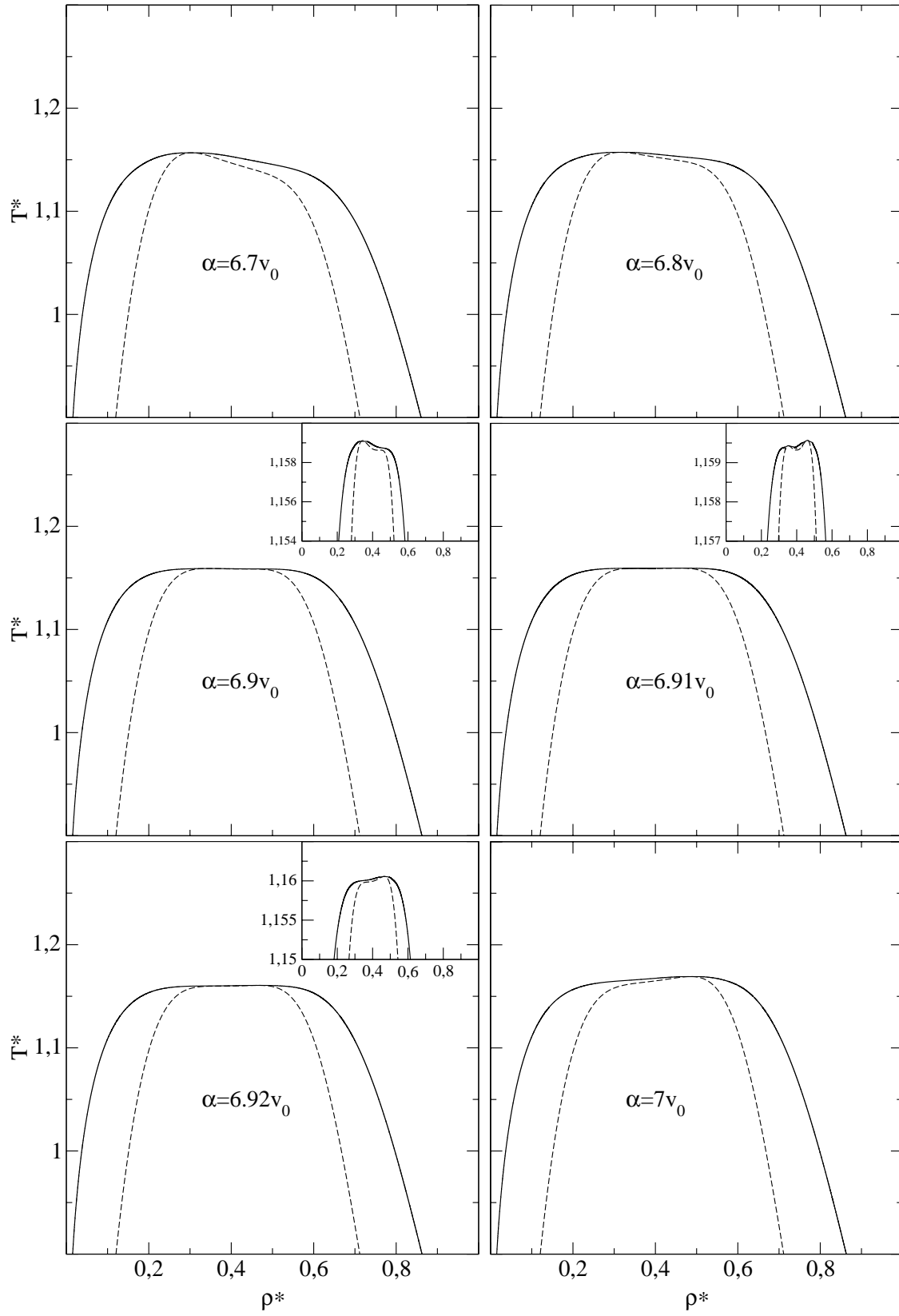Figure 4.17: The same as in fig. (4.12) for $z_0\sigma = 1.67$.

Figure 4.18: The same as in fig. (4.12) for $z_0\sigma = 1.66$. In the case the coexistence curves are very flat near the critical point, the insets show details on a different scale.
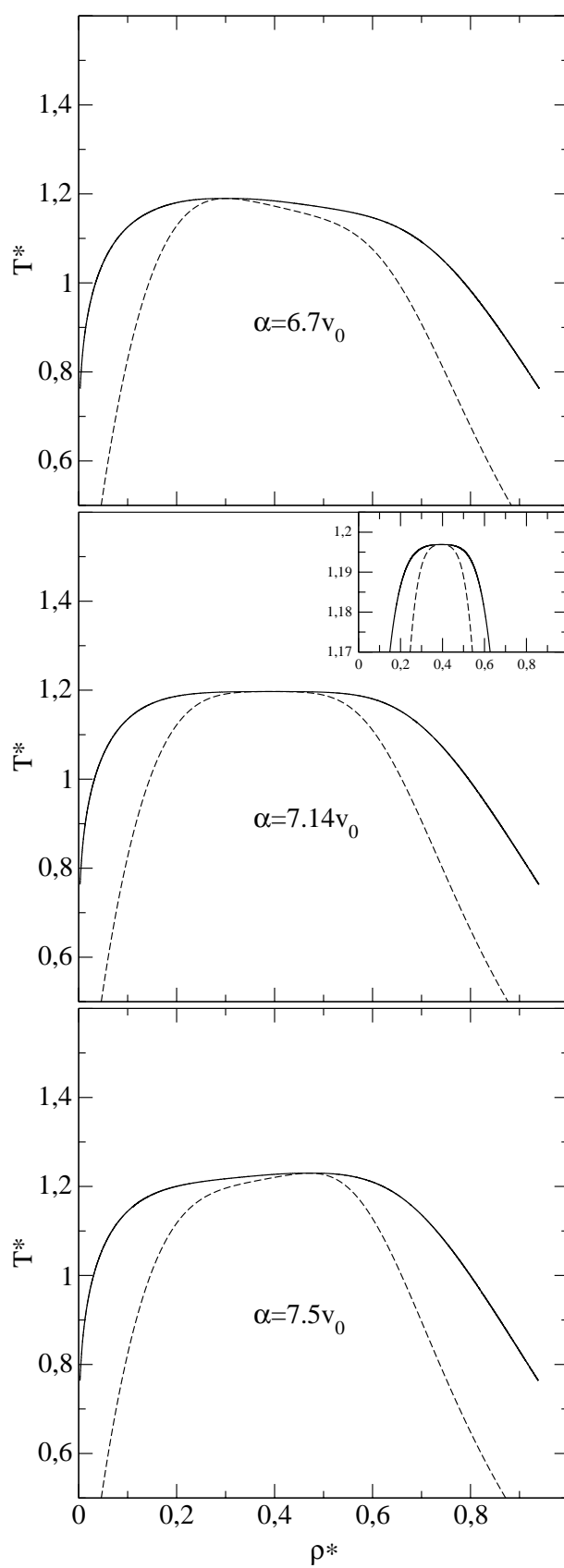
Figure 4.19: The same as in fig. (4.12) for $z_0\sigma = 1.65$.

of α is increased from $\alpha = 0$ (where $z(\rho)\sigma = 1.8$) to $\alpha = 100v_0$; $v_0 = \frac{\pi\sigma^3}{6}$ is the HS volume. In the limit $\alpha \to \infty$ the case $z(\rho)\sigma = 1.6$ is recovered: so the phase diagram for $\alpha = 100v_0$ and $z_0\sigma = 1.8$ should be close to the one of fig. 4.11 ($z_0\sigma = 1.6$).

If we consider the series $z_0\sigma = 1.8$ we observe one critical point and, as α is increased from 0 to $3v_0$, that $\rho_c^\star$ and $T_c^\star$ decrease. For $\alpha = 5.1v_0$ a shoulder appears on the high-density side of the liquid-vapor coexistence curve, which becomes more pronounced when further increasing α, so that at $\alpha = 5.3v_0$ a metastable critical point of a liquid-liquid transition occurs, turning into a stable one at $\alpha = 5.5v_0$. At $\alpha = 5.7v_0$ the temperature of the low-density critical point is lowered and at $\alpha \sim 5.9v_0$ this critical point turns into a metastable one. When further increasing α this critical point becomes a shoulder on the low density side of the coexistence curve which gradually vanishes as α becomes larger. The remaining single critical point shifts, as further increasing α, dramatically to smaller $\rho^\star$-values. The parameters of the critical points are given in table (4.7). The density difference of the two critical points is approximately $\rho_{c,2}^\star - \rho_{c,1}^\star \sim 0.68 - 0.23 = 0.45$ for $\alpha v_0 = 5.5$ and remains nearly constant over the α-range where double criticality occurs. Note the non-monotonic behavior of $\rho_{2,c}^\star$ and $T_{2,c}^\star$ as α is increased.

α/v_0	$\rho_{c,1}^\star$	$T_{c,1}^\star$	$\rho_{c,2}^\star$	$T_{c,2}^\star$
0	0.314	1.219		
3	0.267	1.033		
5.1	0.231	0.894		
5.3	0.230	0.883	$0.679^\diamond$	$0.806^\diamond$
5.5	0.230	0.872	0.681	0.853
5.7	0.232	0.863	0.676	0.900
5.9	$0.238^\diamond$	$0.855^\diamond$	0.668	0.948
6.1			0.658	0.995
6.3			0.648	1.041
9			0.514	1.522
20			0.275	1.801
100			0.308	1.390
∞			0.306	1.392

Table 4.7: Parameters of the critical points $(\rho_c^\star, T_c^\star)$ of a fluid with a density-dependent pair potential given by eqs. (4.88) and (4.89) for $z_0\sigma = 1.8$. Metastable critical points are marked with a diamond.

A similar sequence of phase diagrams is found for $z_0\sigma = 1.7$; it is depicted in fig. (4.14).

α/v_0	$\rho_{c,1}^\star$	$T_{c,1}^\star$	$\rho_{c,2}^\star$	$T_{c,2}^\star$
0	0.310	1.299		
3	0.283	1.185		
5.5	0.259	1.070		
5.7	0.260	1.062		
5.9	0.262	1.055		
6.1	0.266	1.050		
6.3	0.274	1.045	0.579	1.047
6.5			0.580	1.083
9			0.488	1.442
100			0.307	1.391

Table 4.8: The same as in table (4.7) for $z_0\sigma = 1.7$.

As we increase α the two stable critical points first appear now at $\alpha \sim 6.3 v_0$ and the difference of the critical point densities $\rho_{c,2}^\star - \rho_{c,1}^\star \sim 0.58 - 0.27 = 0.31$ is smaller than in the previous case. The parameters of the critical points are given in table 4.8.

We have then produced further series of phase diagrams for $z_0\sigma = 1.69, z_0\sigma = 1.68, z_0\sigma = 1.67$ and $z_0\sigma = 1.66$ (see figs. (4.15)- (4.18)): in all cases two critical points were found for different α-values, i.e., at $\alpha = 6.4 v_0$, $\alpha = 6.55 v_0$, $\alpha = 6.7 v_0$ and $\alpha = 6.91 v_0$, respectively. For $z_0\sigma = 1.66$ the two critical points are no longer well separated, the density difference being now only $\rho_{c,2}^\star - \rho_{c,1}^\star \sim 0.46 - 0.35 = 0.11$. Furthermore the α-range, where double criticality occurs is very limited compared to the previous cases.

If we further decrease $z_0\sigma$ to 1.65 where only a weak ρ-dependence of the Yukawa screening length $z(\rho)\sigma$ is observed (see fig. (4.9)) the two critical points merge, resulting in a very flat coexistence curve for $\alpha = 7.14 v_0$. A preliminary study of the critical exponent

$z_0\sigma$	α/v_0	$\rho_{c,1}^\star$	$\rho_{c,2}^\star$	$\rho_{c,2}^\star - \rho_{c,1}^\star$
1.8	5.5	0.230	0.681	0.451
1.7	6.3	0.274	0.579	0.305
1.69	6.4	0.282	0.559	0.277
1.68	6.55	0.295	0.537	0.242
1.67	6.7	0.311	0.504	0.193
1.66	6.91	0.353	0.460	0.107

Table 4.9: Density difference of the two critical points for different z_0 values.

β has shown that $\beta \sim 1/4$ - the value of a tricritical point that occurs when two order parameters vanish at the same time [97].

To conclude the parameter α triggers the appearance and position of a shoulder on the high- and low-density side of the coexistence curve, the existence of a metastable or stable second critical point - if the z_0 value allows a second critical point - while z_0 triggers the existence of two critical points and - if two critical points are present - their density difference. Table (4.9) shows the density difference of the two critical point for different z_0 values and fig. (4.20) the α-range where double criticality occurs as a function of z_0.
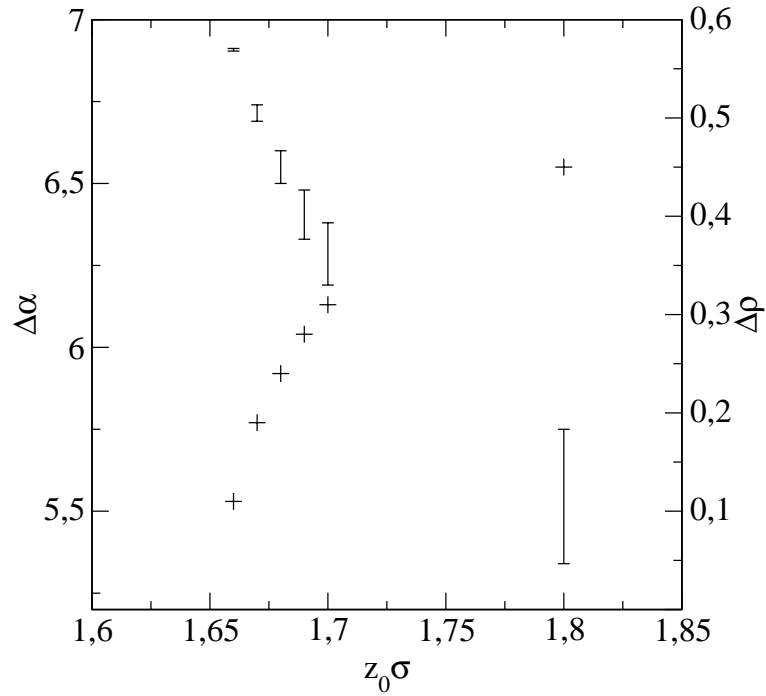

Figure 4.20: Bars (lefthand-side scale): range of the values of α where double criticality occurs as a function of $z_0\sigma$. Pluses (righthand-side scale): density difference of the two critical points as a function of $z_0\sigma$.

4.3 SCOZA for a Binary Symmetric Fluid

For the one-component Yukawa fluid the SCOZA provides very accurate predictions for the thermodynamic properties and the phase diagrams as was demonstrated recently in a comparison with Monte Carlo simulations [59]. As one can expect this promising approach to be of similar accuracy in the case of fluid mixtures, it is of interest to study the SCOZA for a simple model system, namely the binary symmetric fluid (see section 3.1.3) that exhibits - due to the competition between fluid demixing and liquid-vapor phase transition - already a rich phase behavior (see [12]).

4.3.1 Basics

Here we consider a binary symmetric HC1Y mixture. The expression for ϕ_{11} is then

$$\phi_{11}(r) = \begin{cases} \infty & r \leq 1 \\ -\frac{e^{-z_2(r-1)}}{r} & r > 1 \end{cases}, \qquad (4.90)$$

where z_2 is the screening length of the potential; the hard-sphere diameter σ and the interaction strength of the attractive tail ϵ_{11} have been set equal to unity. Thus the usual reduced quantities $\rho_i^\star = \rho_i \sigma^3$, where ρ_i are the partial densities, $\rho^\star = \rho \sigma^3$ and $T^\star = \frac{kT\sigma}{\epsilon_{11}}$ can be identified as ρ_i, ρ and kT. To describe the thermodynamic state of the system we further introduce the concentration of species 1, $x = \frac{\rho_1}{\rho}$ and the packing fraction $\eta = \frac{\pi}{6}\rho$.

For this system the closure relation to the OZ relations for a mixture (2.27) in the MSA is

$$\begin{cases} g_{ij}(r) = 0 & r \leq 1 \\ c_{ij}(r) = -\beta \phi_{ij}(r) & r > 1 \end{cases}. \qquad (4.91)$$

In the version of the SCOZA considered here the closure relation reads

$$\begin{cases} g_{ij}(r) = 0 & r \leq 1 \\ c_{ij}(r) = c_{ij}^{\text{HS}}(r) + K_2^{ij}\phi_{ij}(r) & r > 1 \end{cases}, \qquad (4.92)$$

introducing state dependent parameters K_2^{ij} as multipliers of the $\phi_{ij}(r)$-term of the MSA outside the core. Further we add a second term that represents the pure hard-sphere direct correlation function $c_{ij}^{HS}(r)$. The SCOZA closure (4.92) reduces to the one of the MSA (4.91) if we fix $K_2^{ij} = -\beta$ and set $c_{\text{HS}} = 0$ for $r > 1$; in the SCOZA, in contrast, the parameters K_2^{ij} are not fixed a priori but instead are determined so that thermodynamic consistency is partly fulfilled (see below). The HS parts of the direct correlation functions,

$c_{ij}^{\text{HS}}(r)$, are independent of the attractive tails; the fact that the HS reference system ($\sigma_{ij} \equiv \sigma = 1$) is a one-component system yields $c_{ij}^{\text{HS}}(r; \rho, x) \equiv c_{\text{HS}}(r; \rho)$. Hence, we can use again the Waisman parameterization [42] for c_{HS} with its mathematical conveniences.

The parameters $K_2^{ij}(\beta, \rho, x)$ are obtained by requiring that the compressibility and energy route yield thermodynamically self-consistent results. The symmetry relations of the system lead to

$$K_2^{11}(\beta, \rho, x) = K_2^{22}(\beta, \rho, 1 - x) \tag{4.93}$$

$$K_2^{12}(\beta, \rho, x) = K_2^{12}(\beta, \rho, 1 - x). \tag{4.94}$$

We introduce now an additional approximation for the K_2's which has been motivated by the simpler MSA closure

$$
\begin{aligned}
K_2^{11}(\beta, \rho, x) &= K_2^{12}(\beta, \rho, x) \\
&= K_2^{12}(\beta, \rho, 1 - x) = K_2^{11}(\beta, \rho, 1 - x) = K_2^{22}(\beta, \rho, x) \\
&\equiv K_2(\beta, \rho, x) = K_2(\beta, \rho, 1 - x), \tag{4.95}
\end{aligned}
$$

reducing thus the number of unknown functions from three to one which will be denoted by $K_2(\beta, \rho, x)$. Thus the closure relations (4.92) read ($i, j = 1, 2$)

$$
\begin{cases}
g_{ij}(r) = 0 & r < 1 \\
c_{ii}(r) = K_2(\beta, \rho, x)\frac{e^{-z_2(r-1)}}{r} + K_1(\rho)\frac{e^{-z_1(\rho)(r-1)}}{r} & r > 1 \\
c_{12}(r) = \alpha K_2(\beta, \rho, x)\frac{e^{-z_2(r-1)}}{r} + K_1(\rho)\frac{e^{-z_1(\rho)(r-1)}}{r} & r > 1
\end{cases} \tag{4.96}
$$

The SCOZA requires consistency between the compressibility route and the internal energy route. In the latter the relation between the structure and thermodynamic properties of the system is provided by the excess internal energy (over the ideal gas) per unit volume, $u := \frac{U^{ex}}{V}$, given as an integral over the pair potentials weighted by the radial distribution functions (2.29), i.e.,

$$
\begin{aligned}
u &= 2\pi \sum_{ij} \rho_i \rho_j \int \phi_{ij}(r) g_{ij}(r) r^2 dr \tag{4.97} \\
&= -2\pi \rho^2 \int_1^\infty \frac{e^{-z_2(r-1)}}{r} \left[x^2 g_{11}(r) + 2x(1-x)\alpha g_{12}(r) + (1-x)^2 g_{22}(r) \right] r^2 dr \\
&= -2\pi \rho^2 e^{z_2} \left(x^2 \hat{g}_{11}(z_2) + 2x(1-x)\alpha \hat{g}_{12}(z_2) + (1-x)^2 \hat{g}_{22}(z_2) \right),
\end{aligned}
$$

where $\hat{g}_{ij}(z)$ denotes the Laplace transform of $r g_{ij}(r)$.

According to the compressibility route the thermodynamic properties are obtained from the relations (2.31)

$$\rho_1 \frac{\partial \beta \mu_1}{\partial \rho_1} = 1 - \rho_1 \tilde{c}_{11}(k = 0)$$

$$\rho_2 \frac{\partial \beta \mu_2}{\partial \rho_2} = 1 - \rho_2 \tilde{c}_{22}(k=0)$$

$$\rho_1 \frac{\partial \beta \mu_1}{\partial \rho_2} = -\rho_1 \tilde{c}_{12}(k=0)$$

$$\rho_2 \frac{\partial \beta \mu_2}{\partial \rho_1} = -\rho_2 \tilde{c}_{12}(k=0). \tag{4.98}$$

In the case of thermodynamic consistency, i.e., if the thermodynamics stems from a unique Helmholtz free energy density $f = \frac{F}{V}$ one obtains with

$$u = \frac{\partial \beta f^{ex}}{\partial \beta}, \quad \frac{\partial f^{ex}}{\partial \rho_1} = \mu_1^{ex}, \quad \frac{\partial f^{ex}}{\partial \rho_2} = \mu_2^{ex} \tag{4.99}$$

the consistency conditions

$$\frac{\partial^2 u}{\partial \rho_1^2} = \frac{\partial}{\partial \beta} \left(\frac{\partial^2 \beta f^{ex}}{\partial \rho_1^2} \right) = \frac{\partial}{\partial \beta} \left(\frac{\partial \beta \mu_1^{ex}}{\partial \rho_1} \right)$$

$$= \frac{\partial}{\partial \beta} \left(-\tilde{c}_{11}(k=0) \right)$$

$$\frac{\partial^2 u}{\partial \rho_2^2} = \frac{\partial}{\partial \beta} \left(-\tilde{c}_{22}(k=0) \right)$$

$$\frac{\partial^2 u}{\partial \rho_1 \partial \rho_2} = \frac{\partial}{\partial \beta} \left(-\tilde{c}_{12}(k=0) \right). \tag{4.100}$$

Due to the assumption introduced in eq. (4.95) that reduces the number of unknown functions from three to one, only one PDE for the determination of this unknown function is necessary. So instead of the coupled system of PDEs (4.100) we only need one PDE; we have decided to use the following linear combination of the PDEs of (4.100) which leads to the consistency relation between the internal energy route and the reduced isothermal compressibility

$$\rho \frac{\partial^2 u}{\partial \rho^2} = \frac{1}{\rho} \left(\rho_1^2 \frac{\partial^2 u}{\partial \rho_1^2} + 2\rho_1 \rho_2 \frac{\partial^2 u}{\partial \rho_1 \rho_2} + \rho_2^2 \frac{\partial^2 u}{\partial \rho_2^2} \right)$$

$$= \frac{\partial}{\partial \beta} \left(1 - \frac{1}{\rho} \sum_{ij} \rho_i \rho_j \tilde{c}_{ij}(k=0) \right)$$

$$= \frac{\partial}{\partial \beta} \left(\frac{1}{\chi^{red}} \right), \tag{4.101}$$

with

$$\chi^{red} = \left(1 - \frac{1}{\rho} \sum_{ij} \rho_i \rho_j \tilde{c}_{ij}(k=0) \right)^{-1} = \left(\frac{\partial \beta P}{\partial \rho} \right)^{-1}. \tag{4.102}$$

The advantage of the resulting PDE is the fact that we can treat x just as a parameter, i.e. the PDE can be solved independently for different values of x.

The task is now to express χ^{red} as a function of u so that eq. (4.101) becomes a PDE for the internal energy.

4.3.2 Equimolar Binary Symmetric Mixture

First, we consider the simpler equimolar case. If we choose the parameter $\alpha \geq 1$, i.e., the attraction between unlike particles is larger than between like particles, no demixing transition occurs and the liquid-vapor transition is entirely situated in the $x = \frac{1}{2}$ plane. We thus restrict in the following our considerations to the special case where the concentration of the two components is equal, i.e., $\rho_1 = \rho_2 = \frac{\rho}{2}$.

Due to the symmetry relation

$$h_{11}(r; \rho, x = \frac{1}{2}) = h_{22}(r; \rho, x = \frac{1}{2}) \tag{4.103}$$

and introducing correlation functions $h_{\pm}, c_{\pm}$

$$h_{\pm} \quad := \quad \frac{h_{11} \pm h_{12}}{2} \tag{4.104}$$

$$c_{\pm} \quad := \quad \frac{c_{11} \pm c_{12}}{2} \tag{4.105}$$

the OZ equations decouple into two equations, each of them representing an OZ equation of a pure fluid (denoted by + or -)

$$h_{\pm} = c_{\pm} + \rho c_{\pm} \otimes h_{\pm}. \tag{4.106}$$

The closure relations for the linear combinations of the correlation functions now read

$$\begin{cases} h_+(r) = -1 & r < 1 \\ c_+(r) = K_2(\beta, \rho, x)\frac{1+\alpha}{2}\frac{e^{-z_2(r-1)}}{r} + K_1(\rho)\frac{e^{-z_1(\rho)(r-1)}}{r} & r > 1 \end{cases} \tag{4.107}$$

and

$$\begin{cases} h_-(r) = 0 & r < 1 \\ c_-(r) = K_2(\beta, \rho, x)\frac{1-\alpha}{2}\frac{e^{-z_2(r-1)}}{r} & r > 1 \end{cases}. \tag{4.108}$$

The analytic solution of the OZ equation with the closure relation (4.107) for the '+'-system has been studied extensively in [44, 63, 52].

The closure relation for the '-'-system is characterized by a different core condition for $h_-(r)$. Nevertheless, an analytic solution of the OZ equation with closure relation (4.108) can be derived, either via the Laplace transform technique of via the factorization method of Baxter [74]; details of the calculation can be found in Appendix A.

We now introduce $q = \frac{(1+2\eta)^2}{(1-\eta)^2}$ and the quantity

$$f = (1 - \eta)\sqrt{\frac{1}{\chi^{red}}}. \tag{4.109}$$

Thus eq. (4.101) becomes

$$\frac{2f}{(1-\eta)^2}\frac{\partial f}{\partial u}\frac{\partial u}{\partial \beta} = \rho\frac{\partial^2 u}{\partial \rho^2}. \tag{4.110}$$

In an effort to turn this relation into a PDE for u, f has to be expressed as a function of ρ and u. According to Høye and Blum [98] and sticking to the notation used in that article the inverse compressibility via the fluctuation theorem for an equimolar fluid mixture is

$$
\begin{aligned}
\frac{1}{\chi^{red}} &= 1 - \frac{1}{\rho}\sum_{i,j}\rho_i\rho_j\tilde{c}_{ij}(k=0) \\
&= \frac{1}{\rho}\sum_j \rho_j\left(\frac{A_j}{2\pi}\right)^2 = \left(\frac{A_+}{2\pi}\right)^2,
\end{aligned}
\tag{4.111}
$$

where we have used $A_1 = A_+ + A_-$, $A_2 = A_+ - A_-$ and $A_- = 0$ (see eq. (A.8) of Appendix A). Using the analytic expression for A_+ given in [63], f can be written as [59]

$$f = -\frac{(z_1^2 - z_2^2) + 4\sqrt{q}\left(\gamma_2^+ - \gamma_1^+\right)}{4\left(\frac{z_1}{z_2}\gamma_2^+ - \frac{z_2}{z_1}\gamma_1^+\right)} - \frac{z_1^2 - z_2^2}{z_1 z_2}\frac{\gamma_1^+\gamma_2^+\left(\gamma_2^+ - \gamma_1^+\right)}{\left(\frac{z_1}{z_2}\gamma_2^+ - \frac{z_2}{z_1}\gamma_1^+\right)^2} \tag{4.112}$$

where the quantities γ_1^+ and γ_2^+ are given by

$$
\begin{aligned}
\gamma_1^+ &= 2 - \sqrt{q} - \frac{U_1}{U_0} \\
\gamma_2^+ &= 2 - \sqrt{q} - \frac{W_1}{W_0}.
\end{aligned}
\tag{4.113}
$$

The ratio

$$\frac{W_1}{W_0} = \frac{4 + 2z_2 - z_2^2}{2(2 + z_2)}\frac{\tau_2 I_2^+ - 1}{\sigma_2 I_2^+ - 1} \tag{4.114}$$

depends on the integral,

$$I_2^+ = 4\pi\rho\int_1^\infty dr r e^{-z_2(r-1)}g_+(r), \tag{4.115}$$

the expression $\frac{U_1}{U_0}$ is obtained from (4.114) and (4.115) by replacing the index 2 by 1. The quantities τ_i and σ_i depend only on the screening lengths z_i and are given by

$$
\begin{aligned}
\sigma_i &= \frac{1}{2z_i}\left(\frac{z_i - 2}{z_i + 2} + e^{-z_i}\right) \\
\tau_i &= \frac{1}{2z_i}\left(\frac{z_i^2 + 2z_i - 4}{4 + 2z_i - z_i^2} + e^{-z_i}\right) \quad (i = 1, 2).
\end{aligned}
\tag{4.116}
$$
$$\tag{4.117}$$

With (4.115) and with the definition of the integral

$$I^- = 4\pi\rho\int_1^\infty dr r e^{-z_2(r-1)}g_-(r) \tag{4.118}$$

the excess internal energy per unit volume, u, eq. (4.97) can be rewritten as

$$u = -\frac{\rho}{2}\left(\frac{1+\alpha}{2}I_2^+ + \frac{1-\alpha}{2}I^-\right). \tag{4.119}$$

The partial derivative, $\frac{\partial f}{\partial u}$, appearing in eq. (4.110) now becomes

$$\frac{\partial f}{\partial u} = \frac{\partial f}{\partial \gamma_1^+}\frac{\partial \gamma_1^+}{\partial u} + \frac{\partial f}{\partial \gamma_2^+}\frac{\partial \gamma_2^+}{\partial u}. \tag{4.120}$$

In order to determine the derivatives $\frac{\partial \gamma_1^+}{\partial u}$ and $\frac{\partial \gamma_2^+}{\partial u}$ we need additional analytic results. To this end we use a further equation given in [59],

$$\left[4\left(2 - \sqrt{q} - \alpha_1\right)\left(\sqrt{q} - x^+\right) - z_1^2\right]^2$$
$$\left\{4\left(z_2^2 - 4(y^+)^2\right)(y^+ - x^+)^2 - (z_1^2 - z_2^2)(z_1^2 - z_2^2 + 4((y^+)^2 - (x^+)^2))\right\}$$
$$= -\frac{384\eta z_1^4}{(z_1+2)^2(z_1^2-z_2^2)\sigma_1^2}K_1\left(y^+ - x^+\right)^4 \tag{4.121}$$

with

$$x^+ = \sqrt{q} - \frac{z_1^2}{4\gamma_1^+} \tag{4.122}$$

$$y^+ = \sqrt{q} - \frac{z_2^2}{4\gamma_2^+}$$

and

$$\alpha_i = \frac{(4 + 2z_i - z_i^2)\tau_i}{2(2+z_i)\sigma_i} \quad (i = 1,2). \tag{4.123}$$

We write eq. (4.121) formally as $G_1(x^+, y^+, \rho) = 0$, or, with the expressions (4.122) for x^+ and y^+ inserted as $F_1(\gamma_1^+, \gamma_2^+, \rho) = 0$. A second equation can be derived as follows: first, an analog equation to (4.121) including the unknown function K_2 is obtained by exchanging the indices 1 and 2, the quantities x^+ and y^+ and replacing K_1 by $K_2\frac{1+\alpha}{2}$:

$$\left[4\left(2 - \sqrt{q} - \alpha_2\right)\left(\sqrt{q} - y^+\right) - z_2^2\right]^2$$
$$\left\{4\left(z_1^2 - 4(x^+)^2\right)(y^+ - x^+)^2 - (z_1^2 - z_2^2)(z_1^2 - z_2^2 + 4((y^+)^2 - (x^+)^2))\right\}$$
$$= \frac{384\eta z_2^4}{(z_2+2)^2(z_1^2-z_2^2)\sigma_2^2}K_2\frac{1+\alpha}{2}\left(y^+ - x^+\right)^4. \tag{4.124}$$

In the Appendix A it is shown that (A.40)

$$6\eta K_2\frac{1-\alpha}{2} = \left(\frac{1}{4}z_2^2 - (y^-)^2\right)\left(\frac{z_2+2}{z_2^2}\sigma_2\left(4(1-\alpha_2)(1-y^-) - z_2^2\right)\right)^2 \tag{4.125}$$

where

$$y^- = 1 - \frac{z_2^2}{4\gamma_2^-}, \quad \gamma_2^- = 1 - \frac{V_1}{V_0} \tag{4.126}$$

and

$$\frac{V_1}{V_0} = \frac{4 + 2z_2 - z_2^2}{2(2 + z_2)} \frac{\tau_2 I^- - 1}{\sigma_2 I^- - 1}.$$ (4.127)

Elimination of K_2 in eqs. (4.124) and (4.125) yields the second equation

$$\left[4 \left(2 - \sqrt{q} - \alpha_2 \right) \left(\sqrt{q} - y^+ \right) - z_2^2 \right]^2$$
$$\left\{ 4 \left(z_1^2 - 4(x^+)^2 \right) \left(y^+ - x^+ \right)^2 - \left(z_1^2 - z_2^2 \right) \left(z_1^2 - z_2^2 + 4 \left((y^+)^2 - (x^+)^2 \right) \right) \right\}$$
$$= \frac{16}{\left(z_1^2 - z_2^2 \right)} \frac{1 + \alpha}{1 - \alpha} \left(y^+ - x^+ \right)^4 \left(z_2^2 - 4(y^-)^2 \right)$$
$$\left[4 \left(1 - \alpha_2 \right) \left(1 - y^- \right) - z_2^2 \right]^2$$ (4.128)

or schematically written as $G_2(x^+, y^+, y^-, \rho) = 0$, or, $F_2(\gamma_1^+, \gamma_2^+, \gamma_2^-, \rho) = 0$ respectively.

To calculate the derivatives in (4.120) we need to express u as function of γ_2^+ and γ_2^-. Using eqs. (4.113, 4.114, 4.126, 4.127) we obtain with

$$\phi_2 := \frac{2(2 + z_2)}{4 + 2z_2 - z_2^2}$$ (4.129)

$$I_2^+ = \frac{\phi_2 \left(2 - \sqrt{q} - \gamma_2^+ \right) - 1}{\sigma_2 \phi_2 \left(2 - \sqrt{q} - \gamma_2^+ \right) - \tau_2}$$ (4.130)

$$I^- = \frac{\phi_2 \left(1 - \gamma_2^- \right) - 1}{\sigma_2 \phi_2 \left(1 - \gamma_2^- \right) - \tau_2}$$ (4.131)

(4.132)

and thus, via (4.119),

$$u = g(\gamma_2^+, \gamma_2^-, \rho)$$ (4.133)

where

$$g(\gamma_2^+, \gamma_2^-, \rho) = -\frac{\rho}{2} \left(\frac{1 + \alpha}{2} \frac{\phi_2 \left(2 - \sqrt{q} - \gamma_2^+ \right) - 1}{\sigma_2 \phi_2 \left(2 - \sqrt{q} - \gamma_2^+ \right) - \tau_2} + \right.$$
$$\left. \frac{1 - \alpha}{2} \frac{\phi_2 \left(1 - \gamma_2^- \right) - 1}{\sigma_2 \phi_2 \left(1 - \gamma_2^- \right) - \tau_2} \right)$$ (4.134)

Summarizing, we therefore obtain a set of three coupled nonlinear equations

$$F_1 \left(\gamma_1^+, \gamma_2^+, \rho \right) = 0$$
$$F_2 \left(\gamma_1^+, \gamma_2^+, \gamma_2^-, \rho \right) = 0$$
$$u - g(\gamma_2^+, \gamma_2^-, \rho) = 0$$ (4.135)

For given values of ρ and u the zeros of these equations yield γ_1^+, γ_2^+ and γ_2^- in terms of ρ and u.

Eqs. (4.135) are solved numerically with respect to γ_1^+, γ_2^+ and γ_2^- by a Newton-Raphson method. The partial derivatives $\frac{\partial \gamma_1^+}{\partial u}, \frac{\partial \gamma_2^+}{\partial u}$ are determined implicitly through

$$
\begin{pmatrix} \frac{\partial \gamma_1^+}{\partial u} \\ \frac{\partial \gamma_2^+}{\partial u} \\ \frac{\partial \gamma_2^-}{\partial u} \end{pmatrix} = \begin{pmatrix} \frac{\partial F_1}{\partial \gamma_1^+} & \frac{\partial F_1}{\partial \gamma_2^+} & 0 \\ \frac{\partial F_2}{\partial \gamma_1^+} & \frac{\partial F_2}{\partial \gamma_2^+} & \frac{\partial F_2}{\partial \gamma_2^-} \\ 0 & \frac{\partial g}{\partial \gamma_2^+} & \frac{\partial g}{\partial \gamma_2^-} \end{pmatrix}^{-1} \begin{pmatrix} 0 \\ 0 \\ 1 \end{pmatrix}.
\tag{4.136}
$$

Thus eq. (4.110) takes the form

$$
B(\rho, u)\frac{\partial u}{\partial \beta} = C(\rho, u)\frac{\partial^2 u}{\partial \rho^2}
\tag{4.137}
$$

with

$$
\begin{aligned}
B(\rho, u) &= \frac{2f}{(1-\eta)^2}\left[\frac{\partial f}{\partial \gamma_1^+}\frac{\partial F_1}{\partial \gamma_2^+} - \frac{\partial f}{\partial \gamma_2^+}\frac{\partial F_1}{\partial \gamma_1^+}\right]\frac{\partial F_2}{\partial \gamma_2^-} \\
C(\rho, u) &= \rho\left[\left(\frac{\partial F_1}{\partial \gamma_1^+}\frac{\partial F_2}{\partial \gamma_2^+} - \frac{\partial F_2}{\partial \gamma_1^+}\frac{\partial F_1}{\partial \gamma_2^+}\right)\frac{\partial g}{\partial \gamma_2^-} - \frac{\partial F_1}{\partial \gamma_1^+}\frac{\partial F_2}{\partial \gamma_2^-}\frac{\partial g}{\partial \gamma_2^+}\right].
\end{aligned}
\tag{4.138}
$$

All the partial derivatives in eqs. (4.138) are calculated at constant ρ and can be determined analytically using

$$
\frac{\partial F_1}{\partial \gamma_1^+} = \frac{\partial G_1}{\partial x^+}\frac{\partial x^+}{\partial \gamma_1^+} \quad \text{etc.}
\tag{4.139}
$$

The resulting expressions are evaluated at those values of γ_1^+, γ_2^+ and γ_2^- which are solutions of the system of nonlinear equations (4.135) for given values of ρ and u.

The PDE (4.137) is a non-linear parabolic equation that was solved numerically as explained in [54] on $(\beta, \rho) \in [0, \beta_f] \times [0, \rho_0]$. The initial condition and the boundary conditions of the PDE have been chosen as in [59]. For $\beta = 0$, we take $g_+ = g_{\mathrm{HS}}$ and $g_- = 0$, hence

$$
\begin{aligned}
u(\rho, \beta = 0) &= -2\pi\rho^2\frac{1+\alpha}{2}\int_1^\infty dr\, r e^{-z_2(r-1)} g_{\mathrm{HS}}(r) \tag{4.140} \\
u(\rho = 0, \beta) &= 0 \quad \forall \beta \tag{4.141} \\
\frac{\partial^2 u(\rho_0, \beta)}{\partial \rho^2} &= \frac{\partial^2 u(\rho_0, \beta = 0)}{\partial \rho^2} \quad \forall \beta \tag{4.142}
\end{aligned}
$$

In addition, u in eq. (4.140) can be determined analytically: in fact, for $\beta = 0$, $\gamma_1^+(\rho)$ is known explicitly (see Appendix A of [59]). One can solve eq. (4.112) for γ_2^+ as a function

of γ_1^+, f and ρ. If we use the CS expression for χ^{red} to obtain $f(\beta = 0)$ then $\gamma_2^+(\rho, \beta = 0)$ is known. Since $K_2(\rho, \beta = 0) = 0$ we obtain from eq. (4.125)

$$y^-(\beta = 0) = -\frac{1}{2} z_2 \tag{4.143}$$

and with eq. (4.126)

$$\gamma_2^-(\beta = 0) = \frac{z_2^2}{2(2 + z_2)}. \tag{4.144}$$

This yields with eq. (4.133) $u(\rho, \beta = 0)$.

The unphysical region bounded by the spinodal curves where the compressibility diverges, i.e., where f vanishes, is excluded from the integration. Thus below the critical temperature ($\beta > \beta_c$) the PDE is solved in the low and high density physical region where $f > 0$ separately with the additional boundary conditions

$$u(\rho_{S_i}, \beta) = u_S(\rho_{S_i}) \quad i = 1, 2, \quad \beta > \beta_c \tag{4.145}$$

where ρ_{S_1} and ρ_{S_2} are approximates for the densities of the low and high-density branch of the spinodal where $f = 0$. $u_S(\rho)$ - the value of the excess internal energy at density ρ where the compressibility diverges - is determined in the following way: By setting $f = 0$ in eq. (4.112) one obtains $\gamma_1^+ = \gamma_1^+(\rho, \gamma_2^+)$. Inserting this expression in eq. (4.121) one obtains a nonlinear equation for γ_2^+. The solution of this equation allows one to determine the value of $\gamma_2^+(\rho)$ when $f = 0$ thus yielding via the relation $\gamma_1^+ = \gamma_1^+(\rho, \gamma_2^+)$ the corresponding value of $\gamma_1^+(\rho)$ for $f = 0$. If these values of $\gamma_1^+(\rho)$ and $\gamma_2^+(\rho)$ are inserted in eq. (4.128) one obtains a nonlinear equation for γ_2^-. Its solution inserted in eq. (4.133) finally yields $u_S(\rho)$.

The pressure P and chemical potentials μ_1 and μ_2 are obtained by integration of

$$\frac{\partial \beta \mu_1}{\partial \beta} = \frac{\partial}{\partial \beta} \frac{\partial \beta f}{\partial \rho_1} = \frac{\partial}{\partial \rho_1} \frac{\partial \beta f}{\partial \beta} = \frac{\partial u}{\partial \rho_1} \tag{4.146}$$

$$\frac{\partial \beta \mu_2}{\partial \beta} = \frac{\partial u}{\partial \rho_2} \tag{4.147}$$

$$\frac{\partial \beta P}{\partial \beta} = -u + \rho \frac{\partial u}{\partial \rho} \tag{4.148}$$

$$\tag{4.149}$$

with respect to β. Thus

$$\frac{\partial u}{\partial \rho} = x \frac{\partial u}{\partial \rho_1} + (1 - x) \frac{\partial u}{\partial \rho_2} = x \frac{\partial \beta \mu_1}{\partial \beta} + (1 - x) \frac{\partial \beta \mu_2}{\partial \beta}$$

$$= \frac{\partial \beta \mu_1}{\partial \beta} \tag{4.150}$$

In the last equation of (4.150) we set $x = \frac{1}{2}$ and we have used $\mu_1(x = \frac{1}{2}) = \mu_2(x = \frac{1}{2})$. For the values of the thermodynamic quantities at $\beta = 0$ we have used the CS expressions.
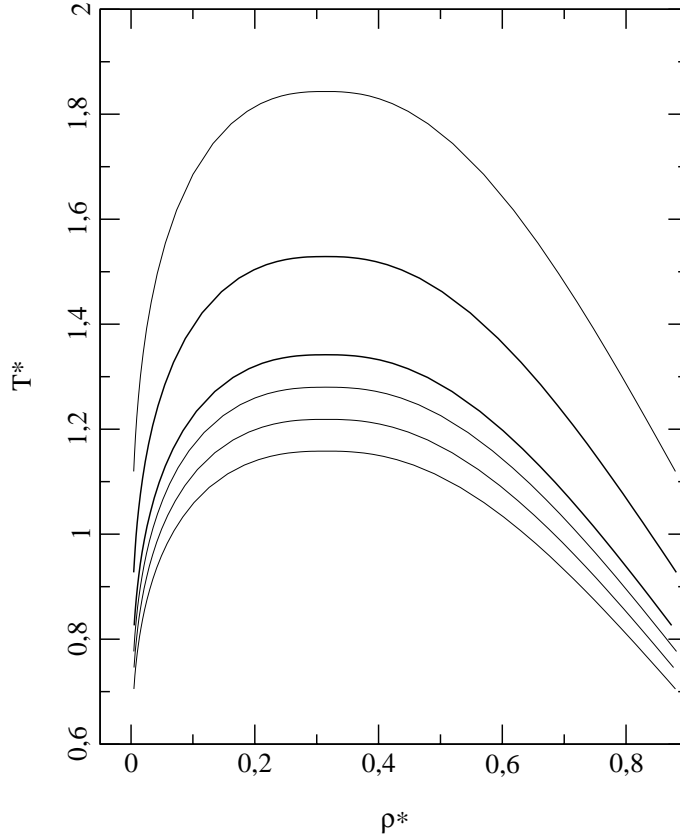
4.3.3   Results

Figure 4.21: Coexistence curves of the equimolar hard-core Yukawa fluid with screening length $z\sigma = 1.8$ in the temperature-density plane for different values of the interaction ratio α. From top to bottom: $\alpha = 2, 1.5, 1.2, 1.1, 1.0, 0.9$.

We consider mixtures with different relative interaction strengths α ranging from $\alpha = 2$, over $\alpha = 1$ to $\alpha = 0.9$. In the first case, $\alpha = 2$, the unlike interaction dominates the like interaction, for $\alpha = 1$ the mixture reduces to a one-component system, while for $\alpha = 0.9$ the like interaction weakly dominates the unlike one. However, the dominance of the like interaction, that triggers the demixing of the fluid mixture is still too weak to lead to a demixing transition within the density and temperature range that is explored, hence the coexisting vapor and fluid phases are both equimolar. In all calculations we set $z\sigma = 1.8$. Table (4.10) shows the values $(\rho_c^\star, T_c^\star)$ of the critical points for the different α values and fig. (4.21) shows the binodal curves. It appears that when α decreases the binodal curve shifts downward with a decrease of the critical temperature from $T_c^\star = 1.843$ at $\alpha = 2$ to $T_c^\star = 1.158$ at $\alpha = 0.9$, respectively. The influence of the variation of α on the critical density $\rho_c^\star$ is much smaller; in fact $\rho_c^\star = 0.313$ and $\rho_c^\star = 0.314$ at $\alpha = 2$ and $\alpha = 0.9$,

respectively. Similar tendencies have been reported in a study by Caccamo *et al.* in [99] using the MHNC theory.

α	2	1.5	1.2	1.1	1	0.9
$\rho_c^\star$	0.313	0.314	0.314	0.314	0.314	0.314
$T^\star$	1.843	1.529	1.342	1.280	1.219	1.158

Table 4.10: Critical densities and temperatures for the equimolar hard-core Yukawa fluid for different values of the interaction ratio α.
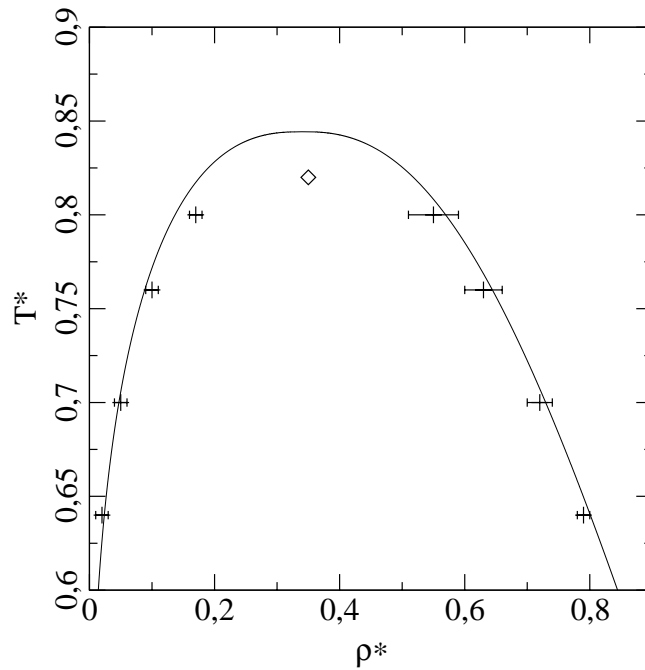

Figure 4.22: Coexistence curve of the equimolar hard-core Yukawa fluid with screening length $z = 2.45$ and interaction ratio $\alpha = 0.90$ in the temperature-density plane. Full line: SCOZA results. Pluses: GEMC results from Caccamo *et al.* [99]. The interpolated estimate of the critical point from MC results is given by a diamond. Statistical uncertainties in the simulation are shown by horizontal bars.

In fig. (4.22) we compare the SCOZA binodal curve for $\alpha = 0.9$ and screening length $z\sigma = 2.45$ with GEMC simulation results reported in [99]. The density of the coexisting liquid phase is slightly overestimated both in the SCOZA and in the MHNC theory [99]. The MC and MHNC results bracket the SCOZA results. A similar behavior was reported in [49] for the one-component fluid.

4.3.4   General Binary Symmetric Fluid

If the unlike particle attraction is weaker than the like particle interactions, i.e., $\alpha < 1$, coexistence of phases of different compositions in the high-density region of the phase diagram will appear. Thus we have to extend our considerations from the $x = \frac{1}{2}$ case to arbitrary values of x. Again we found it convenient to base the formulation of the SCOZA on Baxter's factorization method that has already been extended to mixtures with arbitrary number of components [100] and applied by Blum *et al.* [98] to the case of a mixture with Yukawa closure. Arrieta *et al.* have provided numerical solution algorithms for (multi-)Yukawa [101, 75] multi-component mixtures.

Using Baxter's factorization method the OZ equations for mixtures eqs. (2.27) become (with the simplification $\sigma_i = \sigma_j = \sigma$)

$$2\pi r c_{ij}(r) = -Q'_{ij}(r) + \sum_l \rho_l \int_0^\infty Q_{jl}(t) Q'_{il}(r+t) dt \qquad (4.151)$$

$$2\pi r h_{ij}(r) = -Q'_{ij}(r) + 2\pi \sum_l \rho_l \int_0^\infty (r-t) h_{il}(|r-t|) Q_{lj}(t) dt.$$

We use the latin indices to denote the m fluid components while Greek indices designate the n different Yukawa tails. Summation over a latin and a greek index corresponds to a summation over all components and Yukawa tails, i.e.,

$$\sum_l = \sum_{l=1}^m \quad \text{and} \quad \sum_\nu = \sum_{\nu=1}^n. \qquad (4.152)$$

If these equations are supplemented by the hard-core multi-Yukawa closure

$$\begin{aligned} h_{ij}(r) &= -1 & r < \sigma \\ c_{ij}(r) &= \sum_\nu \widetilde{K}_{\nu ij} \frac{e^{-z_\nu(r-\sigma)}}{r} & r > \sigma, \end{aligned} \qquad (4.153)$$

the factor functions must have the following form:

$$Q_{ij}(r) = Q_{ij}^0(r) + \sum_\nu \frac{1}{z_\nu} D_{\nu ij} e^{-z_\nu(r-\sigma)}, \qquad (4.154)$$

with

$$Q_{ij}^0(r) = \begin{cases} \frac{a_{ij}}{2}(r-\sigma)^2 + b_{ij}(r-\sigma) + \sum_\nu \frac{1}{z_\nu} C_{\nu ij} \left(e^{-z_\nu(r-\sigma)} - 1 \right) & 0 < r < \sigma \\ 0 & \sigma < r \end{cases}. \qquad (4.155)$$

Following Arrieta *et al.* [75] one can show that the unknown coefficients $a_{ij}, b_{ij}, C_{\nu ij}$ can be expressed in terms of $G_{\nu ij} := z_\nu \hat{g}_{ij}(z_\nu) e^{z_\nu \sigma}$ and $D_{\nu ij}$ which satisfy a coupled set of

$2m \cdot m \cdot n$ nonlinear equations

$$\sum_{\tau lmk} A^{(1)}_{\tau \nu mkjl} G_{\tau km} D_{\tau ml} D_{\nu il} + \sum_{\tau lm} A^{(2)}_{\tau \nu mjl} D_{\tau ml} D_{\nu il} + \sum_{l} A^{(3)}_{\nu jl} D_{\nu il} + A^{(4)}_{\nu ij} = 0$$

$$(4.156)$$

$$\sum_{\tau lmk} B^{(1)}_{\tau \nu mklj} G_{\tau km} D_{\tau mj} G_{\nu il} + \sum_{\tau mk} B^{(2)}_{\tau \nu mkij} G_{\tau km} D_{\tau mj}$$

$$+ \sum_{\tau lm} B^{(3)}_{\tau \nu mlj} D_{\tau mj} G_{\nu il} + \sum_{\tau m} B^{(4)}_{\tau \nu mij} D_{\tau mj} + \sum_{l} B^{(5)}_{\nu lj} G_{\nu il} + B^{(6)}_{\nu ij} = 0$$

$$\nu = 1, \ldots, n \quad i, j = 1, \ldots, m$$

$$(4.157)$$

where the only energy-dependent coefficient in the above equation is

$$A^{(4)}_{\nu ij} = 2\pi \widetilde{K}_{\nu ij}.$$

$$(4.158)$$

All other coefficients are calculated from the ρ_i, z_ν and σ, i.e., from the remaining system parameters. Expressions for these coefficients are compiled in Appendix A of [75]. The second system of equations, (4.157), is linear in $\mathbf{D} = \{D_{\nu ij}\}$ for given $\mathbf{G} = \{G_{\nu ij}\}$ and can be written as

$$\sum_{\tau m} O_{\tau \nu mij} D_{\tau mj} = Q_{\nu ij}$$

$$(4.159)$$

with

$$O_{\tau \nu mij}(\rho, \mathbf{G}) = \sum_{lk} B^{(1)}_{\tau \nu mklj} G_{\tau km} G_{\nu il} + \sum_{k} B^{(2)}_{\tau \nu kij} G_{\tau km} + \sum_{l} B^{(3)}_{\tau \nu mlj} G_{\nu il} + B^{(4)}_{\tau \nu mij} \quad (4.160)$$

and

$$Q_{\nu ij}(\rho, \mathbf{G}) = -\sum_{l} B^{(5)}_{\nu lj} G_{\nu il} - B^{(6)}_{\nu ij}.$$

$$(4.161)$$

One can choose the order of the $\{D_{\nu ij}\}$ and $\{Q_{\nu ij}\}$ in the vectors $\mathbf{D}$ and $\mathbf{Q}$ in such a way that the coefficient matrix $\mathbf{O}$ of the linear system (4.159) has a block diagonal form consisting of m blocks of dimension $m \cdot n$. For instance for the binary 2-Yukawa fluid ($m = 2, n = 2$) one obtains

$$\mathbf{O} \cdot \mathbf{D} = \mathbf{Q}$$

$$(4.162)$$

with

$$
\mathbf{O} = \begin{pmatrix}
O_{11111} & O_{21111} & O_{11211} & O_{21211} & 0 & 0 & 0 & 0 \\
O_{11121} & O_{21121} & O_{11221} & O_{21221} & 0 & 0 & 0 & 0 \\
O_{12111} & O_{22111} & O_{12211} & O_{22211} & 0 & 0 & 0 & 0 \\
O_{12121} & O_{22121} & O_{12221} & O_{22221} & 0 & 0 & 0 & 0 \\
0 & 0 & 0 & 0 & O_{11112} & O_{21112} & O_{11212} & O_{21212} \\
0 & 0 & 0 & 0 & O_{11122} & O_{21122} & O_{11222} & O_{21222} \\
0 & 0 & 0 & 0 & O_{12112} & O_{22112} & O_{12212} & O_{22212} \\
0 & 0 & 0 & 0 & O_{12122} & O_{22122} & O_{12222} & O_{22222}
\end{pmatrix}
\tag{4.163}
$$

and

$$
\begin{aligned}
\mathbf{Q}^T &= (Q_{111}, Q_{121}, Q_{211}, Q_{221}, Q_{112}, Q_{122}, Q_{212}, Q_{222}) & (4.164) \\
\mathbf{D}^T &= (D_{111}, D_{211}, D_{121}, D_{221}, D_{112}, D_{212}, D_{122}, D_{222}). & (4.165)
\end{aligned}
$$

Solving this system of $m \cdot m \cdot n$ linear equations (4.162) yields $\mathbf{D}(\rho, \mathbf{G})$.

In the formulation of the SCOZA we will also need the derivatives $\frac{\partial \mathbf{D}}{\partial \mathbf{G}}(\rho, \mathbf{G})$ which are obtained via implicitly differentiating eq. (4.159)

$$
\begin{aligned}
\sum_{\tau m} O_{\tau\nu mij}(\rho, \mathbf{G}) \frac{\partial D_{\tau mj}}{\partial G_{\mu rs}} &= -\sum_{\tau m} \frac{\partial O_{\tau\nu mij}}{\partial G_{\mu rs}}(\rho, \mathbf{G}) D_{\tau mj}(\rho, \mathbf{G}) + \frac{\partial Q_{\nu ij}}{\partial G_{\mu rs}}(\rho, \mathbf{G}) \\
&= -\left(\sum_l B^{(1)}_{\mu\nu srlj} G_{\nu il} + B^{(2)}_{\mu\nu srij} \right) D_{\mu sj}(\rho, \mathbf{G}) \\
&\quad - \left\{ \sum_{\tau m} \left(\sum_k B^{(1)}_{\tau\nu mksj} G_{\tau km} + B^{(3)}_{\tau\nu msj} \right) D_{\tau mj}(\rho, \mathbf{G}) \right. \\
&\qquad\qquad\qquad\qquad \left. - B^{(5)}_{\nu sj} \right\} \delta_{\mu\nu} \delta_{ri}.
\end{aligned}
\tag{4.166}
$$

Thermodynamic quantities required in the PDE of the SCOZA are the inverse reduced isothermal compressibility and the internal energy. The inverse reduced isothermal compressibility calculated via the compressibility route is given by $(x_i = \rho_i/\rho)$ (see [75])

$$
\frac{1}{\chi^{red}} = 1 - \frac{1}{\rho} \sum_{ij} \rho_i \rho_j \tilde{c}_{ij}(k=0) = \sum_j x_j \left(\frac{A_j}{2\pi} \right)^2,
\tag{4.167}
$$

where

$$
A_j = A^0(1 + M_j) - \frac{4}{\sigma^2} B^0 N_j
\tag{4.168}
$$

with

$$
M_j = -\sum_\tau \frac{1}{z_\tau^2} \sum_m \rho_m \left\{ M_\tau^{(a)} D_{\tau mj} + (1 - M_\tau^{(a)} e^{-z_\tau \sigma}) f_{\tau mj} \right\}
$$

$$N_j = \sum_\tau \frac{1}{z_\tau^3} \sum_m \rho_m \left\{ L_\tau^{(a)} D_{\tau m j} + (1 - L_\tau^{(a)} e^{-z_\tau \sigma}) f_{\tau m j} \right\}$$

$$f_{\tau m j} = \frac{2\pi}{z_\tau^2} \sum \rho_k G_{\tau m k} D_{\tau k j}. \qquad (4.169)$$

Expressions for $M_\tau^{(a)}$, $L_\tau^{(a)}$, A^0 and B^0 in terms of ρ_i, z_ν and σ are compiled in the Appendix A of [75]. Inserting the solution of the linear system $\mathbf{D}(\rho, \mathbf{G})$ in the expressions (4.169) yields $A_j(\rho, \mathbf{G})$.

The internal energy via the energy route (4.97) is given by

$$u = -\frac{2\pi\rho^2}{z_2} \left(x^2 G_{211} + \alpha x (1 - x) G_{212} + \alpha x (1 - x) G_{221} + (1 - x)^2 G_{222} \right). \qquad (4.170)$$

If we consider the closure relation of the SCOZA (4.96) we set in eq. (4.153) for the binary 2-Yukawa case ($m = 2, n = 2$)

$$\begin{aligned}
\widetilde{K}_{1ij} &= K_1(\rho) \quad \forall i, j \\
\widetilde{K}_{211} &= \widetilde{K}_{222} = K_2(\rho, x, \beta) \\
\widetilde{K}_{212} &= \widetilde{K}_{221} = \alpha K_2(\rho, x, \beta).
\end{aligned} \qquad (4.171)$$

Inserting $A_j(\rho, \mathbf{G})$ (4.167) in the PDE

$$\frac{\partial}{\partial \beta} \left(\frac{1}{\chi^{red}} \right) = \rho \frac{\partial^2 u}{\partial \rho^2} \qquad (4.172)$$

gives

$$2 \sum_j x_j \frac{A_j}{(2\pi)^2} \sum_{\mu r s} \frac{\partial A_j}{\partial G_{\mu r s}} \frac{\partial G_{\mu r s}}{\partial u} \frac{\partial u}{\partial \beta} = \rho \frac{\partial^2 u}{\partial \rho^2} \qquad (4.173)$$

or

$$B(\rho, u) \frac{\partial u}{\partial \beta} = C(\rho) \frac{\partial^2 u}{\partial \rho^2} \qquad (4.174)$$

with

$$B(\rho, u) = 2 \sum_j x_j \frac{A_j}{(2\pi)^2} \sum_{\mu r s} \frac{\partial A_j}{\partial G_{\mu r s}} \frac{\partial G_{\mu r s}}{\partial u} \qquad (4.175)$$

$$C(\rho) = \rho.$$

We now have to determine A_j, $\frac{\partial A_j}{\partial G_{\mu r s}}$ and $\frac{\partial G_{\mu r s}}{\partial u}$ as functions of ρ and u. In a first step we determine $\mathbf{G}$ for a given value of ρ and u. To this end we establish a set of eight nonlinear equations the solution of which gives $\mathbf{G}(\rho, u)$. The first one is the energy equation (4.170)

$$u + \frac{2\pi\rho^2}{z_2} \left(x^2 G_{211} + \alpha x (1 - x) G_{212} + \alpha x (1 - x) G_{221} + (1 - x)^2 G_{222} \right) = 0 \qquad (4.176)$$

or formally written as $F_1(\rho, G_{211}, G_{212}, G_{221}, G_{222}) = 0$. Further we consider eq. (4.156), with the solution $\mathbf{D}(\rho, \mathbf{G})$ inserted, for $\nu = 1$, $i, j \in \{1, 2\}$ where $A^{(4)}_{1ij} = 2\pi K_1(\rho)$ for $i, j \in \{1, 2\}$, formally written as $F_i(\rho, \mathbf{G}) = 0$ for $i = 2, \ldots, 5$. The remaining three equations are obtained from eq. (4.156) for $\nu = 2$ and eliminating the unknown function $K_2(\rho, x, \beta)$ via the relations

$$
\begin{aligned}
A^{(4)}_{211} &= A^{(4)}_{222} \\
A^{(4)}_{212} &= A^{(4)}_{221} \\
A^{(4)}_{212} &= \alpha A^{(4)}_{211}.
\end{aligned}
\tag{4.177}
$$

For given ρ and u the $\mathbf{G}$ are determined by solving the coupled set of eight nonlinear equations via a Newton-Raphson technique using explicit expressions for the Jacobian. The Jacobi matrix of the system of nonlinear equations in the $\mathbf{G}$ is given by

$$
J = \begin{pmatrix}
0 & 0 & 0 & 0 & \frac{2\pi\rho^2 x^2}{z_2} & \frac{2\pi\rho^2 \alpha x(1-x)}{z_2} & \frac{2\pi\rho^2 \alpha x(1-x)}{z_2} & \frac{2\pi\rho^2 (1-x)^2}{z_2} \\
\frac{\partial F_2}{\partial G_{111}} & \frac{\partial F_2}{\partial G_{112}} & \frac{\partial F_2}{\partial G_{121}} & \frac{\partial F_2}{\partial G_{122}} & \frac{\partial F_2}{\partial G_{211}} & \frac{\partial F_2}{\partial G_{212}} & \frac{\partial F_2}{\partial G_{221}} & \frac{\partial F_2}{\partial G_{222}} \\
\vdots & \vdots & \vdots & \vdots & \vdots & \vdots & \vdots & \vdots \\
\frac{\partial F_8}{\partial G_{111}} & \frac{\partial F_8}{\partial G_{112}} & \frac{\partial F_8}{\partial G_{121}} & \frac{\partial F_8}{\partial G_{122}} & \frac{\partial F_8}{\partial G_{211}} & \frac{\partial F_8}{\partial G_{212}} & \frac{\partial F_8}{\partial G_{221}} & \frac{\partial F_8}{\partial G_{222}}
\end{pmatrix},
\tag{4.178}
$$

where

$$
\begin{aligned}
\frac{\partial F_2}{\partial G_{\mu rs}}(\rho, \mathbf{G}) &= \sum_l A^{(1)}_{\mu\nu sr1l} D_{\mu sl} D_{11l} + \\
&\quad \sum_{\tau lmk} A^{(1)}_{\tau\nu mk1l} G_{\tau km} \left(\frac{\partial D_{\tau ml}}{\partial G_{\mu rs}} D_{11l} + D_{\tau ml} \frac{\partial D_{11l}}{\partial G_{\mu rs}} \right) + \\
&\quad \sum_\tau A^{(2)}_{\tau\nu m1l} \left(\frac{\partial D_{\tau ml}}{\partial G_{\mu rs}} D_{11l} + D_{\tau ml} \frac{\partial D_{11l}}{\partial G_{\mu rs}} \right) + A^{(3)}_{11l} \frac{\partial D_{11l}}{\partial G_{\mu rs}}
\end{aligned}
\tag{4.179}
$$

with $\mathbf{D} = \mathbf{D}(\rho, \mathbf{G})$ and $\frac{\partial \mathbf{D}}{\partial \mathbf{G}}(\rho, u)$ of eq. 4.159 and (4.166) inserted and similarly for the other functions F_i.

The $\mathbf{G}(\rho, u(\rho, \beta - \Delta\beta))$ from the previous temperature step in the solution algorithm of the PDE are taken as initial values of the NR technique. In each step of the iteration, for given $\mathbf{G}$, the linear system (4.159) is solved yielding $\mathbf{D}(\rho, \mathbf{G})$. Then the derivatives $\frac{\partial D_{\tau ml}}{\partial G_{\mu rs}}(\rho, \mathbf{G})$ are obtained by solving the linear equations (4.166). These solutions are inserted in the expression for J. Convergence in the NR method is achieved if the relative difference of two successive values of G is less than 10^{-10}. Furthermore it is checked whether the solution is physical, i.e., if $G_{12} = G_{21}$. With this solution $\mathbf{G}(\rho, u)$ one calculates $\mathbf{D}(\rho, u)$ (4.159), $A_j(\rho, u)$ (4.168, 4.169) and $\frac{\partial \mathbf{D}}{\partial \mathbf{G}}(\rho, u)$ (4.166).

The derivatives $\frac{\partial A_j}{\partial G_{\mu r s}}$ are obtained from (4.168) and are given by

$$\frac{\partial A_j}{\partial G_{\mu r s}} = A_j^0 \frac{\partial M_j}{\partial G_{\mu r s}} - \frac{4}{\sigma^2} B_j^0 \frac{\partial N_j}{\partial G_{\mu r s}}, \tag{4.180}$$

where

$$\frac{\partial M_j}{\partial G_{\mu r s}} = -\sum_\tau \frac{1}{z_\tau^2} \sum_m \rho_m \left\{ M_\tau^{(a)} \frac{\partial D_{\tau m j}}{\partial G_{\mu r s}} + (1 - M_\tau^{(a)} e^{-z_\tau \sigma}) \frac{\partial f_{\tau m j}}{\partial G_{\mu r s}} \right\}$$

$$\frac{\partial N_j}{\partial G_{\mu r s}} = \sum_\tau \frac{1}{z_\tau^3} \sum_m \rho_m \left\{ L_\tau^{(a)} \frac{\partial D_{\tau m j}}{\partial G_{\mu r s}} + (1 - L_\tau^{(a)} e^{-z_\tau \sigma}) \frac{\partial f_{\tau m j}}{\partial G_{\mu r s}} \right\}$$

$$\frac{\partial f_{\tau m j}}{\partial G_{\mu r s}} = \frac{2\pi}{z_\tau^2} \sum_k \rho_k \left(\delta_{\mu \tau} \delta_{mr} \delta_{ks} D_{\tau k j} + G_{\tau m k} \frac{\partial D_{\tau k j}}{\partial G_{\mu r s}} \right). \tag{4.181}$$

The derivatives $\frac{\partial G_{\mu r s}}{\partial u}$ are obtained by implicitly differentiating the equations $F_i = 0$ for $i = 1, \ldots, 8$ via

$$\begin{pmatrix} \frac{\partial G_{111}}{\partial u} \\ \frac{\partial G_{112}}{\partial u} \\ \vdots \\ \frac{\partial G_{222}}{\partial u} \end{pmatrix} = J^{-1} \cdot \begin{pmatrix} -1 \\ 0 \\ \vdots \\ 0 \end{pmatrix}. \tag{4.182}$$

Inserting the values of $\mathbf{G}(\rho, u)$, $\mathbf{D}(\rho, u)$ and $\frac{\partial D_{\tau m l}}{\partial G_{\mu r s}}(\rho, \mathbf{G})$ in eqs. (4.180, 4.181) and in the Jacobian J of (4.182) finally gives $\frac{\partial A_j}{\partial G_{\mu r s}}(\rho, u)$ and $\frac{\partial G_{\mu r s}}{\partial u}(\rho, u)$.

The PDE (4.101) is again a nonlinear diffusion equation, that was solved as in the one-component case for different values of x on $(\beta, \rho) \in [0, \beta_f] \times [0, \rho_0]$. The initial condition $u(\rho, x, \beta = 0)$ is obtained by making use of the fact that the direct correlation functions c_{ij} coincide with those of a one-component HS gas and taking into account the results for the one-component system. Thus with

$$\begin{aligned} G_{1ij}(\rho, x, \beta = 0) &= G_1(\rho, \beta = 0) \quad \text{cf. eq.(4.65)} \quad i, j = 1, 2 \\ G_{2ij}(\rho, x, \beta = 0) &= G_2(\rho, \beta = 0) \quad \text{cf. eq.(4.67)} \quad i, j = 1, 2 \end{aligned} \tag{4.183}$$

one obtains $u(\rho, x, \beta = 0)$ from the energy equation (4.170). The boundary conditions are those of eqs. (4.60) and (4.62).

As in the one-component system we have to exclude the region where thermodynamic stability requirements are not satisfied. In this unphysical region the fluid can no longer be present in a single homogeneous phase and phase separation occurs. In section 3.1.2 the phase stability conditions of a general binary fluid were presented. We will specialize these conditions in the following to the binary symmetric fluid. In that case we have to distinguish between the following two types of instability: material and azeotropic

instability. Material instability which leads to the separation into two phases of different compositions is indicated by a divergence of $S_{CC}(0)$. On the other hand, azeotropic instability where the fluid is mechanically unstable while remaining materially stable leading to a separation into two phases of different density but equal compositions is marked by a divergence of χ_T or $S_{NN}(0)$, while $S_{CC}(0)$ remains finite. The azeotropic instability of a binary symmetric fluid occurs at $x = 1/2$ and for this concentration $\delta = \rho(v_1 - v_2) = \frac{1}{2}\rho\left(\tilde{h}_{11}(0) - \tilde{h}_{22}(0)\right) = 0$. Thus $S_{NN}(0) = \chi^{red}$ may remain finite even if $S_{CC}(0)$ diverges. So material and mechanical instability can be distinguished in the $x = 1/2-$plane [102].

Both criteria of mechanical and material instability, i.e. diverging $S_{NN}(0)$ or $S_{CC}(0)$ have been merged into one criterion by Arrieta *et al.* [75] which we have used in our calculations. In this criterion it is checked whether the $\tilde{h}_{ij}(0)$ become infinite so that one of the structure factors is infinite. If

$$
\begin{aligned}
\Delta(0) &= \left(\det\left(\delta_{ij} + \sqrt{\rho_i\rho_j}\,\tilde{h}_{ij}(0)\right)\right)^{-1/2} \\
&= \left(\det\left(\delta_{ij} - \sqrt{\rho_i\rho_j}\,\tilde{c}_{ij}(0)\right)\right)^{1/2} = \det(\delta_{ij} - \sqrt{\rho_i\rho_j\bar{Q}_{ij}}) \leq 0
\end{aligned} \tag{4.184}
$$
$$\tag{4.185}$$

the solution is considered unphysical where

$$
\bar{Q}_{ij} = \int_0^\infty Q_{ij}(r)dr = \frac{1}{6}A_j\sigma^3 - \frac{1}{2}b_j\sigma^2 - \sum_\tau \frac{1}{z_\tau^2}\left(C_{\tau ij}M_\tau^{(a)} - f_{\tau ij}\right) \tag{4.186}
$$

with

$$
\begin{aligned}
b_j &= b_0(1 + M_j) + A^0 N_j \tag{4.187} \\
C_{\tau ij} &= f_{\tau ij}e^{-z_\tau\sigma} - D_{\tau ij}, \tag{4.188}
\end{aligned}
$$

and eqs. (4.168) and (4.169). b_0 is calculated from ρ and σ (see Appendix A of [75]).

The boundary conditions on the spinodal lines are

$$
u(\rho_S, \beta) = u_S(\rho_S) \tag{4.189}
$$

where the density ρ_S is the approximation for the spinodal density on the discrete density grid at a given temperature. It is located at that point where $\Delta(0)$ changes sign and becomes negative. $u_S(\rho)$ is the value of the excess internal energy where $\Delta(0) = 0$. This is determined by solving the set of eight nonlinear equations

$$
\begin{aligned}
\Delta(0)(\rho, \mathbf{G}) &= 0 \\
F_i(\rho, \mathbf{G}) &= 0 \quad i = 2, \ldots, 8, \tag{4.190}
\end{aligned}
$$

for **G** using a Newton Raphson technique where the Jacobian of the nonlinear system is provided. This Jacobian can be calculated in a straightforward way analogous to the one of eq. (4.178). Inserting the solution $\mathbf{G}(\rho)$ in the energy equation (4.170) finally yields $u_S(\rho)$. For the system of the binary symmetric HCY fluid that we have investigated, three cases of instability regions in the interval $[0, \rho_0]$ for a given value of x and T have to be distinguished that are shown in fig. (4.23).
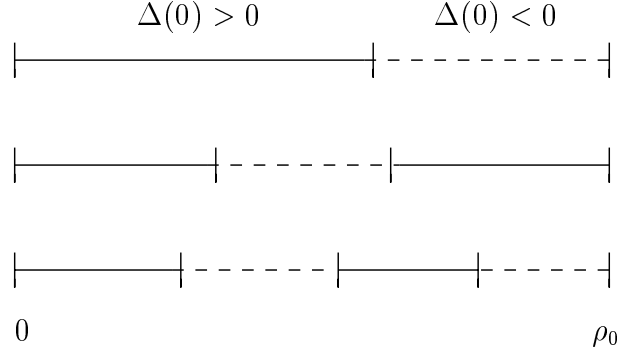
Figure 4.23: The 3 different cases of the instability region on the interval $[0, \rho_0]$ for a given value of x and T for a HC1Y fluid. The full lines are the stable regions where $\Delta(0) > 0$, while the dashed lines represent the unstable regions that are excluded from the integration of the PDE.

Once $u(\rho, x, \beta)$ has been determined the quantities relevant for the calculation of the phase diagram, the pressure P and the chemical potentials μ_i ($i = 1, 2$) are obtained by integrating $\frac{\partial \beta P}{\partial \beta}$ and $\frac{\partial \beta \mu}{\partial \beta}$ with respect to β from

$$\frac{\partial \beta \mu_1}{\partial \beta} = \frac{\partial u}{\partial \rho} + \frac{1-x}{\rho}\frac{\partial u}{\partial x} \tag{4.191}$$

$$\frac{\partial \beta \mu_2}{\partial \beta} = \frac{\partial u}{\partial \rho} - \frac{x}{\rho}\frac{\partial u}{\partial x} \tag{4.192}$$

$$\frac{\partial \beta P}{\partial \beta} = -u + \rho\frac{\partial u}{\partial \rho} \tag{4.193}$$

$$\tag{4.194}$$

with the CS values for βP and $\beta \mu_i$ values for βP and $\beta \mu$ as integration constants at $\beta = 0$

$$\beta P(\rho, x, \beta = 0) = \rho\frac{1 + \eta + \eta^2 - \eta^3}{(1 - \eta)^3}$$

$$\beta \mu_i(\rho, x, \beta = 0) = \ln \rho_i + \frac{8\eta - 9\eta^2 - 3\eta^3}{(1 - \eta)^3}. \tag{4.195}$$
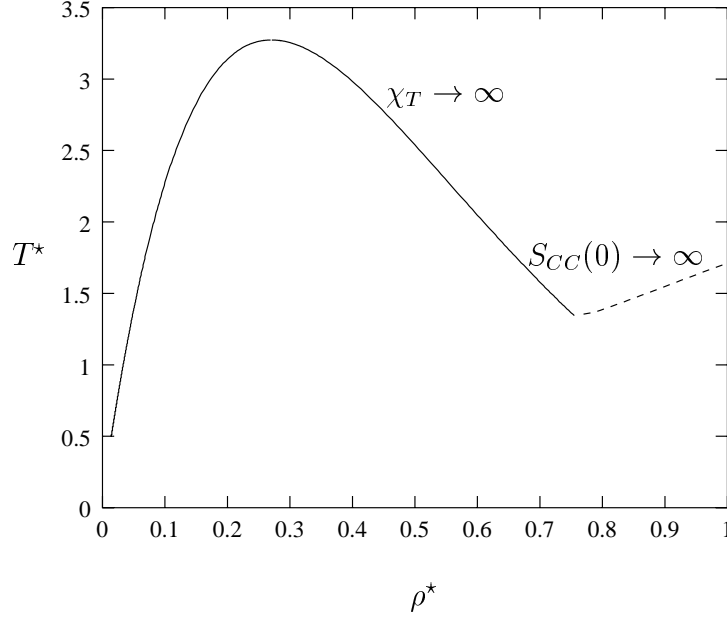
4.3.5   Results

Figure 4.24: Phase stability line in the temperature-density plane for an equimolar HCY mixture with $\alpha = 0.9$ and $z\sigma = 0.8$. Different line symbols are used for the density regimes in which either χ_T (full line) or $S_{CC}(0)$ (dashed line) diverges.

Fig. (4.24) shows the phase stability line of a binary symmetric fluid for $x = 1/2$. Note that the stable phase is now and also in the following plots above the stability line. In fig. (4.24) this line consists of two parts: along the low-density part up to densities of ~ 0.76 the compressibility diverges whereas $S_{CC}(0)$ remains finite while for densities larger than ~ 0.76 the behavior of χ_T and $S_{CC}(0)$ is reversed. The latter part of this curve represents the critical consolution line - also called the λ-line - while the low-density part is a typical liquid-vapor spinodal. The threshold density $\rho_t^\star$ that is separating the two regimes is given by $\rho_t^\star = 0.76$. As seen in the figure the critical temperature of the consolution points increases with increasing density. This can be understood in the following way: since we consider the case $\alpha < 1$, i.e. the unlike interaction is less favorable than the like interactions, self-aggregation is the driving mechanism of liquid-liquid separation and it is the stronger the higher one chooses the particle density since in this case the particles approach each other closely enough to feel the strongest attractive regions of the Yukawa potential.

A necessary condition for the mixture to be in equilibrium is given by the fact that

the Gibbs free energy

$$G = U - TS + PV \tag{4.196}$$

must have a minimum. Self-aggregation leads on the one hand to a reduction in the entropy and thus to a positive contribution $-TS$ in the Gibbs free energy, on the other hand to a reduction of the internal energy U. This latter contribution is less and less negative the lower the density is for the reason given above. So by decreasing the density the entropic part that favors a homogeneous fluid mixture plays a more dominant role and leads to a cross over from the demixing phase separation regime to the liquid-vapor phase separation regime.
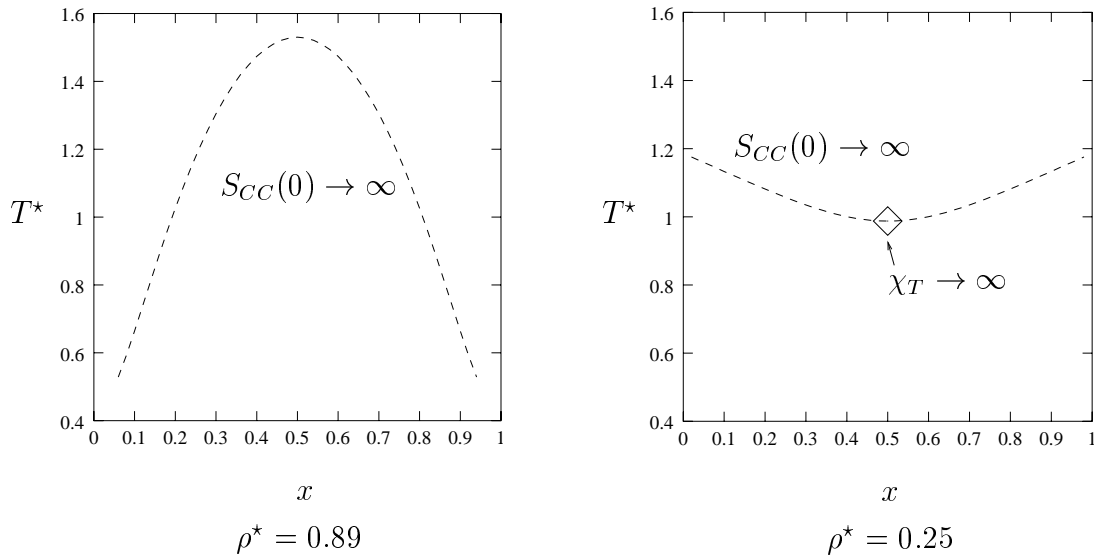
Figure 4.25: Phase stability lines in the temperature-concentration plane for a HCY mixture with $\alpha = 0.65$ and $z\sigma = 1.8$. The point where χ_T diverges is marked by a diamond. Everywhere else $S_{CC}(0)$ diverges (dashed line).

The spinodal line in the temperature-concentration plane is shown in fig. (4.25) for two different values of the density. This figure shows that the curvature changes as the density is varied. For the density $\rho^\star = 0.89$ all points of the instability line are characterized by a divergence of $S_{CC}(0)$ while for $\rho^\star = 0.25$ $S_{CC}(0)$ diverges everywhere except at $x = 1/2$ where χ_T diverges. The curvature change of the stability line as the density varies is due to the following reasons: The concave phase stability line (at high $\rho^\star$) can be explained with the same arguments as above when the increase of the critical consolution temperature with the density was examined. It was argued that at higher density the energetic contribution to the Gibbs free energy plays the dominant role. If we leave the equimolar concentration the number of cross interactions decreases and since the

like interactions are more attractive the internal energy of the homogeneous non-equimolar mixture is smaller compared to that of the homogenous equimolar case with the same total fluid density. So, less energy is necessary at $x \neq 1/2$ to bring the system from a demixed state back to a homogeneous phase than in the equimolar case. Thus at high density the stability curve decreases as one leaves the equimolar concentrations. The reverse behavior is found, however, at lower densities, where the liquid-liquid spinodal curve increases when one moves away from $x = 1/2$. This behavior is driven by the entropic contribution to G, the entropy of mixing being maximal at the equimolar concentration.
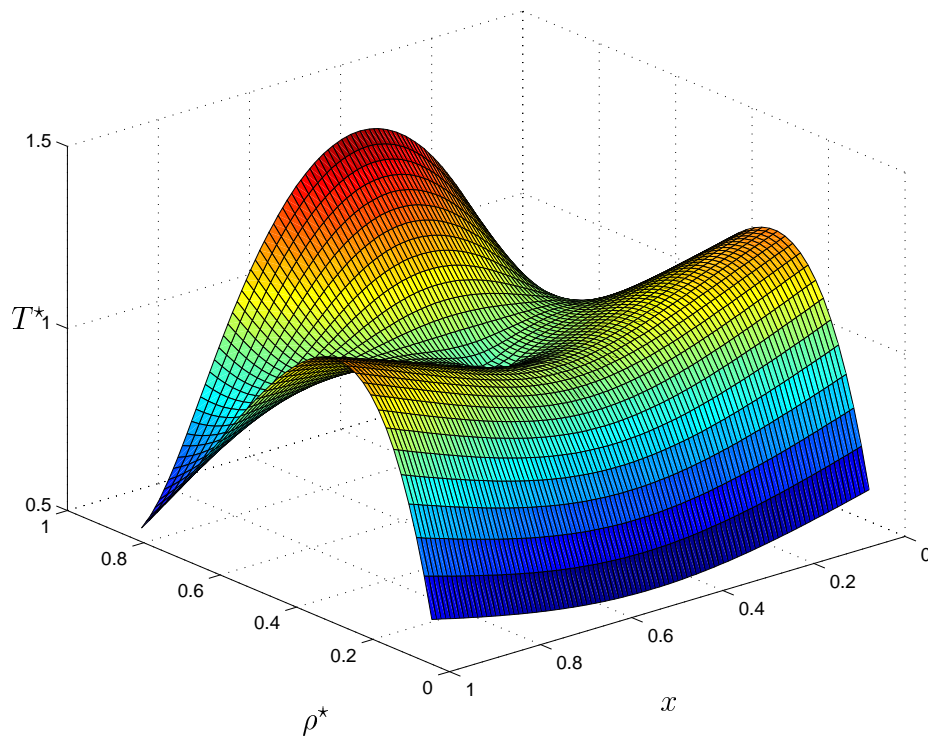

Figure 4.26: 3-dimensional view of the phase stability behavior of a HCY mixture with $\alpha = 0.65$ and $z\sigma = 1.8$ in the $T^\star - \rho^\star - x$ space.

A three-dimensional plot of the phase stability behavior in the $T^\star - \rho^\star - x$ space is shown in fig. (4.26). Now, let us assume that we approach the phase stability boundary from above on different paths. We fix the concentration x to $1/2$, fix the density and reduce the temperature until we reach the stability boundary. If we choose a density above the threshold value $\rho^\star > \rho_t^\star$ and reduce the temperature until we cross the stability boundary where $S_{CC}(0)$ diverges, self-aggregation will take place and the fluid is going to demix into a 1-rich and a 2-rich phase. For $\rho < \rho_t^\star$, where $\chi_T \to \infty$ the fluid becomes

mechanically unstable and separates into a mixed liquid and vapor phase. By further reducing the density the scenario will again change and the fluid will decompose into 3 phases: a homogenous vapor, a 1-rich and a 2-rich fluid.

In order to understand the demixing separation on a structural level we recall that for $x = 1/2$ (eq. 2.34)

$$
\begin{aligned}
S_{NN}(0) &= 2\left(S_{11}(0) + S_{12}(0)\right) \\
S_{CC}(0) &= \frac{1}{2}\left(S_{11}(0) - S_{12}(0)\right).
\end{aligned}
\tag{4.197}
$$

Thus from $S_{CC}(0) \to \infty$ [while $S_{NN}(0) < \infty$] it follows that $S_{11}(0) \to \infty$ and $S_{12}(0) \to -\infty$, or equivalently, $\int \left(g_{12}(r) - 1\right) d^3r \to -\infty$ which means that $g_{12}(r) < 1$ at macroscopic distances. Therefore particles tend to surround themselves with like particles, and avoid the presence of unlike particles in their neighborhood. This is the mechanism of self-aggregation.

The different types of phase diagrams of a binary symmetric mixture (see section 3.1.3) that where found in the mean field study of [12] were also recovered within the SCOZA. We calculated the phase diagrams by solving the coupled set of equations (3.13) to (3.15) with a Newton-Raphson technique. Fig. (4.27) shows a series of phase diagrams for $z\sigma = 1.8$ and $\alpha = 0.65,\ 0.70,\ 0.75$. Another series of phase diagrams is shown in fig. (4.28) for $z\sigma = 2.5$. The sequence of types of phase diagrams is the same in the two series, only the critical points are shifted to lower temperature for $z\sigma = 1.8$. The change of the type of phase diagram is triggered by the parameter α. For the interaction parameter α, which characterizes the ratio between the unlike and the like interactions we have chosen values smaller than one: this guarantees, that, apart from the vapor-liquid transition, we shall also encounter for sufficiently small α a fluid-fluid decomposition. As α is decreased the λ-line shifts to lower densities and the sequence of the types of phase diagrams is type I $\to$ type II $\to$ type III. The three-dimensional phase diagram for $z\sigma = 1.8$ and $\alpha = 0.70$ (type II) is shown in fig. (3.3).

It becomes apparent from the figures that the SCOZA is able to get very close to the tricritical point. This is in contrast to the ORPA results for a related problem presented in the following chapter.
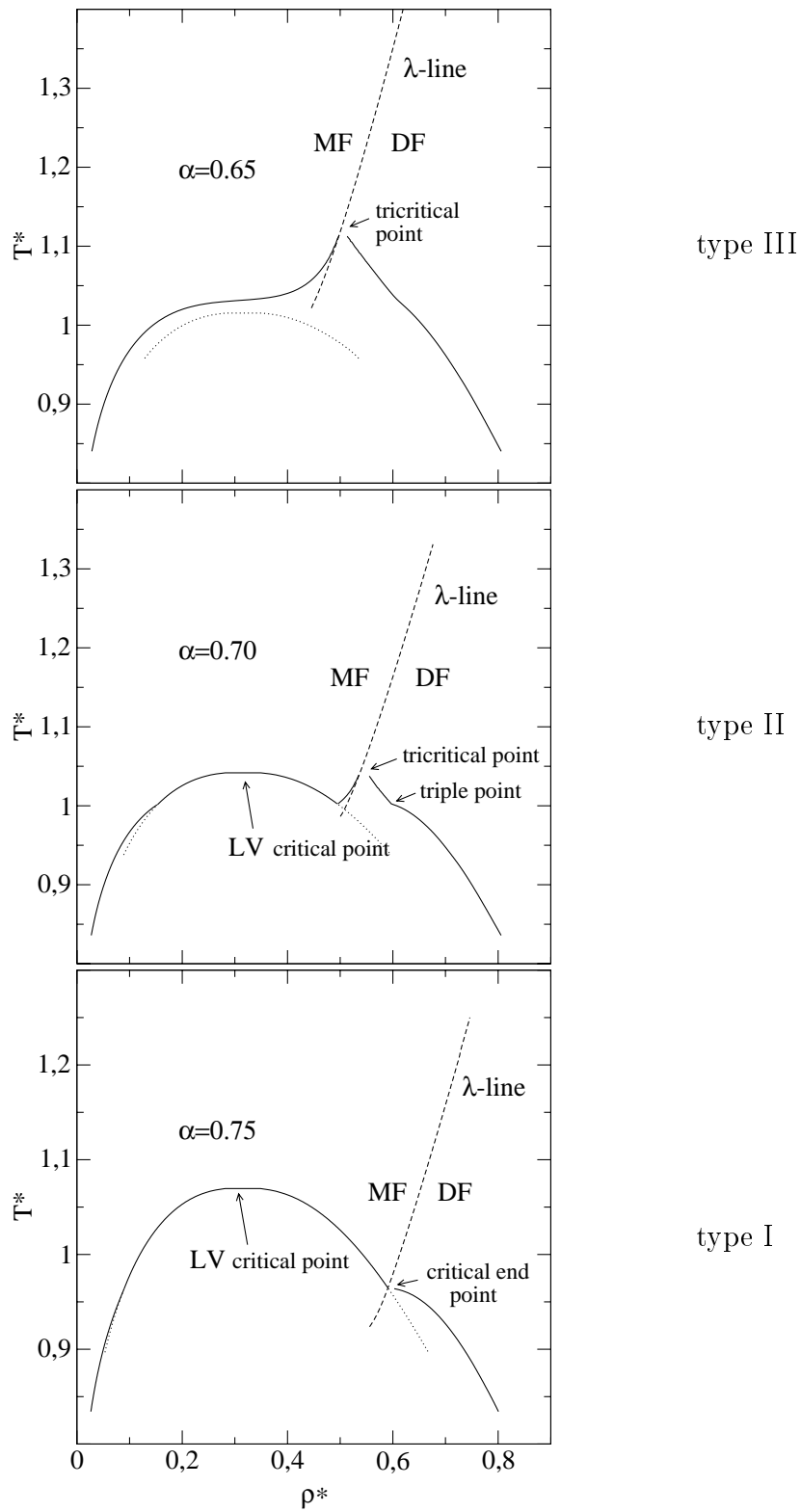
Figure 4.27: SCOZA phase diagrams in the $T^\star - \rho^\star$- plane for various α values and $z\sigma = 1.8$. The full lines represent first-order phase coexistence, the dashed lines the λ-line and the dotted curves metastable V-MF transitions.
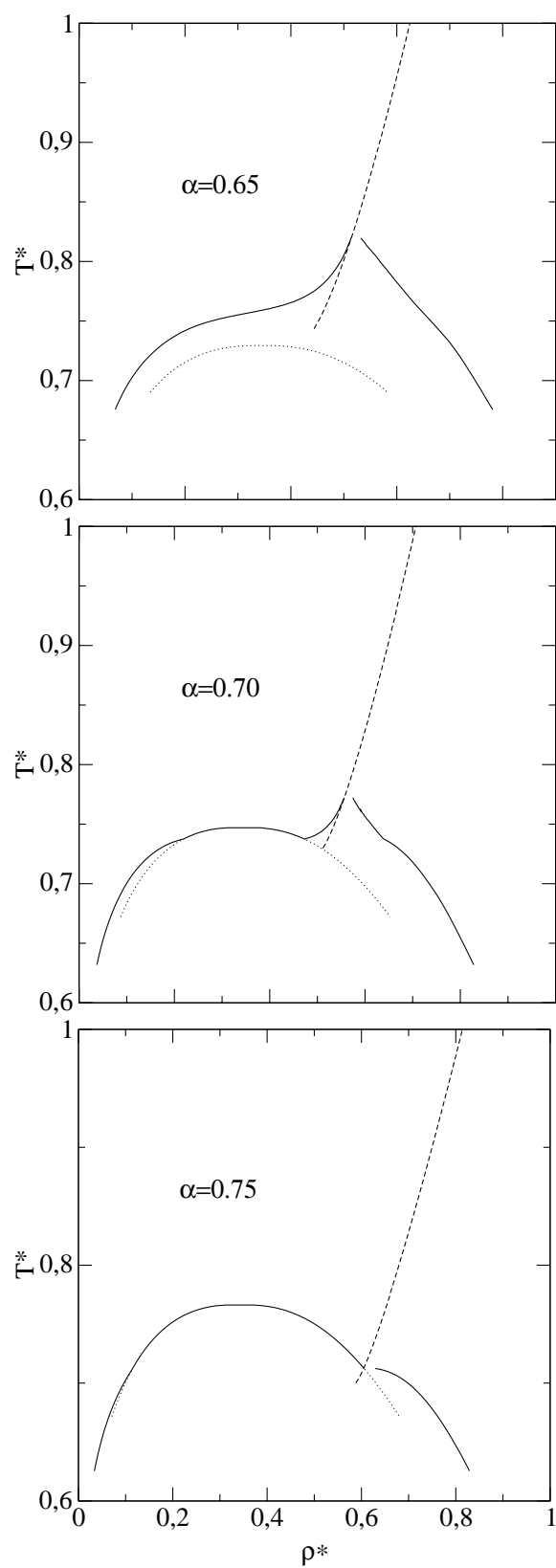
Figure 4.28: The same as in fig. (4.27) for $z\sigma = 2.5$

Part III

Confined Fluids

Chapter 5

Fluid Mixtures in Porous Media

5.1 Introduction

In the previous section we have investigated the phase behavior of a binary symmetric bulk fluid. As expected, we have found a much richer variety of phase diagrams than in a one-component fluid. The system that we are going to treat in the following is even more complex: we investigate a binary symmetric fluid that is confined in a disordered porous material (matrix) and study, in particular, the influence of the properties of the matrix and of the matrix-fluid interactions on the phase behavior.

Investigations of the properties of fluids in thermal equilibrium with a disordered porous structure have become a very challenging field in liquid state physics [13] during the past years and the number of experimental and theoretical studies in this field has largely increased. Due to the importance of adsorption on porous materials in many technological applications such as catalysis, gas separation, gas purification or others a large amount of experimental data on gas adsorption on porous substrates have been accumulated over the years [103]. Another point of interest in experimental research has been the study of liquids adsorbed in porous media. Investigations have been focused on the influence of the properties of the porous media on the critical behavior and on the process of phase separation of a liquid adsorbed in this material. This research was motivated by de Gennes [104] who suggested that binary mixtures adsorbed in porous media near the critical point may be thought as experimental realizations of the random field Ising model (RFIM) [105] – a spin model of random magnets. In this model the random field describes the spatially varying preference of the pore network for the adsorption of one of the fluid components.

Experimental studies have revealed that a porous matrix (even if it occupies only a small fraction of the volume) can have a substantial influence on the phase behavior of the liquid: ^{4}He and N_2 in high-porosity aerogel [14] are two examples where the near-critical liquid-vapor (LV) curve is narrowed drastically under the influence of a matrix. The effects become of course richer and more interesting in the case that the fluid is a binary mixture: for example, experiments on a ^{3}He-^{4}He mixture inside a highly porous silica-gel or a porous gold matrix have shown a drastic modification of the superfluid transition [15].

Stimulated by these experimental results, considerable effort has been dedicated in the last decade to developing theoretical tools that allow the investigation of structural and thermodynamic properties of liquids in quenched porous media. Experimental results in dilute silica gels (porous materials with high porosity where the porosity can be as high as 99.9%) were interpreted by the RFIM. On the other hand, it has been argued that experiments in Vycor (which is a glass with a fairly low porosity) can be interpreted in terms of wetting phenomena in a confined geometry with no randomness [106]. Theoretical studies of confined fluids have generally been limited to 'single pore' models with idealized pore geometries, (e.g. fluids confined to narrowly spaced plane walls, cylindrical or spherical pores [107]) which lack the ability to represent a truly disordered structure. In reality, however, porous solids are often disordered, containing an interconnected network of pores of various sizes and shapes. On the other hand, confinement in the pores plays no role in the RFIM. Hence, both approaches do not seem sufficient to describe the vast variety of phase behavior observed. Consequently, a more realistic continuum description for the fluid/solid system was required which is able to comprise randomness, confinement and connectivity between the pores.

Such an approach was proposed by Madden and Glandt [16] who modeled such a system as a special binary mixture: the porous solid is modeled as a rigid arrangement of particles that is not affected by the introduction of the liquid. The configuration of the immobile matrix particles is assumed to have been formed by an instantaneous thermal quench of a fluid in equilibrium at a higher temperature; that is, the quenched particles are distributed according to an equilibrium ensemble at a higher temperature in the absence of the fluid. The fluid particles (or annealed particles) that constitute the second component are allowed to move in the volume that is not occupied by the matrix. In contrast to a 'standard' two-component equilibrium mixture, there is no structural response of the matrix to the particles in the fluid.

The main problem in the description of the system lies in the two successive averages required for the calculation of thermodynamic and structural properties: one average is

taken over the configurations of the liquid, keeping the matrix particles in fixed positions, and the second average is then taken over different matrix configurations. The first steps to solving this complex problem were proposed by Madden and Glandt, who derived cluster expansions for the distribution functions; integral equations for the correlation functions, which are similar to the OZ equations in standard liquid-state theory, have been presented. In subsequent work, Given and Stell have applied the replica method (introduced originally in the theory of spin glasses [17]) to this problem [108, 109, 18] and have provided a powerful tool on which many of the present-day approaches in this field are based. The replica trick exploits a mathematical isomorphism between a partly quenched system and a limiting case of a corresponding equilibrium system, which consists of the now mobile matrix particles and of s noninteracting identical copies of the liquid: the properties of the quenched system are obtained by considering the limit $s \to 0$ of the properties of the equilibrium system, which, in turn, can be treated by standard liquid state theories. Given and Stell presented in their work the (now correct) formulation of the so called replica OZ (ROZ) equations, the counterpart of the OZ relations in standard liquid state theory: they relate the liquid-liquid, the liquid-matrix, and the matrix-matrix correlation functions. Finally, thermodynamic relations for such systems have been presented by Rosinberg *et al.* [110, 111].

Integral equation theories which use approximate closures to the ROZ equations have been applied to the calculation of pair distribution functions [112, 113, 114, 115]. Comparison with results from Monte Carlo simulations [113, 114] indicated that the approach has an accuracy comparable to that of bulk liquid state theory. Further theoretical research has focused on the phase behavior of fluids in disordered porous materials. Page and Monson [116] observed in their Monte Carlo simulation of a Lennard-Jones fluid that is confined in a rigid matrix of spherical obstacles a significant narrowing of the liquid-vapor coexistence curve as well as the evidence of a second fluid-fluid phase transition at low temperature. Kaminsky and Monson [117] and Ford and Glandt [118] applied a mean-field theory to model systems and showed that both the critical temperature and the critical density decrease with increasing matrix concentration. Kierlik *et al.* [35] have applied an improved perturbation theory – the optimized cluster theory – to describe phase diagrams of Lennard-Jones fluids. They observed that the liquid-vapor coexistence curve was similar to that of a bulk fluid, although displaced and narrowed. Additionally, the theory predicted the appearance of a second fluid-fluid transition at low temperatures. Their results were compared with GCMC simulations in [119].

Recently, a formalism to treat systems containing partly quenched mixtures with electrostatic interactions between various species [120] and to treat diatomic fluids adsorbed

in porous matrices has been presented [121].

So far, only the phase behavior of one-component liquids in a porous medium has been investigated, while practically no attention has been paid to describe binary liquids in a porous matrix. However, a study of such a system is of interest due to the following two reasons: first, similar to the homogeneous case, the step from a one-component to a binary liquid offers - due to the increased number of parameters - a much richer variety. A further important motivation to proceed to liquid mixtures is the fact that several experiments have been made for such systems.

Using the replica trick we have generalized the formulation of the theory to the binary mixture in a porous matrix (which represents a very special three-component system) [34, 122]: we have proceeded along similar lines as in the one-component case and derived the ROZ equations which now consist of one decoupled equation for the matrix correlation functions h_{00} and c_{00} (as in the case of a one-component liquid) and a set of eight coupled integral-equations for the set of the remaining correlation functions (vs. three coupled equations in the case of a simple liquid). These equations can be solved along with one of the standard liquid state closures (such as Percus-Yevick or hypernetted chain approximation) using efficient numerical algorithms, like the one proposed by Lomba *et al.* [113] for the simple one-component case. As a further closure relation we have also considered the random phase approximation (RPA) – as already done by Kierlik and co-workers [35] in the one-component case – along with an optimization criterion in the closure relation (ORPA [31, 32, 29]), that guarantees that the pair distribution functions vanish inside the core region. We show that the solution of the ROZ equations together with the ORPA closure relation can be mapped on the solution of a variational problem: a suitably defined functional (which turns out to be a second order contribution to the free energy) is minimized with respect to variations of the direct correlation functions inside the core region. The formalism arising from this route is rather complex even for a simple closure relation like the ORPA.

In our investigations we applied the theory on the calculations of phase diagrams [19, 123, 124]. As in the bulk system we found three different types of phase diagrams depending on the values of the coupling strengths of the fluid-fluid and matrix-fluid interactions, and the matrix properties. The transition between the different types of phase diagrams was found to be not only triggered by internal parameters (i.e. parameters that characterize the fluid-fluid interactions) but also by external parameters (i.e. parameters that characterize the matrix and the matrix-fluid interactions). Similar as in the case of the bulk fluid, one can produce - for a given matrix density - trends in the types of phase diagram by varying the parameter α, i.e., the ratio of the unlike to the like interactions.

In addition, we could show, that such trends can also be induced by varying the external parameters, keeping the internal parameters fixed.

Due to the complexity of the system we have used a thermodynamic perturbation theory - the ORPA - instead of the more sophisticated SCOZA that is up to now restricted to the case of a bulk fluid due to its complex concept. The theoretical results were compared with GCMC simulations and the ORPA was found to give - despite its simplicity - (at least qualitative) information of how a variation of the system parameters influences the phase behavior. Thus, systematic trends could be worked out on a qualitative basis.

The remaining part of this chapter is organized as follows: after a description of the potentials that characterize our model in sect. 5.2, we present briefly, in sect. 5.3, the ORPA which is used as a closure to the ROZ equations and collect the expressions (free energy, chemical potential and pressure) that are necessary to calculate phase diagrams. Section 5.4 describes the results: comparison is made between simulation results and ORPA predictions and trends in the variation of the phase diagrams induced by the different system parameters are discussed.

5.2   The System

The system we have studied is a symmetric binary HCY mixture in thermal equilibrium with a disordered porous (hard-sphere) matrix of immobile particles realized by a frozen configuration of particles of the same size as the fluid particles. A picture of this model is shown in fig. (5.1).

All the interactions of the system can be written as $[\beta = 1/(k_B T)]$

$$\beta \Phi_{ij}(r) = \begin{cases} \infty & r < \sigma \\ -\dfrac{K_{ij}}{r}\exp[-z(r-\sigma)] & r \geq \sigma \end{cases} . \tag{5.1}$$

A value 0 of index i or j denotes the matrix particles, while 1 and 2 denote the two components of the fluid. The diameter σ is assumed to be equal for all interactions and z is the screening length. The contact values K_{ij} are parameterized as follows:

$$K_{00} = 0 \qquad K_{11} = K_{22} \tag{5.2}$$

$$K_{12} = \alpha K_{11} \qquad K_{01} = K_{02} = y K_{11}. \tag{5.3}$$

We define a reduced temperature via $T^\star = \sigma/K_{11}$ (in the following $T^\star$ is denoted by T). Further system variables are the partial densities, ρ_i, of species i, the concentration of

matrix particle
('quenched' particle)

fluid particles of component 1 and 2
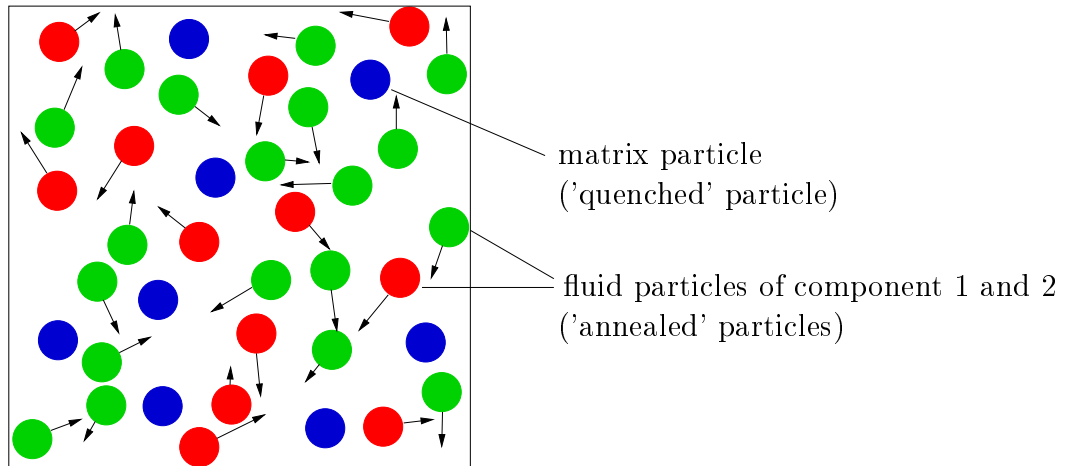('annealed' particles)

Figure 5.1: Model of a binary fluid inside a porous matrix. The matrix particles are fixed; the fluid particles are allowed to equilibrate in the rigid matrix structure. All particles are of the same size.

species 1 of the fluid $x = \rho_1/(\rho_1 + \rho_2)$, the fluid density $\rho_f = \rho_1 + \rho_2$ and the matrix density ρ_0 (densities will be given in units of σ^3 throughout this chapter). In all calculations presented here, unless otherwise stated, the potentials have been truncated at $r_c = 2.5\sigma$, and $z\sigma$ was chosen to be 2.5; this concerns both the simulations and the theoretical calculations.

5.3   Thermodynamic Perturbation Theory

5.3.1   Replica Trick

A binary liquid inside a porous (one-component) matrix can be considered as a very special three-component liquid, where the particles of the matrix are fixed in place and are not affected by the mobile particles of the liquid. Physical quantities are hence obtained by two successive averages: one average is taken over the degrees of freedom of the fluid particles (where the positions of the matrix particles are kept fixed) and the other average is performed over all possible degrees of freedom of the matrix particles. The actual calculation of such averages turns out to be very difficult; to circumvent these problems, Given and Stell have applied the replica method (introduced originally in [17]) to liquid-state systems [108, 109, 18]: this method exploits a mathematical isomorphism between a partly quenched system and a limiting case of a corresponding equilibrium system, that

is usually denoted as the replicated system. We briefly demonstrate this trick for the case of a binary liquid, using a canonical ensemble both for the matrix and the binary liquid. For a given matrix configuration (the positions of the N_0 matrix particles are denoted by $\mathbf{q}^{N_0} = \{\mathbf{q}_i\}$), and a given temperature T_1 ($\beta_1 = 1/k_B T_1$), and volume V, the free energy A is given by

$$-\beta_1 A(N_1, N_2, V, T_1; \mathbf{q}^{N_0}) = \ln Z(\mathbf{q}^{N_0}), \tag{5.4}$$

$Z(\mathbf{q}^{N_0})$ being the usual canonical partition function, i.e.,

$$Z(\mathbf{q}^{N_0}) = \frac{1}{N_1! N_2!} \int d^3 r^{N_1} d^3 s^{N_2} \exp\left[-\beta_1 \left(H_{01} + H_{02} + H_{11} + H_{12} + H_{22}\right)\right]. \tag{5.5}$$

The H_{ij} are the configurational parts of the Hamilton functions describing the interactions between matrix particles and particles of the liquid. The positions of the N_1 (resp. N_2) fluid particles of component 1 (resp. component 2) are denoted by $\mathbf{r}^{N_1} = \{\mathbf{r}_i\}$ (resp. $\mathbf{s}^{N_2} = \{\mathbf{s}_i\}$). The free energy of the quenched system, $\bar{A}$, where the matrix particles are distributed according to a canonical ensemble at a temperature T_0 ($\beta_0 = 1/k_B T_0$), is obtained via averaging over the $\mathbf{q}^{N_0}$, i.e.,

$$-\beta_1 \bar{A} = -\beta_1 \bar{A}(N_0, N_1, N_2, V, T_1, T_0) = \frac{1}{N_0! Z_0} \int d^3 q^{N_0} \exp\left[-\beta_0 H_{00}(\mathbf{q}^{N_0})\right] \ln Z(\mathbf{q}^{N_0}) \tag{5.6}$$

where Z_0 is a normalizing factor. The logarithm in the above expression makes the calculation of the average very difficult. However, using the identity $\ln x = \lim_{s \to 0} dx^s/dx$ one obtains

$$-\beta_1 \bar{A} = \frac{1}{Z_0} \lim_{s \to 0} \frac{d}{ds} \left[\frac{1}{N_0!} \int d^3 q^{N_0} \exp\left[-\beta_0 H_{00}(\mathbf{q}^{N_0})\right] \left[Z(\mathbf{q}^{N_0})\right]^s\right]. \tag{5.7}$$

The bracketed term in the above equation is denoted by $Z^{\text{rep}}(s)$ and can explicitly be written for integer values of s as an iterated integral

$$
\begin{aligned}
Z^{\text{rep}}(s) \;=\;& \frac{1}{N_0! \, (N_1!)^s \, (N_2!)^s} \int d^3 q^{N_0} \; d^3 r_1^{N_1} \cdots d^3 r_s^{N_1} \; d^3 s_1^{N_2} \cdots d^3 s_s^{N_2} \;\; \exp\left[-\beta_0 H_{00}(\mathbf{q}^{N_0})\right] \times \\
& \exp\left[-\beta_1 \sum_{\alpha=1}^{s} \left[H_{01}^\alpha(\mathbf{q}^{N_0}, \mathbf{r}_\alpha^{N_1}) + H_{02}^\alpha(\mathbf{q}^{N_0}, \mathbf{s}_\alpha^{N_2})\right]\right] \times \\
& \exp\left[-\beta_1 \sum_{\alpha=1}^{s} \left[H_{11}^\alpha(\mathbf{r}_\alpha^{N_1}) + H_{12}^\alpha(\mathbf{r}_\alpha^{N_1}, \mathbf{s}_\alpha^{N_2}) + H_{22}^\alpha(\mathbf{s}_\alpha^{N_2})\right]\right].
\end{aligned}
\tag{5.8}
$$

If we assume that the interactions between the particles of the system can be described via pair potentials Φ_{ij}, then (5.8) is the equilibrium partition function of a system with the following configurational part of the Hamilton function

$$
\begin{aligned}
H \;=\;& \sum_{\substack{i<j \\ i,j\in\{1,\ldots,N_0\}}} \Phi_{00}(\mathbf{q}_i,\mathbf{q}_j) \;+\; \sum_{\alpha=1}^{s} \sum_{\substack{i,j \\ i\in\{1,\ldots,N_0\} \\ j\in\{1,\ldots,N_1\}}} \Phi_{01}^{\alpha}(\mathbf{q}_i,\mathbf{r}_{\alpha,j}) \;+ \\
& \sum_{\alpha=1}^{s} \sum_{\substack{i,j \\ i\in\{1,\ldots,N_0\} \\ j\in\{1,\ldots,N_2\}}} \Phi_{02}^{\alpha}(\mathbf{q}_i,\mathbf{s}_{\alpha,j}) \;+\; \sum_{\alpha=1}^{s}\sum_{\beta=1}^{s} \sum_{\substack{i<j \\ i,j\in\{1,\ldots,N_1\}}} \Phi_{11}^{\alpha\beta}(\mathbf{r}_{\alpha,i},\mathbf{r}_{\beta,j}) \;+ \\
& \sum_{\alpha=1}^{s}\sum_{\beta=1}^{s} \sum_{\substack{i,j \\ i\in\{1,\ldots,N_1\} \\ j\in\{1,\ldots,N_2\}}} \Phi_{12}^{\alpha\beta}(\mathbf{r}_{\alpha,i},\mathbf{s}_{\beta,j}) \;+\; \sum_{\alpha=1}^{s}\sum_{\beta=1}^{s} \sum_{\substack{i<j \\ i,j\in\{1,\ldots,N_2\}}} \Phi_{22}^{\alpha\beta}(\mathbf{s}_{\alpha,i},\mathbf{s}_{\beta,j}) \\
\;=\;& H_{00}(\mathbf{q}^{N_0}) \;+ \\
& \sum_{\alpha=1}^{s} \left[H_{01}^{\alpha}(\mathbf{q}^{N_0},\mathbf{r}_{\alpha}^{N_1}) + H_{02}^{\alpha}(\mathbf{q}^{N_0},\mathbf{s}_{\alpha}^{N_2}) + H_{11}^{\alpha}(\mathbf{r}_{\alpha}^{N_1}) + H_{12}^{\alpha}(\mathbf{r}_{\alpha}^{N_1},\mathbf{s}_{\alpha}^{N_2}) + H_{22}^{\alpha}(\mathbf{s}_{\alpha}^{N_2}) \right] \quad (5.9)
\end{aligned}
$$

$\Phi_{rs}^{\alpha\beta}$ denotes the pair interaction between a fluid particle of component r in replica α with a particle of component s in replica β, $\mathbf{r}_{\alpha,j}$ is the position of particle number j of fluid component 1 in replica α, etc., and the system is characterized by the following pair potentials

$$
\begin{aligned}
\Phi_{01}^{\alpha}(\mathbf{q}_i,\mathbf{r}_{\alpha,j}) &= \Phi_{01}(\mathbf{q}_i,\mathbf{r}_{\alpha,j}) \\
\Phi_{02}^{\alpha}(\mathbf{q}_i,\mathbf{s}_{\alpha,j}) &= \Phi_{02}(\mathbf{q}_i,\mathbf{s}_{\alpha,j}) \\
\Phi_{11}^{\alpha\beta}(\mathbf{r}_{\alpha,i},\mathbf{r}_{\beta,j}) &= \delta_{\alpha\beta}\Phi_{11}(\mathbf{r}_{\alpha,i},\mathbf{r}_{\beta,j}) \\
\Phi_{12}^{\alpha\beta}(\mathbf{r}_{\alpha,i},\mathbf{s}_{\beta,j}) &= \delta_{\alpha\beta}\Phi_{12}(\mathbf{r}_{\alpha,i},\mathbf{s}_{\beta,j}) \\
\Phi_{22}^{\alpha\beta}(\mathbf{s}_{\alpha,i},\mathbf{s}_{\beta,j}) &= \delta_{\alpha\beta}\Phi_{22}(\mathbf{s}_{\alpha,i},\mathbf{s}_{\beta,j}).
\end{aligned}
\quad (5.10)
$$

(5.8) represents the canonical partition function of a fully equilibrated $(2s+1)$-component system, consisting of the matrix and of s identical copies (so-called replicas, denoted by the Greek index) of the liquid mixture where the interaction of the liquid particles has a very special feature: pairs of liquid particles interact only if they belong to the same replica.

In the following we assume $T_0 = T_1 \equiv T$, hence

$$
-\beta\bar{A} = \frac{1}{Z_0}\lim_{s\to 0}\frac{d}{ds}Z^{\mathrm{rep}}(s) \;=\; \lim_{s\to 0}\frac{d}{ds}\left[-\beta A^{\mathrm{rep}}(s)\right]. \quad (5.11)
$$

Thus we have related the thermodynamic potential of the partly quenched system to the limiting case of the thermodynamic potential of a fully equilibrated system. Structure functions and further thermodynamic properties of the partly quenched system can now be obtained from the corresponding quantities of the fully equilibrated replicated system by special prescriptions, involving throughout limits $s \to 0$: a complete set of these rules are compiled in ref. [110]. E.g. the correlation functions of the partly quenched system are obtained via

$$h_{ij}(r) = \lim_{s \to 0} h_{ij}^{rep}(r; s). \tag{5.12}$$

Note that the limiting case $s \to 0$ cannot be interpreted physically: firstly, a physical interpretation of the replicated system as an equilibrium mixture of $(s + 1)$ components is only valid if s is an integer. Furthermore, although in the limit $s \to 0$ the replicated system becomes an equilibrium system containing only the quenched particles, we still have nontrivial correlation functions describing the correlations between a pair of annealed particles in the same replica and a pair of particles in different replicas. Instead, one must envision the replica method merely as a mathematical tool which tells us how to relate the thermodynamic potential of a partly quenched system to that of a fully equilibrated system.

5.3.2   The structure

The replica Ornstein-Zernike equation

The structure of a binary liquid inside a porous matrix can be most readily determined via the ROZ equations that relate the fluid-fluid, matrix-fluid, and matrix-matrix direct $c_{ij}(r)$ and total $h_{ij}(r)$ correlation functions. These relations are derived from the standard OZ equations for the fully equilibrated $(2s + 1)$-component system, exploiting the symmetry of the replicated system and taking the limit $s \to 0$. So one finally arrives at the following set of integral-equations where $\otimes$ represents a convolution:

$$
\begin{aligned}
h_{00} &= c_{00} + \rho_0 c_{00} \otimes h_{00} \\
\mathbf{h}_{01} &= \mathbf{c}_{01} + \mathbf{h}_{01} \otimes \rho_0 c_{00} + \boldsymbol{\rho}_1 \mathbf{h}_{11} \otimes \mathbf{c}_{01} - \boldsymbol{\rho}_1 \mathbf{h}_{12} \otimes \mathbf{c}_{01} \\
\mathbf{h}_{11} &= \mathbf{c}_{11} + \mathbf{h}_{01} \otimes \rho_0 \mathbf{c}_{01}^{\mathrm{T}} + \boldsymbol{\rho}_1 \mathbf{h}_{11} \otimes \mathbf{c}_{11} - \boldsymbol{\rho}_1 \mathbf{h}_{12} \otimes \mathbf{c}_{12} \\
\mathbf{h}_{12} &= \mathbf{c}_{12} + \mathbf{h}_{01} \otimes \rho_0 \mathbf{c}_{01}^{\mathrm{T}} + \boldsymbol{\rho}_1 \mathbf{h}_{12} \otimes \mathbf{c}_{11} + \boldsymbol{\rho}_1 \mathbf{h}_{11} \otimes \mathbf{c}_{12} - 2\boldsymbol{\rho}_1 \mathbf{h}_{12} \otimes \mathbf{c}_{12},
\end{aligned}
\tag{5.13}
$$

where the superscript T denotes the transpose of a vector and $\otimes$ stands for a convolution. The following matrix-notation has been introduced [122]

$$\boldsymbol{\rho}_1 = \left(\begin{array}{cc} \rho_1 & 0 \\ 0 & \rho_2 \end{array} \right) \quad \mathbf{h}_{01} = \left(\begin{array}{c} h_{01} \\ h_{02} \end{array} \right) \quad \mathbf{c}_{01} = \left(\begin{array}{c} c_{01} \\ c_{02} \end{array} \right) \tag{5.14}$$

$$\mathbf{h}_{11} = \left(\begin{array}{cc} h_{11} & h_{12} \\ h_{12} & h_{22} \end{array} \right) \quad \mathbf{c}_{11} = \left(\begin{array}{cc} c_{11} & c_{12} \\ c_{12} & c_{22} \end{array} \right) \quad \mathbf{h}_{12} = \left(\begin{array}{cc} h_{13} & h_{14} \\ h_{14} & h_{24} \end{array} \right) \quad \mathbf{c}_{12} = \left(\begin{array}{cc} c_{13} & c_{14} \\ c_{14} & c_{24} \end{array} \right),$$

where h_{13} (resp. h_{24}) is the $(s \to 0)$-limit of the correlation function between particles of species 1 (resp. 2) of different replicas. Further, h_{14} is the $(s \to 0)$-limit of the correlation function between unlike particles of different replicas. Within the present framework which describes fluids in contact with porous media, these functions are called 'blocking parts' of the correlation functions denoted by

$$h_{11}^b = h_{13}, \quad h_{12}^b = h_{14}, \quad h_{22}^b = h_{24} \tag{5.15}$$

and

$$h_{11}^c = h_{11} - h_{11}^b, \quad h_{12}^c = h_{12} - h_{12}^b, \quad h_{22}^c = h_{22} - h_{22}^b \tag{5.16}$$

are the so called connected parts of the correlation functions. Given and Stell [18] introduced the two correlation functions h_{ij}^c and h_{ij}^b by their diagrammatic expansion. It should be borne in mind that $h_{13}^{rep}, h_{14}^{rep}, h_{24}^{rep}$, describe the correlation between particles of different replicas which do not interact directly. They only interact indirectly through the mediation of the quenched particles. So, the connected parts of the correlation functions describe correlations between a pair of fluid particles that are transmitted through successive layers of fluid particles whereas the blocking parts describe correlations between fluid particles blocked or separated from each other by matrix particles. Note that, though the matrix particles are immobile, they tend to order the fluid particles on either side of them and thus are capable of mediating correlations through a layer of matrix particles. At very low matrix porosities, i.e. very high densities of the matrix, the volume accessible to fluid particles is divided into small cavities. In this limit the functions h_{ij}^c describe correlations between fluid particles in the same cavity, whereas h_{ij}^b describe correlations between fluid particles in different cavities.

The ROZ equations (5.13) form a set of nine integral-equations, eight of them being coupled.

Integral-equation closure relations

The ROZ equations can now be solved with one of the standard closure relations of liquid state theory [4], such as the Percus-Yevick (PY) or the hypernetted chain (HNC)

approximation. The method used here is a hybrid of the iterative Picard scheme and the Newton-Raphson technique which was developed by Gillan [125]. The numerical solution of the ROZ equations is based on an algorithm introduced by Labik, Malijevsky and Vonka (LMV algorithm [126]), an extension of Gillan's work, which was originally proposed for solving numerically the OZ equations for homogeneous liquids (and mixtures) and extended by Lomba [113] to the case of the ROZ equations. We have calculated the correlation functions of the reference system by solving the ROZ equations along with the PY closure.

The optimized random phase approximation

To close the ROZ equations we have chosen the ORPA (see section 2.2.2). Applying the ORPA to the replicated system and taking the limiting case $s \to 0$ one obtains the properties of the partly quenched system.

The replicated system is now a $(2s + 1)$-component system with a very special set of interatomic potentials $\Phi_{ij}(r)$. Most importantly, since the particles belonging to different replicas do not interact, one has $\phi_{13} = \phi_{14} = \phi_{24} = 0$. We assume that the matrix particles are pure hard spheres; then the RPA closure relations read

$$
\begin{array}{rcll}
c_{00}^{\text{rep}}(r; s) & = & c_{\text{r};00}^{\text{rep}}(r; s) & \\
c_{ij}^{\text{rep}}(r; s) & = & c_{\text{r};ij}^{\text{rep}}(r; s) + c_{\text{p};ij}^{\text{rep}}(r; s) & \text{for } i,j = 01, 02, 11, 12, 22 \\
c_{ij}^{\text{rep}}(r; s) & = & c_{\text{r};ij}^{\text{rep}}(r; s) & \text{for } i,j = 13, 14, 24.
\end{array}
\tag{5.17}
$$

with $c_{\text{p};ij}^{\text{rep}}(r; s) = -\beta \Phi_{\text{p};ij}(r)$, while the core conditions now read $h_{\text{p};ij}(r) = 0$ for $r < \sigma_{ij}$, $ij = 01, 02, 11, 12, 13$. Since there is no risk of ambiguity, we can suppress in the following the arguments r and k of the functions; the arguments are obvious from the following notation: functions in k-space carry a tilde, while all other functions are in r-space. Using the symmetry properties of the replicated system the expression for the excess free energy (2.56) in the replicated system, $(A^{\text{rep}})^* = -\beta A_{\text{ex}}^{\text{rep}}(s)/V$ is given by

$$
\begin{aligned}
(A^{\text{rep}})^* (s) = {} & (A_{\text{r}}^{\text{rep}})^* (s) + \\
& \frac{1}{2} \left[s \sum_{i=1,2} \rho_i^2 \tilde{c}_{\text{p};ii}^{\text{rep}}(s) + 2s \sum_{\substack{i<j \\ i=0,1}} \rho_i \rho_j \tilde{c}_{\text{p};ij}^{\text{rep}}(s) \right]_{k=0} - \frac{1}{2} \left[s \sum_{i=1,2} \rho_i c_{\text{p};ii}^{\text{rep}}(s) \right]_{r=0} \\
& - \frac{1}{2(2\pi)^3} \int d^3k \left\{ \ln \det \left[1 - \widetilde{\mathsf{C}}^{\text{rep}}(s) \right] - \ln \det \left[1 - \widetilde{\mathsf{C}}_{\text{r}}^{\text{rep}}(s) \right] \right\},
\end{aligned}
\tag{5.18}
$$

where we have used the matrix notation C introduced in subsect. 2.2.2. Again, closer investigation of the symmetry of the two matrices appearing in the above equation allows

to derive the following identity which can be applied to both contributions of the above integral

$$
\begin{aligned}
\ln \det &\left[1 - \widetilde{\mathsf{C}}^{\mathrm{rep}}(s) \right] \\
&= (s-1) \ln \left\{ \left[1 - \rho_1 \left(\tilde{c}_{11}^{\mathrm{rep}}(s) - \tilde{c}_{13}^{\mathrm{rep}}(s) \right) \right] \left[1 - \rho_2 \left(\tilde{c}_{22}^{\mathrm{rep}}(s) - \tilde{c}_{24}^{\mathrm{rep}}(s) \right) \right] \right. \\
&\qquad\qquad\qquad\qquad\qquad\qquad \left. -\rho_1 \rho_2 \left[\tilde{c}_{12}^{\mathrm{rep}}(s) - \tilde{c}_{14}^{\mathrm{rep}}(s) \right]^2 \right\} + \\
&\quad \ln \left\{ \left[1 - \rho_0 \tilde{c}_{00}^{\mathrm{rep}}(s) \right] \left\{ \left[1 - \rho_1 \tilde{c}_{11}^{\mathrm{rep}}(s) - \rho_1 (s-1) \tilde{c}_{13}^{\mathrm{rep}}(s) \right] \times \right. \right. \\
&\qquad\qquad \left[1 - \rho_2 \tilde{c}_{22}^{\mathrm{rep}}(s) - \rho_2 (s-1) \tilde{c}_{24}^{\mathrm{rep}}(s) \right] - \rho_1 \rho_2 \left[\tilde{c}_{12}^{\mathrm{rep}}(s) + (s-1) \tilde{c}_{14}^{\mathrm{rep}}(s) \right]^2 \left.\right\} - \\
&\qquad\qquad s \rho_0 \rho_1 \left[\tilde{c}_{01}^{\mathrm{rep}}(s) \right]^2 \left[1 - \rho_2 \tilde{c}_{22}^{\mathrm{rep}}(s) - (s-1) \tilde{c}_{24}^{\mathrm{rep}}(s) \right]^2 - \\
&\qquad\qquad 2 s \rho_0 \rho_1 \rho_2 \tilde{c}_{01}^{\mathrm{rep}}(s) \tilde{c}_{02}^{\mathrm{rep}}(s) \left[\tilde{c}_{12}^{\mathrm{rep}}(s) + (s-1) \tilde{c}_{14}^{\mathrm{rep}}(s) \right] - \\
&\qquad\qquad s \rho_0 \rho_2 \left[\tilde{c}_{02}^{\mathrm{rep}}(s) \right]^2 \left[1 - \rho_1 \tilde{c}_{11}^{\mathrm{rep}}(s) - (s-1) \tilde{c}_{13}^{\mathrm{rep}}(s) \right]^2 \left.\right\}.
\end{aligned}
\tag{5.19}
$$

The free energy of the quenched system, $\bar{A}$, is now obtained via $\bar{A} = \lim_{s \to 0} \frac{d}{ds} A^{\mathrm{rep}}(s)$ [110, 35]

$$
\begin{aligned}
\bar{A}^* = {}& A_{\mathrm{r}}^* - \mathcal{A}[\mathsf{C}] + \mathcal{A}[\mathsf{C}_{\mathrm{r}}] + \\
& \frac{1}{2} \left[\rho_1^2 \tilde{c}_{\mathrm{p};11} + \rho_2^2 \tilde{c}_{\mathrm{p};22} + 2 \rho_0 \rho_1 \tilde{c}_{\mathrm{p};01} + 2 \rho_0 \rho_2 \tilde{c}_{\mathrm{p};02} + 2 \rho_1 \rho_2 \tilde{c}_{\mathrm{p};12} \right]_{k=0} - \\
& \frac{1}{2} \left[\rho_1 c_{\mathrm{p};11} + \rho_2 c_{\mathrm{p};22} \right]_{r=0}
\end{aligned}
\tag{5.20}
$$

where the functional $\mathcal{A}[\mathsf{C}]$ is defined as follows

$$
\begin{aligned}
\mathcal{A}[\mathsf{C}] = {}& \frac{1}{2(2\pi)^3} \int d^3 k \left\{ \ln \left\{ \left(1 - \rho_1 \tilde{c}_{11}^{c} \right) \left(1 - \rho_1 \tilde{c}_{22}^{c} \right) - \rho_1 \rho_2 \left[\tilde{c}_{12}^{c} \right]^2 \right\} - \right. \\
& \frac{1}{\left[1 - \rho_1 \tilde{c}_{11}^{c} \right] \left[1 - \rho_2 \tilde{c}_{22}^{c} \right] - \rho_1 \rho_2 \left[\tilde{c}_{12}^{c} \right]^2} \times \\
& \left[\rho_1 \tilde{c}_{13} \left(1 - \rho_2 \tilde{c}_{22}^{c} \right) + \rho_2 \tilde{c}_{24} \left(1 - \rho_1 \tilde{c}_{11}^{c} \right) + 2 \rho_1 \rho_2 \tilde{c}_{14} \tilde{c}_{12}^{c} + \right. \\
& \left. \left. \frac{\rho_0}{1 - \rho_0 \tilde{c}_{00}} \left(\rho_1 \tilde{c}_{01}^2 \left(1 - \rho_2 \tilde{c}_{22}^{c} \right) + \rho_2 \tilde{c}_{02}^2 \left(1 - \rho_1 \tilde{c}_{11}^{c} \right) + 2 \rho_1 \rho_2 \tilde{c}_{01} \tilde{c}_{02} \tilde{c}_{12}^{c} \right) \right] \right\}
\end{aligned}
\tag{5.21}
$$

and $\mathcal{A}[\mathsf{C}_{\mathrm{r}}]$ is obtained from the above expression by substituting the c_{ij}'s by $c_{\mathrm{r};ij}$'s.

Finally one can show [34] that for the above expression of the free energy the following relation holds

$$
\left(\frac{\delta \bar{A}^*}{\delta c_{\mathrm{p};ij}} \right)(r) = \frac{2 - \delta_{ij}}{2} \rho_i \rho_j \left[g_{\mathrm{r};ij}(r) + h_{\mathrm{p};ij}(r) \right]
\tag{5.22}
$$

which means that the minimization of the functional $\bar{A}^*[\mathsf{C}_{\mathrm{p}}]$ with respect to variations of the $c_{\mathrm{p};ij}(r)$ inside the core region is equivalent to the hard core condition. This fact is in particular useful for the *numerical* solution of the ORPA: although, of course, the

numerical solutions of integral-equations and of the minimization of the functional should lead to the same results we found that – from the numerical point of view - in some cases it can be more convenient to solve the minimization problem.

5.3.3   Numerical details

For the numerical solution of the ORPA we have discretized the correlation functions both in r- and k-space, using typically 1024 grid-points and a mesh-size of $\Delta r = 0.01\sigma$. For a given system, we first calculate the correlation functions $h_{\mathrm{r};ij}$ and $c_{\mathrm{r};ij}$ of the reference system by solving the ROZ equations (5.13) along with the Percus-Yevick (PY) closure [4] using the LMV-algorithm [126] adapted to the present problem [113]. The iterative algorithm is considered to be converged if the difference $\Delta\Gamma_{ij}$ between two successive values of the functions $\Gamma_{ij} = (h_{ij} - c_{ij})r$ satisfies

$$\sum_{ij} \sum_{l} \left[\Delta\Gamma_{ij}(r_l)\right]^2 \Delta r < 10^{-5}. \tag{5.23}$$

In eq. (5.23) the first summation is done over all pairs of indices while the second sum is taken over all grid points of the r-mesh.

Then we solve the ORPA by minimizing $\mathcal{A}$ (5.21) using the steepest-descent method to obtain the correlation functions $h_{\mathrm{p};ij}$ and $c_{\mathrm{p};ij}$. The advantage of this minimization algorithm lies in the fact that an explicit calculation of the functional is not required; we only need its derivatives, i.e. the $h_{\mathrm{p};ij}$'s, which we easily obtain from the so-called residual ROZ-equations [34]. Starting from an initial guess for the direct correlation functions inside the core region (for instance, the simple RPA expression or the solution at some lower density) we create with these gradients a sequence of new, improved direct correlation functions until we obtain a minimum in the functional within a sufficient accuracy. The step size in this search is triggered by a parameter ξ which measures the degree of violation of the core condition by the resulting perturbation parts of the total correlation functions, $H_{\mathrm{p};ij}(r) = rh_{\mathrm{p};ij}(r)$

$$\xi = \left\{ \left[\sum_{j=1,2} \sum_{k:r_k<\sigma_{0j}} \left(H_{\mathrm{p};0j}(r_k)\right)^2 + \sum_{i,j=1,2;i\leq j} \sum_{k:r_k<\sigma_{ij}} \left(H_{\mathrm{p};ij}(r_k)\right)^2 \right] \Delta r \right\}^{1/2}. \tag{5.24}$$

For each system the ROZ have been solved along isotherms separated by $\Delta T = 0.002$ (0.0001 near critical regions) with a grid size in density of 0.005 and 0.0125 in concentration.

5.3.4 Thermodynamic Properties

In order to calculate phase equilibria we have to equate the pressure and the chemical potentials; in the following we present expressions for these quantities.

The chemical potentials $\mu_i = \mu_i^{\mathrm{id}} + \mu_{\mathrm{r};i}^{\mathrm{ex}} + \mu_{\mathrm{p};i}$ are calculated as follows ('ex' denotes the excess part over the ideal part, 'id'): the reference parts are obtained via numerical integration of the compressibility equation, i.e.,

$$
\begin{aligned}
\left(\frac{\partial \beta \mu_{\mathrm{r};1}^{\mathrm{ex}}}{\partial \rho_f}\right)_{T,x,\rho_0} &= -x[\tilde{c}_{\mathrm{r};11}^c]_{k=0} - (1-x)[\tilde{c}_{\mathrm{r};12}^c]_{k=0} \\
\left(\frac{\partial \beta \mu_{\mathrm{r};2}^{\mathrm{ex}}}{\partial \rho_f}\right)_{T,x,\rho_0} &= -(1-x)[\tilde{c}_{\mathrm{r};22}^c]_{k=0} - x[\tilde{c}_{\mathrm{r};12}^c]_{k=0}
\end{aligned}
\tag{5.25}
$$

using as an integration constant at $\rho_f = 0$ the Carnahan-Starling expression for the excess chemical potential of a one-component system of hard spheres at packing fraction $\eta = (\pi/6)\rho_0\sigma^3$ [118]

$$
\beta\mu_{\mathrm{r};i}^{\mathrm{ex}}(\rho_f = 0) = \frac{8\eta - 9\eta^2 + 3\eta^3}{(1-\eta)^3} \qquad i = 1, 2.
\tag{5.26}
$$

Further, the ideal parts of the chemical potentials are given by $\beta\mu_i^{\mathrm{id}} = \ln \rho_i$ $(i = 1, 2)$ and for the perturbation parts of the μ_i's one is able to derive closed expressions in the version of the ORPA used in this contribution (which is equivalent to the MSA) within the energy route [51]

$$
\beta\mu_{\mathrm{p};1} = \beta\mu_1 - \beta\mu_{\mathrm{r};1} = -\left[\rho_f x \tilde{c}_{\mathrm{p};11} + \rho_0 \tilde{c}_{\mathrm{p};01} + \rho_f(1-x)\tilde{c}_{\mathrm{p};12}\right]_{k=0} + \frac{1}{2}\left[c_{\mathrm{p};11}\right]_{r=0},
$$

$$
\beta\mu_{\mathrm{p};2} = \beta\mu_2 - \beta\mu_{\mathrm{r};2} = -\left[\rho_f(1-x)\tilde{c}_{\mathrm{p};22} + \rho_0 \tilde{c}_{\mathrm{p};02} + \rho_f x \tilde{c}_{\mathrm{p};12}\right]_{k=0} + \frac{1}{2}\left[c_{\mathrm{p};22}\right]_{r=0}.
\tag{5.27}
$$

The pressure, $P = P^{\mathrm{id}} + P_{\mathrm{r}}^{\mathrm{ex}} + P_{\mathrm{p}}$, is calculated as follows: the ideal contribution is $\beta P^{\mathrm{id}} = \rho_f$; the reference part to the pressure is obtained via numerical integration of the compressibility relation

$$
\left(\frac{\partial \beta P_{\mathrm{r}}^{\mathrm{ex}}}{\partial \rho_f}\right)_{T,x,\rho_0} = -\rho_f \left\{x^2[\tilde{c}_{\mathrm{r};11}^c]_{k=0} + 2x(1-x)[\tilde{c}_{\mathrm{r};12}^c]_{k=0} + (1-x)^2[\tilde{c}_{\mathrm{r};22}^c]_{k=0}\right\};
\tag{5.28}
$$

Note that the integration constants are irrelevant if one wants to determine only the phase diagram.

Finally, the perturbation part of the pressure is calculated from the Gibbs-Duhem relation

$$
\beta P_{\mathrm{p}} = \bar{A}^\star - \bar{A}_{\mathrm{r}}^\star + \beta \sum_{i=1,2} \rho_i \mu_{\mathrm{p};i},
\tag{5.29}
$$

where the difference of the free energies is taken from (5.20).

Phase diagrams were determined from numerical solution of the equilibrium conditions Eqs. (3.11) – (3.12) as explained in section 3.1.3; these coupled non-linear equations were solved via a Newton-Raphson procedure.

As we approach the critical or tricritical points the above systems of equations become ill-conditioned. In all the phase diagrams presented in the following section we have plotted the coexistence curves as far as reliable numerical solutions were available, the open segments representing those regions where no numerical solution could be found.

For the determination of the critical temperature and density, T_c and ρ_c, the results were extrapolated under the assumption that the coexistence curve can be described by a scaling type law and the law of rectilinear diameters, i.e.

$$\rho_l - \rho_g = B(T - T_c)^{\beta} \qquad (\rho_l + \rho_g)/2 = \rho_c + A(T - T_c) \qquad (5.30)$$

Eqs. (5.30) were fitted to the coexistence curves by taking A,B, and β as adjustable parameters. Due to the well-known fact that the ORPA (being a conventional liquid state theory) fails to describe correctly the critical region [7], the values of β (generally between 1/3 or 1/2 depending on matrix density) obtained by the curve fitting should not be considered as reliable estimates of a critical exponent.

5.4   Results

5.4.1   Comparison with simulations

The computer simulations, carried out for four different matrix densities $\rho_0 = 0$, 0.05, 0.15 and 0.3 at $\alpha = 0.7$, $y = 1$, $z\sigma = 2.5$, $r_c = 2.5\sigma$, have been compared with ORPA results (for technical details of the GCMC simulations we refer to [19] and references quoted therein). The MC results are shown in fig. (5.2) by the symbols. In the range of temperatures $T \approx 0.7$ - 0.8 one observes, for $\rho_0 = 0$, a first order V-MF transition with critical temperature $T_c \approx 0.72 - 0.73$ and critical density $\rho_c \approx 0.35$ and a line of second order demixing transitions terminating at a tricritical point with temperature $T_{tc} \approx 0.73$, slightly higher than the critical temperature, and density $\rho_{tc} \approx 0.57$. This diagram is of type II. When the matrix density increases, the temperature range, within which the equimolar liquid exists, decreases and the phase diagram evolves towards a type I diagram. At $\rho_0 = 0.3$ the phase diagram in the temperature range $0.49 - 0.52$ reveals that (within
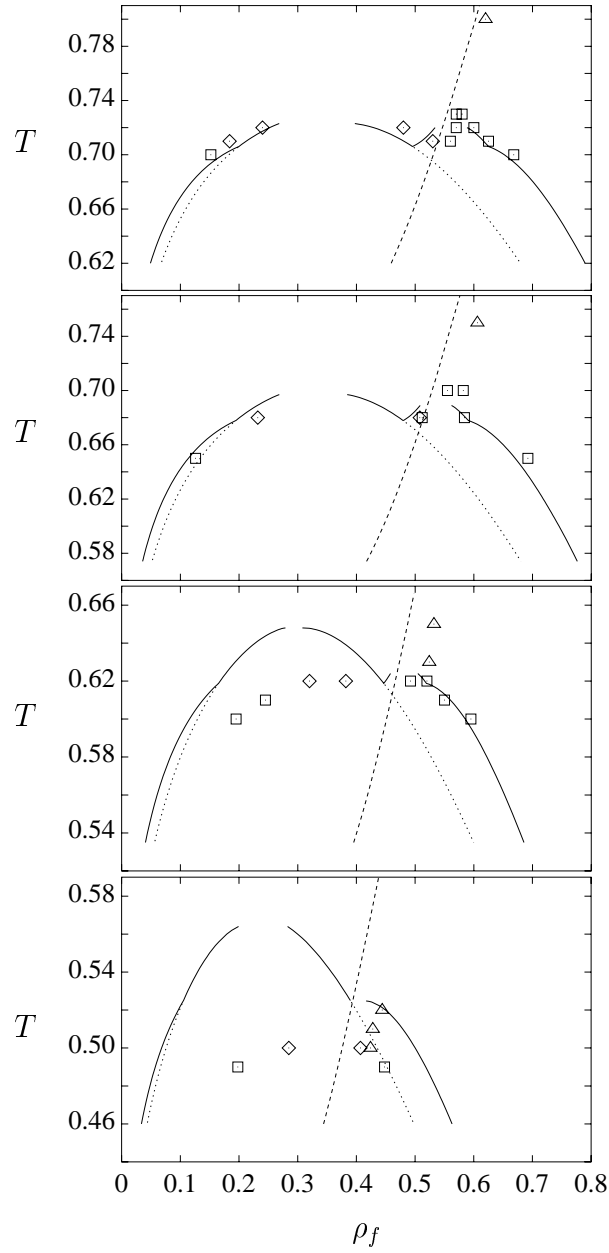
Figure 5.2: Variation with matrix density ρ_0 of the phase diagram of a binary fluid mixture in contact with a porous matrix ($\alpha = 0.7$, $y = 1$ and $z\sigma = 2.5$): comparison between GCMC [19] and ORPA results. $\rho_0 = 0$, 0.05, 0.15, and 0.30 (from top to bottom). Symbols: GCMC simulations (diamonds: V-MF equilibrium; squares: V-DF or MF-DF equilibrium; triangles: λ-line). Lines: ORPA results (full line: V-MF, V-DF or MF-DF coexistence curve; dotted line: metastable V-MF transitions; dashed line: λ-line).
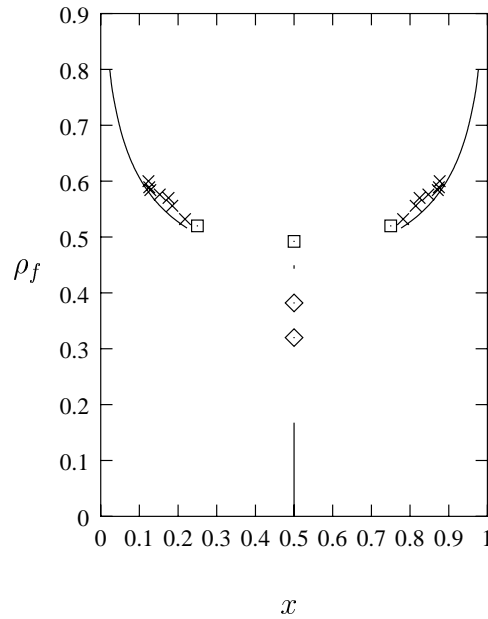
Figure 5.3: Demixing transition of a binary fluid in contact with a porous matrix of density $\rho_0 = 0.15$ ($\alpha = 0.7$, $y = 1$ and $z\sigma = 2.5$): ρ_f as a function of concentration x for $T = 0.62$. The symbols denote GCMC simulations (diamonds: V-MF equilibrium; squares: MF-DF equilibrium; crosses: first order demixing transition) the lines ORPA results.

accuracy of the simulation results) the tricritical temperature, or possibly the temperature of the critical end point, is close and slightly below the critical temperature (~ 0.51).

Comparison of the phase diagrams with ORPA results is also illustrated in fig. (5.2). At $\rho_0 = 0$ excellent agreement is obtained for the V-MF and MF-DF transition densities, the fluid concentrations of the demixed phase and the λ-line. This agreement deteriorates, however, with increasing ρ_0. Although in the ORPA the same sequence of types of phase diagrams occurs as in the simulations and general trends (lowering of the critical temperature and narrowing of the V-MF coexistence curve with increasing matrix density) are correctly reproduced, marked differences are observed on a quantitative level. In particular, for $\rho_0 \geq 0.15$, the critical temperature is found to be higher than in the simulations; also the ratio of the critical to tricritical or end point temperature increases with ρ_0, while it remains close to 1 in the simulations. Furthermore, the critical density shifts to lower values in contrast to the simulations where it remains nearly constant. On the other hand, the concentrations of the demixed phase remain accurate even at a high matrix density as illustrated in fig. (5.3) for $\rho_0 = 0.15$. As noted in the previous section, the determination of the equilibrium densities of the different phases in the simulations

are affected by uncertainties of the order of 2-3 % for $\rho_0 \neq 0$ and ~ 1 % for $\rho_0 = 0$. In view of these error bars the difference between the theory and the simulations at the higher matrix densities is significant. The major source of error is likely to be found in the use of the ORPA, in particular in that of the PY type closure to solve the ROZ equations for the reference hard sphere system in the framework of the replica theory [114]. Differences of similar size between simulation and ORPA results were observed in the one-component case [119].

5.4.2 Variation of α

The variation of the phase diagram with α (ratio of the interaction strengths between unlike and like particles) is shown in figs. (5.4)-(5.6) for the matrix densities $\rho_0 = 0$ and 0.1. In the latter case the matrix-fluid interaction was either a pure hard sphere ($y = 0$) or a hard sphere + Yukawa interaction ($y = 1$). For the bulk mixture we observe – in qualitative agreement with the mean-field results of Wilding *et al.* [12] and subsect. 4.3.5 – variation of the phase diagram from type III to type II to type I as we increase α from 0.65 to 0.90. At $\alpha = 0.9$ no demixing transition could be observed down to a temperature $T = 0.55$, below which the ORPA equations no longer could be solved. At this temperature and α value a freezing transition is also possible and the demixing transition does not exist anymore in the fluid phase. Over the range of α values considered the critical temperature and density do not vary appreciably with α. An increase of the matrix density from 0 to 0.1 (at $y = 1$) does not alter this behavior or the sequence of phase diagrams (from type III to type I) but lowers T_c and T_{tc} by $\sim 10\%$ and shifts the densities of the tricritical and CEP points to slightly lower densities. A change of y from 1 to 0 at fixed matrix density $\rho_0 = 0.1$ lowers T_c by $\sim 10\%$, shifts ρ_c from ~ 0.32 to ~ 0.26 and delays the appearance of the CEP as one increases α.

5.4.3 Variation of y

The variation with the parameter y (expressing the ratio between the fluid-fluid and the matrix-fluid interactions) is shown in fig. (5.7) and (5.8) for the two cases $\rho_0 = 0.05$, $\alpha = 0.7$ and $\rho_0 = 0.1$, $\alpha = 0.73$. A positive value of y represents an attraction between matrix and fluid particles while a negative value represents a repulsion. For the lower matrix density $\rho_0 = 0.05$, the sequence of phase diagrams is found to be type III $\rightarrow$ type II $\rightarrow$ type III when y decreases from positive to negative values. A V-MF transition appears near $y \sim 2$ (a precise location cannot be found due to numerical problems in the
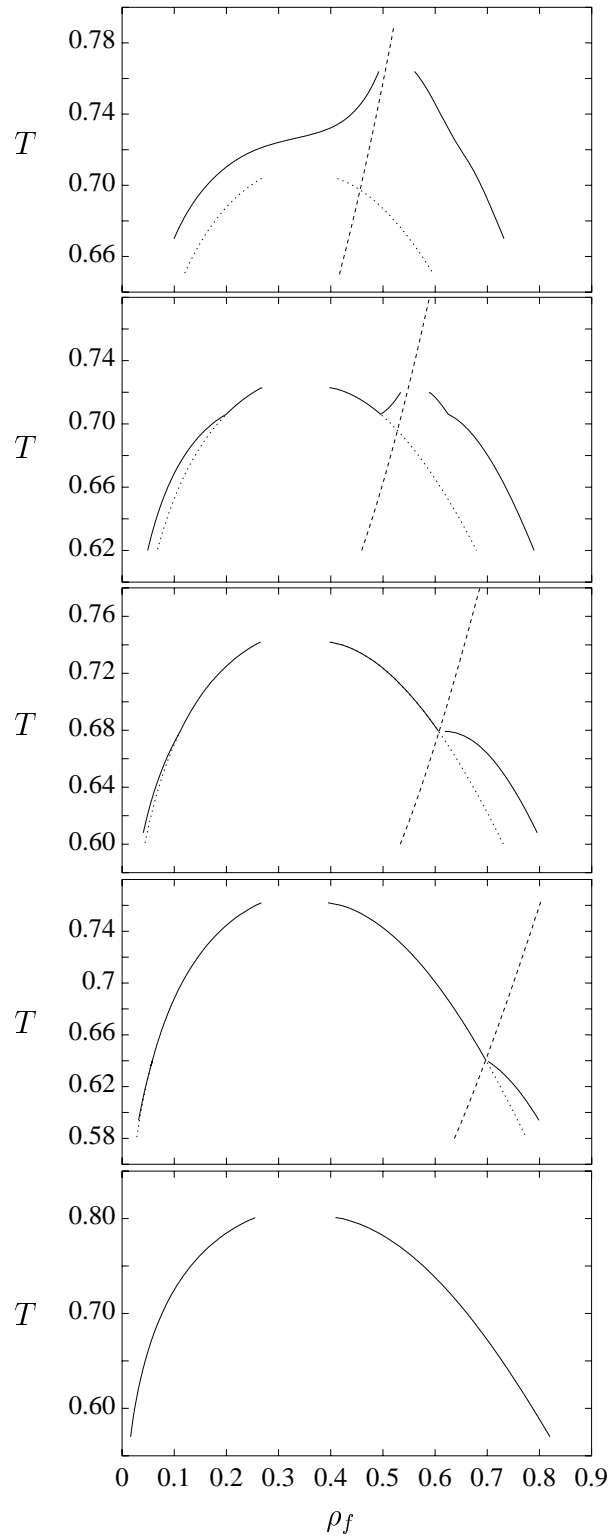
Figure 5.4: Variation with α of the phase diagram of the binary fluid mixture in thermal equilibrium with a porous matrix from ORPA. $\rho_0 = 0$: $\alpha = 0.65$, 0.70, 0.75, 0.80 and 0.90 (from top to bottom); Full line: V-MF, V-DF or MF-DF coexistence curves; dotted line: metastable V-MF transition; dashed line: λ-line.
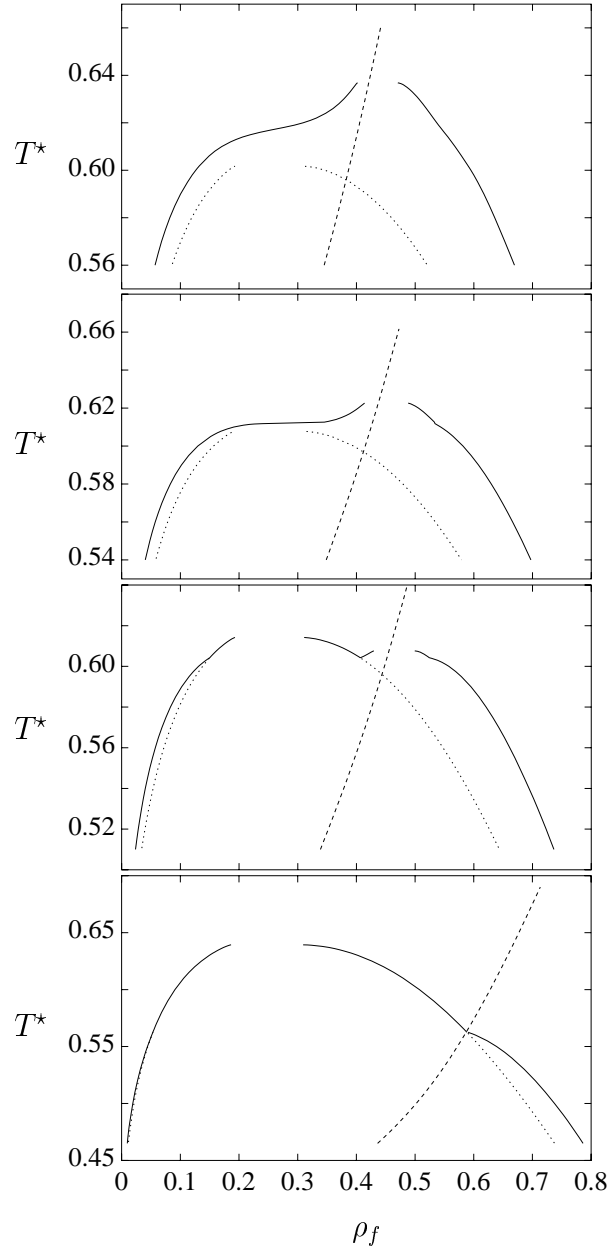
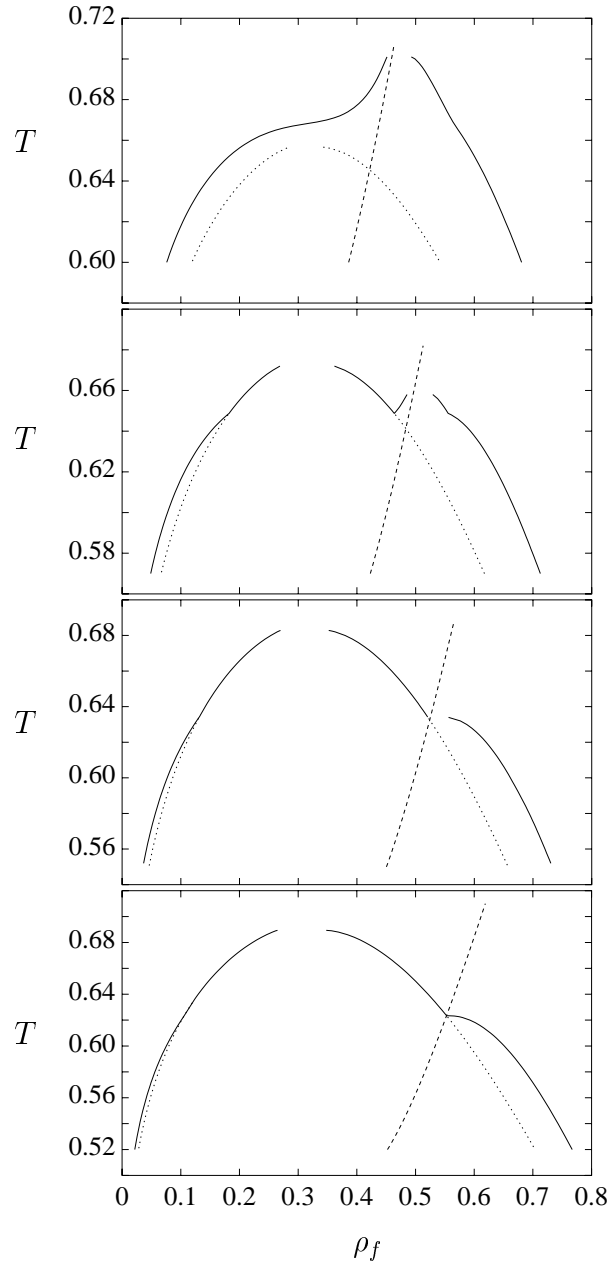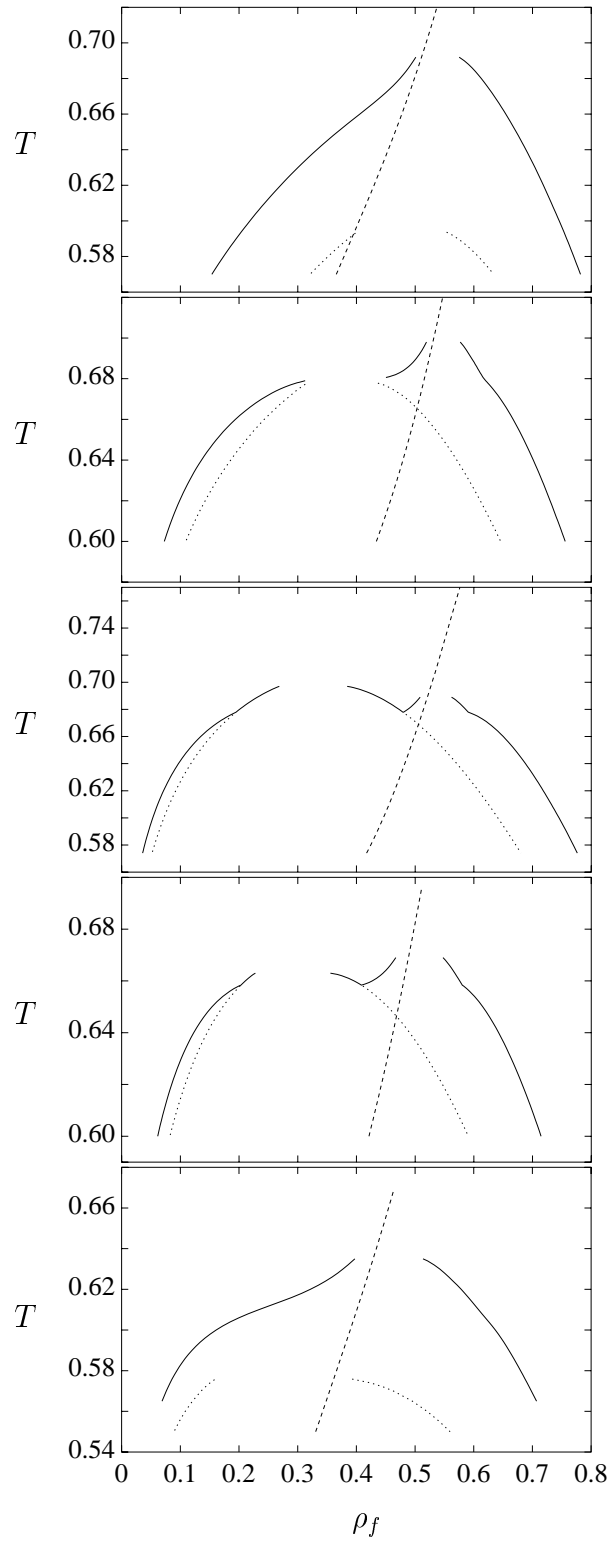Figure 5.5: The same as in fig. (5.4) for $\rho_0 = 0.1$, $y = 0$: $\alpha = 0.68$, 0.70, 0.72 and 0.80 (from top to bottom).

Figure 5.6: The same as in fig. (5.4) for $\rho_0 = 0.1$, $y = 1$: $\alpha = 0.65$, 0.70, 0.73, and 0.75 (from top to bottom).

Figure 5.7: Variation with y of the phase diagram of the binary fluid mixture in thermal equilibrium with a porous matrix from ORPA. $\rho_0 = 0.05$, $\alpha = 0.7$: $y = 3.5, 2, 1, 0, -1$ (from top to bottom). Full line: V-MF, V-DF or MF-DF coexistence curves; dotted line: metastable V-MF transition; dashed line: λ-line.
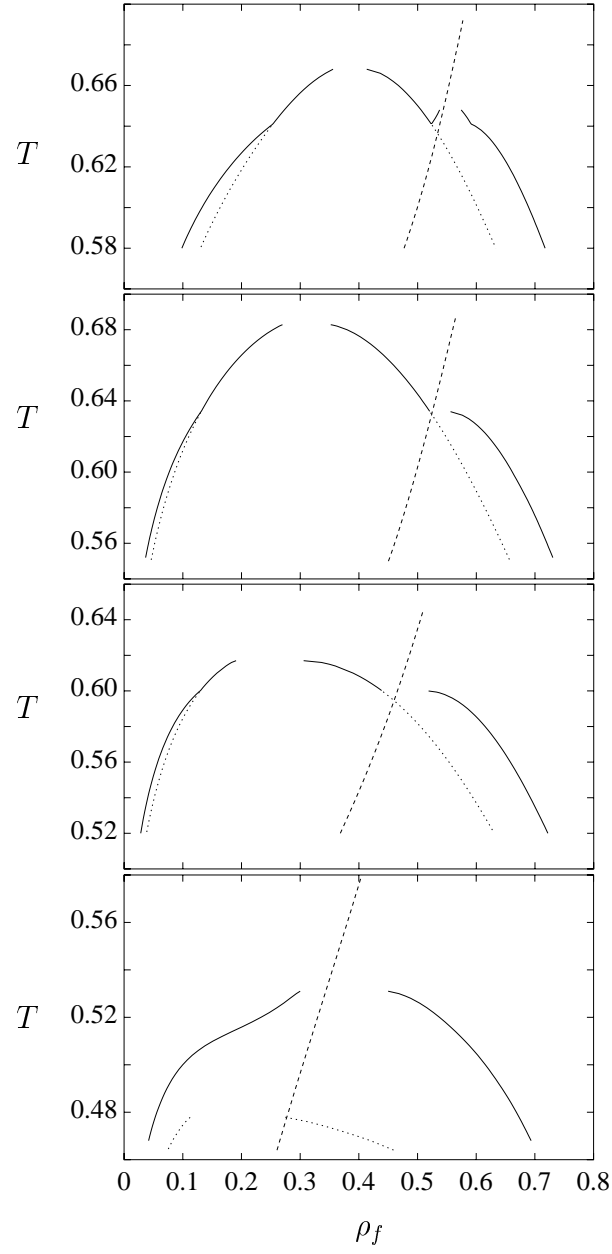
Figure 5.8: The same as in fig. (5.7) for $\rho_0 = 0.10$, $\alpha = 0.73$: $y = 2$, 1, 0, -1 (from top to bottom).

critical region as mentioned above) and exists only in a small range of y-values extending roughly from 2 to -0.5. The phase diagram is again of type III for the more strongly repulsive matrix-fluid interactions $y = -1$. A qualitatively similar behavior is observed for the larger matrix density $\rho_0 = 0.1$; here the type II phase behavior occurs at least for $0 < y < 2$.

The ORPA allows us to determine the metastable V-MF transitions (hidden below the V-DF coexistence curve); these are marked in figs. (5.7)-(5.8) by dotted lines. From fig. (5.7), it is apparent that, when the matrix is strongly attractive ($y = 3.5$), the λ-line (extended into the V-DF coexistence region) intersects the metastable first order V-MF coexistence line at a density smaller than the (metastable) critical density, $\rho_c^{\mathrm{V-MF}}$, while for the repulsive matrix-fluid interaction ($y = -1$) the intersection is observed for densities larger than $\rho_c^{\mathrm{V-MF}}$. As pointed out by Wilding *et al.* [12] in their mean-field study of a symmetric binary *bulk* mixture these differences in the metastable equilibrium may be of relevance for the dynamic properties of the system. Therefore, when, in the case of a repulsive matrix, the fluid is quenched from a high temperature state into the coexistence region slightly below the metastable critical point one can expect "two-stage demixing". This means, the system will first separate into a V- and a MF-phase; then the equimolar liquid will demix [12]. In contrast, for an attractive matrix ($y = 3.5$), the fluid will demix and phase separate simultaneously ("one-stage demixing" [12]).

5.4.4   Variation of ρ_0

The influence of the matrix density on the phase diagram of the mixture is shown in figs. (5.9) and (5.10) for two values, 0 and 1, of the parameter y and $\alpha = 0.7$. As discussed in the comparison of simulation and theoretical results, in both cases, at $\rho_0 = 0$, we have a type II diagram characterized by a tricritical point (where the λ-line of the second order demixing transition terminates) as well as a triple point where the G, the L and the DF coexist. As we increase ρ_0, at $y = 1$ (attractive tail in the matrix-fluid interaction) the tricritical temperature T_{tc} decreases; at $\rho_0 \sim 0.3$ the first order transition between the MF and the DF has vanished, giving rise to a CEP at T_{cep} (type I phase diagram). It can be observed that the existence of a CEP leads to a kink in the V-MF curve, clearly visible in the ORPA data, a phenomenon which has been discussed in a simulation study of the pure mixture in [127]. The situation is completely different if the matrix-fluid interactions are hard sphere potentials ($y = 0$). We now arrive with increasing ρ_0 at a type III phase diagram; for $\rho_0 \sim 0.1$ the V-MF transition becomes metastable and hidden below the V-DF transition (type III phase diagram). As discussed in the previous subsection, the
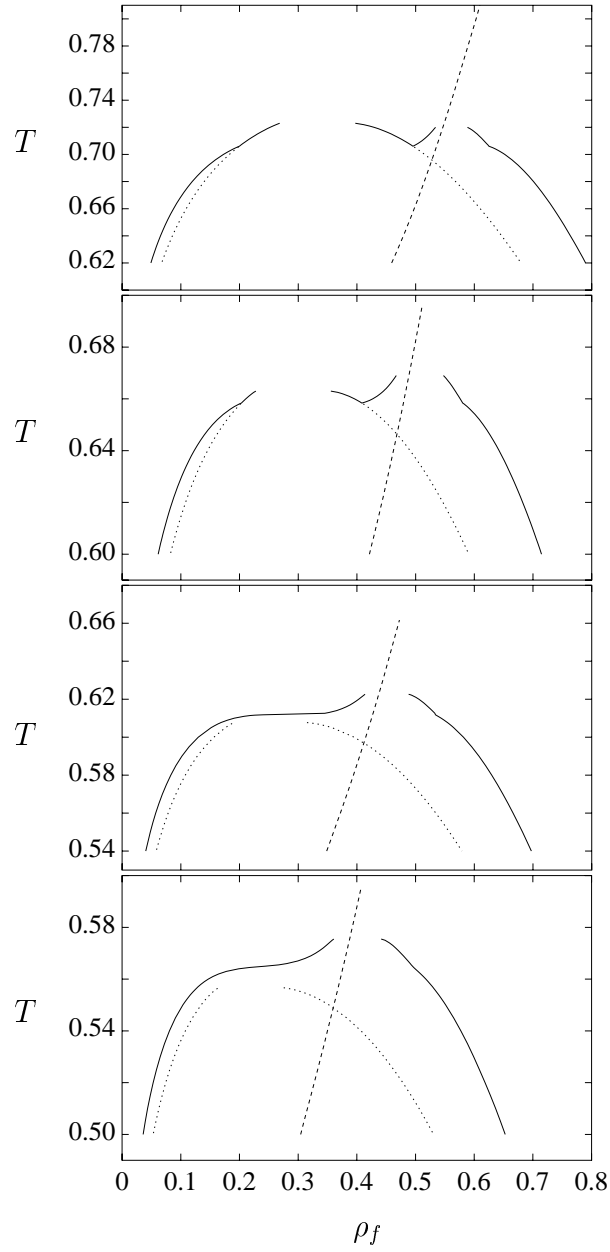
Figure 5.9: Variation with matrix density ρ_0 of the phase diagram of the binary fluid mixture in thermal equilibrium with a porous matrix from ORPA. $y = 0$, $\alpha = 0.7$: ρ_0 = 0., 0.05, 0.10 and 0.15 (from top to bottom). Full line: V-MF, V-DF or MF-DF coexistence curves; dotted line: metastable V-MF transition; dashed line: λ-line.
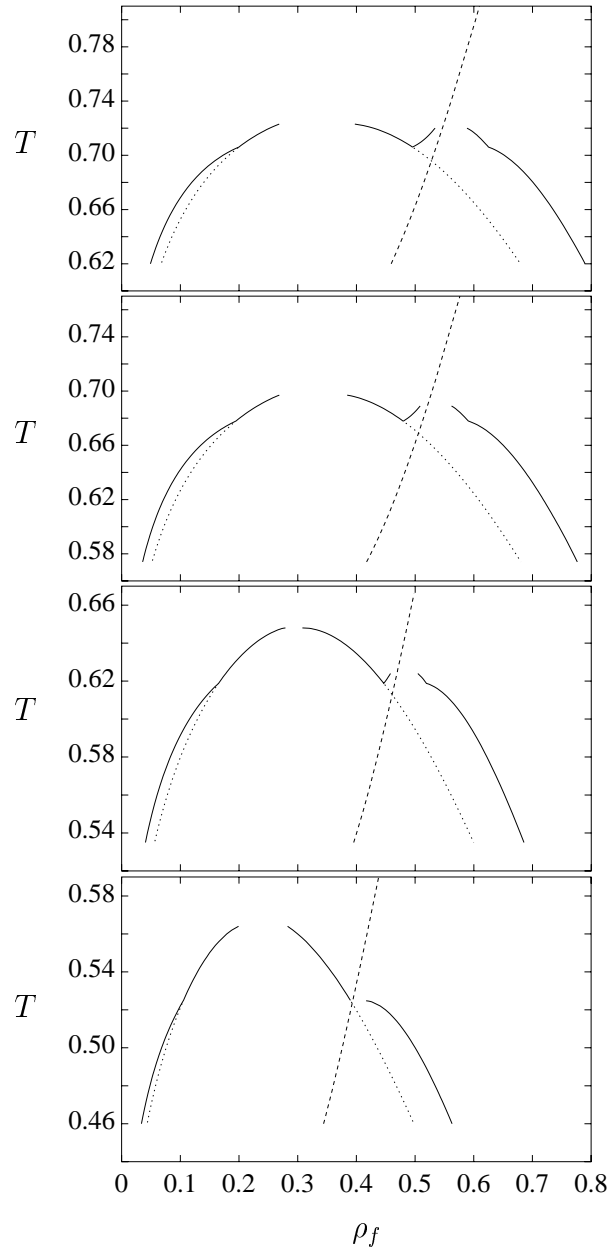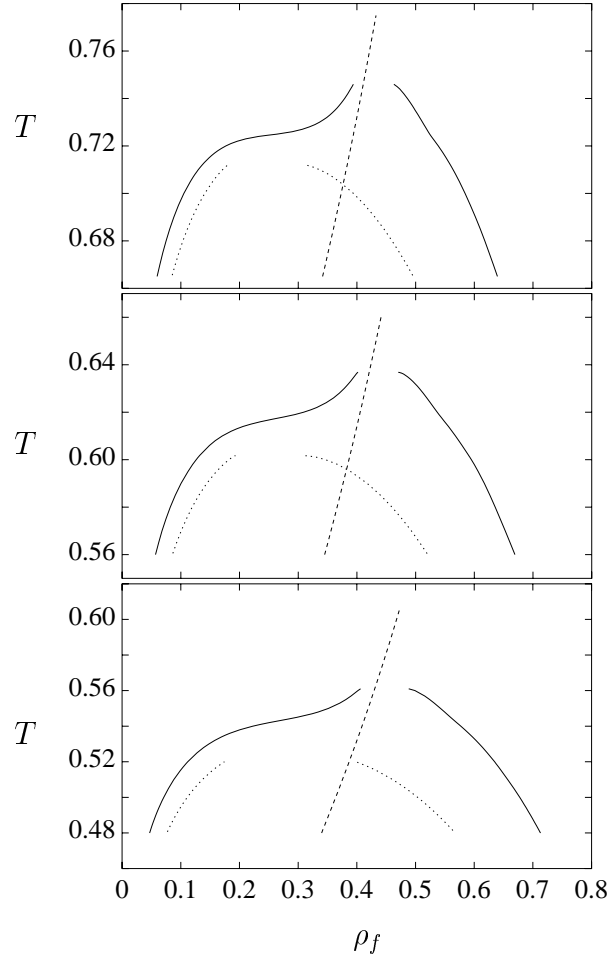
Figure 5.10: The same as in fig. (5.7) for $y = 1$, $\alpha = 0.7$: $\rho_0 = 0$, 0.05, 0.15 and 0.30 (from top to bottom).

metastable V-MF transition can lead to a "two-stage demixing".
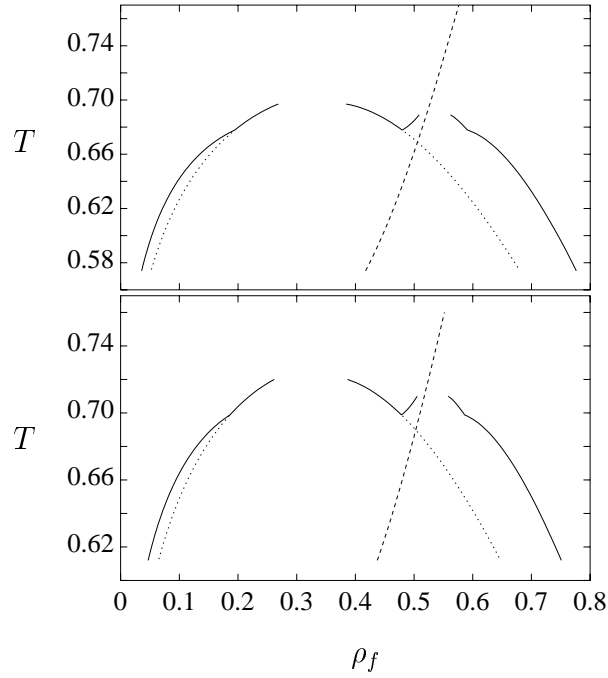
5.4.5 Variations of z and r_c

Figure 5.11: Variation with screening length z of the phase diagram of the binary fluid mixture in thermal equilibrium with a porous matrix from ORPA. Parameters: $y = 0$, $\alpha = 0.68$, and $\rho_0 = 0.10$. $z\sigma = 2$, 2.5 and 3 (from top to bottom). Full line: V-MF, V-DF or MF-DF coexistence curves; dotted line: metastable V-MF transition; dashed line: λ-line.

The change in phase diagram entailed by variation of the screening length z of the Yukawa potential is shown in fig. (5.11) for $\rho_0 = 0.10$, $\alpha = 0.68$, and $y = 0$. A change of $z\sigma$ from 2 to 3 mainly lowers the tricritical temperature and the critical temperature of the metastable V-MF transition, but otherwise leaves the critical density and type of phase diagram (type III) unchanged.

Increasing the range of the Yukawa potential from $r_c = 2.5\sigma$ (value at which most of the ORPA calculations have been performed to allow comparison with the MC simulations) to 8σ raises the critical temperature while preserving the shape of the phase diagram (cf. fig. (5.12)). We only observe a narrowing of the V-MF coexistence.

Figure 5.12: Variation with cut-off radius r_c of the phase diagram of the binary fluid mixture in thermal equilibrium with a porous matrix from ORPA. Top curve: $r_c = 2.5\sigma$; bottom curve $r_c = 8\sigma$. The other parameters are $y = 1$, $\alpha = 0.7$, and $\rho_0 = 0.05$. Full line: V-MF, V-DF or MF-DF coexistence curves; dotted line: metastable V-MF transition; dashed line: λ-line.

Chapter 6

Conclusion and Outlook

The Self-Consistent Ornstein Zernike Approximation (SCOZA) is an advanced liquid-state method that remains successful in the critical region; it enforces consistency between the compressibility route and the energy route to thermodynamics. SCOZA is known to give accurate results for the phase diagram and the critical behavior of a fluid.

We have generalized the formulation of the SCOZA to the case of a hard-core multi-Yukawa fluid. This has enabled us to treat various systems with pair potentials that can be parameterized in terms of linear combinations of Yukawa tails: the LJ potential and the Girifalco potential that describes the interaction between fullerene particles. We have calculated phase diagrams of these systems and compared the results with previous theoretical and simulation studies. The comparison has shown that the SCOZA provides very accurate estimates for the critical point parameters. The determination of the phase diagrams of $C_{n \geq 60}$ fullerenes showed - in contrast to previous studies by Caccamo *et al.* [91] - that the range of the liquid range decreases as one increases the size of the fullerene molecules.

We have furthermore presented results for a HCY system with density-dependent interaction range $z(\rho)$. Such investigations should be of relevance for the phase transitions in colloidal systems and liquid metals which are usually described by density-dependent pair potentials. By varying the two parameters of $z(\rho)$ that describe the height and location of its maximum we generated a series of phase diagrams and observed different types of critical behavior: in particular, phase diagrams with two critical points where found, one corresponding to a stable or metastable gas-liquid transition, the other one to stable or metastable liquid-liquid transitions. In the case when the two critical points merge a preliminary study of the critical exponent β showed evidence that in this case a tricritical point occurs. The development of the SCOZA done in this work offers for the

first time to study these phenomena in a quantitative way. More detailed investigations in this direction are currently done.

We have also generalized the SCOZA to a binary symmetric fluid. Mean-filed theory predicts for this mixture the existence of three generic phase diagrams. These phase diagrams are also obtained in the present study and the transition between these types is found to be triggered by the parameter α - the ratio of the unlike to the like species interaction. A comparison with MC studies is planned. We also consider the further development of enforcing self-consistency between the energy route and the routes to the partial compressibilities (eq. 2.31) which would require the solution of a coupled set of three PDEs to be worth pursuing. Closer investigations of the critical behavior of binary mixtures will be done in future work.

Furthermore, we have studied a binary symmetric mixture when it is in thermal equilibrium with a disordered porous matrix. Results obtained within the framework of the ROZ integral equation theory in combination with the ORPA closure have provided detailed information on the influence of matrix density and parameters defining the interactions between the particles of the binary mixture and between the mixture- and the matrix-particles. The three types of phase diagrams that occur in the bulk mixture are also encountered by the ROZ theory for both the bulk and the confined mixture. A major achievement of this work is to supply a non-ambiguous correspondence between the interactions in the partly quenched system (mixture plus porous matrix) and the type of phase diagram to which they give rise. In the bulk binary mixture the change in phase diagram is triggered by only one parameter (the parameter α). In the present system the situation is more complex bringing into play a combination of several parameters α, y (the ratio of matrix-fluid and fluid-fluid interactions) and the porosity (via ρ_0). Small changes in each of these parameters have been shown to lead to qualitative changes of the phase diagrams. In particular, for a given fluid and matrix, it is apparent that the phase diagram can be changed drastically by varying the porosity of the medium which is the parameter most readily controllable in experiment. Comparison with GCMC simulations and ORPA results showed that for low matrix densities the agreement is excellent and that ORPA is able to predict - at least in a qualitative way - trends in the phase behavior.

Appendix A

On the Analytic Solution of the OZ Equation for Yukawa Systems

We solve the Ornstein-Zernike equation

$$h(r) = c(r) + \rho \int d^3r' c(r') h(|\mathbf{r} - \mathbf{r}'|) \tag{A.1}$$

supplemented by the closure relation

$$
\begin{aligned}
h(r) &= 0 && \text{for} \quad r < 1 \\
c(r) &= K\frac{e^{-z(r-1)}}{r} && \text{for} \quad r > 1,
\end{aligned}
\tag{A.2}
$$

using two different approaches.

A.1   Baxter's Factorization Technique

The first approach is based on the Wiener-Hopf factorization of the direct correlation function introduced by Baxter [74]. He showed that the original OZ equation can be rewritten as

$$rc(r) = -Q'(r) + 2\pi\rho \int_r^R Q'(t)Q(t-r)dt \tag{A.3}$$

$$rh(r) = -Q'(r) + 2\pi\rho \int_0^R (r-t)h(|r-t|)Q(t)dt, \tag{A.4}$$

where $Q(r)$ is the so-called factor function. Baxter then showed that $Q(r)$ has the following properties: $Q(r)$ is a real, continuous function, $Q(r) = 0$ for $r < 0$ and $Q(r) = 0$ for $r > R$ if $c(r) = 0$ for $r > R$. He thus immediately obtained the PY solution for hard-spheres

($c(r) = 0$ for $r > 1$). Høye and Blum [24] showed that Baxter's approach is also applicable for an infinitely ranged $c(r)$ of the form of a linear combination of Yukawas and derived the analytic solution. They showed that from the form of $c(r)$ outside the core (A.2) and eq. (A.3) it follows that $Q(r)$ must be of the form

$$Q(r) = Q_0(r) + de^{-zr} \quad \text{for} \quad r > 0 \tag{A.5}$$

where

$$Q_0(r) = \begin{cases} \frac{a}{2}(r^2 - 1) + b(r - 1) + c\left(e^{-zr} - e^{-z}\right) & 0 < r < 1 \\ 0 & 1 < r \end{cases} \tag{A.6}$$

with yet undetermined coefficients a, b, c and d. We insert $Q(r)$ given by (A.5) and (A.6) into eq. (A.4). For $r < 1$ one then gets using the core condition

$$\begin{aligned} 0 &= -Q_0'(r) + 2\pi\rho \int_0^\infty (r - t) \underbrace{h(|r - t|)Q_0(t)}_{=0 \text{ for } r<1} dt \\ &\quad + 2\pi\rho \int_0^\infty (r - t)h(|r - t|)de^{-zt}dt \\ &= -Q_0'(r) - 2\pi\rho de^{-zr} \int_0^\infty uh(u)e^{-zu}du \\ &= -\left(ar + b - z(c + d)e^{-zr}\right) - 2\pi\rho de^{-zr}\hat{h}(z), \end{aligned} \tag{A.7}$$

where $\hat{h}(z)$ is the Laplace transform of $rh(r)$. By equating terms of equal r dependence one gets

$$\begin{aligned} a &= 0 \\ b &= 0 \\ z(c + d) &= 2\pi\rho d\hat{h}(z). \end{aligned} \tag{A.8}$$

Using these coefficients for Q and inserting this function in eq. (A.3) one gets for $r > 1$

$$\begin{aligned} Ke^{-z(r-1)} &= dze^{-zr} + 2\pi\rho \int_r^1 \underbrace{Q(t - r)Q_0'(t)}_{=0 \text{ for } r>1} dt \\ &\quad - 2\pi\rho dz \int_r^\infty Q(t - r)e^{-zt}dt \\ &= dze^{-zr}\left(1 - 2\pi\rho q(z)\right), \end{aligned} \tag{A.9}$$

where

$$\begin{aligned} q(z) &= \int_0^\infty Q(t)e^{-zt}dt \\ &= \sigma(z) - \tau(z)e^{-z} \end{aligned} \tag{A.10}$$

with

$$\sigma(z) = -\frac{c}{z}e^{-z} + \frac{c+d}{2z}$$

$$\tau(z) = -\frac{1}{2z}ce^{-z}. \tag{A.11}$$

Therefore one obtains from (A.9)

$$e^z K = dz\left(1 - 2\pi\rho q(z)\right). \tag{A.12}$$

We further need some expression for $\hat{h}(z)$. We take the analytic continuation of eq. (A.7) for $r > 1$ and subtract it from eq. (A.4) for $r > 1$

$$rh(r) = zde^{-zr} + 2\pi\rho \int_0^\infty (r-t)h(|r-t|)Q(t)dt \tag{A.13}$$

to obtain

$$rh(r) = -zce^{-zr} + 2\pi\rho \int_0^r (r-t)h(|r-t|)Q(t)dt. \tag{A.14}$$

The last integral is just a convolution integral. So one obtains after Laplace transformation

$$\hat{h}(s) = -\frac{zc}{z+s}e^{-z}e^{-s} + 2\pi\rho\hat{h}(s)q(s) \tag{A.15}$$

and therefore

$$(1 - 2\pi\rho q(z))\hat{h}(z) = -\frac{c}{2}e^{-2z}. \tag{A.16}$$

For given $\hat{h}(z)$ eqs. (A.16) and (A.8) are linear in c and d. We introduce ($\eta = \frac{\pi}{6}\rho$)

$$\begin{aligned} I &= 24\eta e^z \hat{h}(z) \\ &= 24\eta \int_1^\infty re^{-z(r-1)}g(r)dr, \end{aligned} \tag{A.17}$$

using the relation $g(r) = h(r)$ which is valid for the '-'-system (cf. subsect. 4.3.2); solving eqs. (A.16) and (A.8) for c and d we obtain

$$\begin{aligned} c &= \left(-1 + \frac{I}{2z}e^{-z}\right)d \\ d &= \frac{\frac{I}{12\eta}e^z}{\left(1 + \frac{1}{2z}(1-e^{-z})I\right)^2}. \end{aligned} \tag{A.18}$$

Inserting this solution in eq. (A.12) yields a nonlinear equation for I

$$6\eta K = \frac{\frac{z}{2}I\left(1 - \frac{I}{2z}e^{-z}\right)}{\left(1 + \frac{1}{2z}(1-e^{-z})I\right)^4}. \tag{A.19}$$

For given K and z the solution of this nonlinear equation yields I and thus $c, d, \hat{h}(z), u$ etc.

A.2   Laplace Transform Technique

The alternative route to the solution is based on the Laplace transform technique that was applied by Waisman [42] to solve the OZ equation with core condition and a direct correlation function of one-Yukawa form. His solution was subsequently simplified by Høye and Stell [71] and generalized to the case of two Yukawas [44, 63, 52].

We consider the core condition

$$h(r) = -\epsilon \quad \text{for} \quad r < 1. \tag{A.20}$$

and recover the original core condition (A.2) in the limit $\epsilon \to 0$. We introduce the functions

$$H(r) = \frac{h(r)}{\epsilon}, \quad C(r) = \frac{c(r)}{\epsilon}. \tag{A.21}$$

They satisfy the OZ relation

$$H(r) = C(r) + \tilde{\rho} \int d^3 r' C(r') H(|\mathbf{r} - \mathbf{r}'|) \tag{A.22}$$

and the closure relations

$$
\begin{aligned}
H(r) &= -1 \quad \text{for} \quad r < 1 \\
C(r) &= \widetilde{K} \frac{e^{-z(r-1)}}{r} \quad \text{for} \quad r > 1
\end{aligned}
\tag{A.23}
$$

with

$$\widetilde{K} = \frac{K}{\epsilon}, \quad \tilde{\rho} = \epsilon\rho, \quad \tilde{\eta} = \epsilon\eta. \tag{A.24}$$

Thus we recover a closure relation that has already been studied by the Laplace transform technique. Waisman found the direct correlation function of this system inside the core to be given by

$$-C(r) = a + br + \frac{1}{2}\tilde{\eta}ar^3 + v\frac{1 - e^{-zr}}{zr} + v^2\frac{\cosh(zr) - 1}{2r\widetilde{K}z^2 e^z}, \quad r < 1 \tag{A.25}$$

where a, b and $v = \widetilde{K}I = \widetilde{K}24\tilde{\eta}e^z\widehat{H}(z)$ satisfy a set of nonlinear equations. Following similar lines as for the two-Yukawa $c(r)$ in [44, 63] these equations can be rewritten as a system of linear equations for a suitable choice of parameters: to this end we introduce the variable

$$\gamma := 2 - \sqrt{q} - \frac{V_1}{V_0}, \text{with } q = \left(\frac{1 + 2\tilde{\eta}}{1 - \tilde{\eta}}\right)^2, \tag{A.26}$$

where the ratio $\frac{V_1}{V_0}$ is given in terms of $I = 24\tilde{\eta}e^z\widehat{H}(z)$ by eqs. (33) and (34) of [44] as

$$\frac{V_1}{V_0} = \frac{4 + 2z - z^2}{2(2 + z)}\frac{\tau I - 1}{\sigma I - 1}. \tag{A.27}$$

where

$$\sigma = \frac{1}{2z}\left(\frac{z-2}{z+2} + e^{-z}\right) \tag{A.28}$$

$$\tau = \frac{1}{2z}\left(\frac{z^2+2z-4}{4+2z-z^2} + e^{-z}\right). \tag{A.29}$$

The above mentioned linear system becomes then (compare with eq. (6) of [63])

$$
\begin{aligned}
A + (2-h)V_0 &= q \\
hA + V_0 &= g
\end{aligned}
\tag{A.30}
$$

with

$$A = (1-\eta)^2\left(1 - \rho\tilde{c}(k{=}0)\right) \tag{A.31}$$

$$h = 1 + \frac{\gamma^2}{\frac{1}{4}z^2}$$

$$g = (\gamma + \sqrt{q})^2 - \frac{1}{4}z^2. \tag{A.32}$$

Solving the system (A.30) for V_0 gives

$$V_0 = \frac{4}{z^2}\left(\frac{1}{4}z^2 - x^2\right)\left(\sqrt{q} - x\right)^2 \tag{A.33}$$

where we defined

$$x := \sqrt{q} - \frac{\frac{1}{4}z^2}{\gamma}. \tag{A.34}$$

From the definitions (A.26) and (A.34) it follows

$$\frac{V_1}{V_0} = 2 - \sqrt{q} - \frac{\frac{1}{4}z^2}{\left(\sqrt{q} - x\right)^2}. \tag{A.35}$$

By inserting the expressions (A.33) and (A.35) in eq. (36) of [44]

$$6\tilde{\eta}\widetilde{K} = \frac{4(z+2)^2\sigma^2}{z^2}V_0\left(\frac{V_1}{V_0} - \alpha\right)^2 \tag{A.36}$$

where

$$\alpha = \frac{(4+2z-z^2)\,\tau}{2\,(2+z)\,\sigma} \tag{A.37}$$

one obtains a nonlinear equation for the quantity x

$$6\tilde{\eta}\tilde{K} = \frac{(z+2)^2\sigma^2}{z^4}\left(\frac{1}{4}z^2 - x^2\right)\left(4(2-\sqrt{q}-\alpha)(\sqrt{q}-x) - z^2\right)^2. \tag{A.38}$$

To obtain the corresponding equation for the original closure relation (A.2) we insert the
expressions (A.24) in eq. (A.38) and take the limit $\epsilon \to 0$. In this limit one gets

$$
\begin{aligned}
I &= 24\epsilon\eta \int_1^\infty e^{-z(r-1)} \frac{h(r)}{\epsilon} dr = 24\eta \int_1^\infty e^{-z(r-1)} h(r) dr = 24\eta e^z \hat{h}(z) \\
q &\to 1 \\
\gamma &\to 1 - \frac{V_1}{V_0} \\
x &\to 1 - \frac{\frac{1}{4}z^2}{\gamma}
\end{aligned}
\tag{A.39}
$$

and thus

$$
6\eta K = \frac{(z+2)^2 \sigma^2}{z^4} \left(\frac{1}{4} z^2 - x^2 \right) \left(4(1-\alpha)(1-x) - z^2 \right)^2 .
\tag{A.40}
$$

By expressing x as a function of I via the eqs. (A.34,A.26,A.27) one can show that
eq. (A.40) is equivalent to the previous formulation eq. (A.19).

Bibliography

[1] J. M. Yeomans, *Statistical Mechanics of Phase Transitions* (Oxford: Clarendon Press, 1992)

[2] K. G. Wilson, Rev. Mod. Phys. **Vol.** 55, 583 (1983)

[3] M.P. Allen and D.J. Tildesley, *Computer Simulations of Liquids* (Oxford, Clarendon, 1990).

[4] J. P. Hansen and I. R. McDonald, *Theory of Simple Liquids* (New York: Academic Press, 1986, 2nd edition)

[5] J. S. Rowlinson, and F. L. Swinton, *Liquids and Liquid Mixtures* (London: Butterworth, 1982)

[6] J. S. Høye, in *New Approaches to Problems in Liquid State Theory* (Eds. C. Caccamo, J.-P. Hansen, and G. Stell, Nato Science Series, Kluwer, Dordrecht, 1998)

[7] A. Parola, L. Reatto, Advances in Physics, **Vol.** 44, 211 (1995)

[8] R. Dickman, G. Stell, Phys. Rev. Lett., **Vol.** 77, 996 (1996)

[9] C. Caccamo, Phys. Rep., **Vol.** 274, 1 (1996)

[10] P. H. Poole, T. Grande, C. A. Angell, and P. F. McMillan, Science, **Vol.** 275, 322 (1997)

[11] N. G. Almarza, E. Lomba, G. Ruiz, C. F. Tejero, Phys. Rev. Lett., **Vol.** 86, 2038 (2001)

[12] N. B. Wilding, F. Schmid, P. Nielaba, Phys. Rev. E, **Vol.** 58, 2201 (1998)

[13] M.-L. Rosinberg, *New Approaches to Problems in Liquid State Theory* (Eds. C. Caccamo, J.-P. Hansen, and G. Stell, NATO Science Series, Kluwer, Dordrecht, 1999)

[14] A. P. Y. Wong and M. H. W. Chan, Phys. Rev. Lett., **Vol.** 65, 2569 (1990), A. P. Y. Wong, S. B. Kim, W. I. Goldburg and M. H. W. Chan, Phys. Rev. Lett., **Vol.** 70, 954 (1993), M. Chan, N. Mulders and J. Reppy, Physics Today, **Vol.** 49 (8), 30 (1996)

[15] S. B. Kim, J. Ma and M. H. W. Chan, Phys. Rev. Lett., **Vol.** 71, 2268 (1993), D. J. Tulimieri D. J., J. Yoon and M. H. W. Chan, Phys. Rev. Lett., **Vol.** 82, 121 (1999)

[16] W. G. Madden and E. G. Glandt, J. Stat. Phys., **Vol.** 51, 537 (1988), W. G. Madden, J. Chem. Phys., **Vol.** 96, 5422 (1992)

[17] S. F. Edwards and P. W. Anderson, J. Phys. F, **Vol.** 5, 965 (1975), S. F. Edwards and C. Jones, J. Phys. A, **Vol.** 9, 1595 (1976)

[18] J. A. Given and G. Stell, Physica A, **Vol.** 209, 495 (1994)

[19] E. Schöll-Paschinger, D. Levesque, J.-J. Weis, and Gerhard Kahl, Phys. Rev. E, **Vol.** 64, 011502 (2001)

[20] T. L. Hill, *Statistical Thermodynamics* (Massachusetts: Addison-Wesley Publishing Company, 1960)

[21] M. Tau, L. Reatto, J. Chem. Phys., **Vol.** 83, 1921 (1985)

[22] L. S. Ornstein, F. Zernike, Proc. Acad. Sci. (Amsterdam), **Vol.** 17, 1452 (1914)

[23] A. B. Bathia, D. E. Thornton, Phys. Rev. B, **Vol.** 2, 3004 (1970)

[24] J. S. Høye, L. Blum, J. Stat. Phys., **Vol.** 16, 399 (1977)

[25] E. Waisman, J. L. Lebowitz, J. Chem. Phys., **Vol.** 56, 3086 (1972); *ibid* **Vol.** 56, 3093 (1972)

[26] M. Wertheim, J. Chem. Phys., **Vol.** 55, 4291 (1971)

[27] L. Mier y Tern, E. Corvera, A. E. Gonzlez, Phys. Rev. A, **Vol.** 39, 371 (1989)

[28] E. R. Smith, Mol. Phys., **Vol.** 3, 823 (1979)

[29] H. C. Andersen, D. Chandler and J. D. Weeks, Advances in Chemical Physics, **Vol.** 34, 105 (1976)

[30] G. Stell, Phys. Rev., **Vol.** 184, 135 (1969); J. Chem. Phys., **Vol.** 55, 1485 (1971)

[31] H. C. Andersen and D. Chandler, J. Chem. Phys., **Vol.** 57, 1918 (1972)

[32] H. C. Andersen, D. Chandler and J. D. Weeks, J. Chem. Phys., **Vol.** 56, 3812 (1972)

[33] H. C. Andersen, J. D. Weeks, and D. Chandler, Phys. Rev. A, **Vol.** 4, 1597 (1971)

[34] E. Paschinger, Diploma thesis, Technische Universität Wien (1999)

[35] E. Kierlik, M. L. Rosinberg, G. Tarjus, and P. A. Monson, J. Chem. Phys., **Vol.** 106, 264 (1997)

[36] K. Huang, *Statistical Mechanics*, (New York: John Wiley & Sons, 1963)

[37] Schwabl, *Statistische Mechanik*, (Berlin: Springer, 2000)

[38] P. H. van Konynenburg, R. L. Scott, Philos. Trans. R. Soc. London, Ser. A, **Vol.** 51, 495 (1980)

[39] Dominique Levesque, J.-J. Weis, private communication

[40] J.-J. Weis, M.J.P. Nijmeijer, J.M Tavares, M.M. Telo da Gamma, Phys. Rev. E, **Vol.** 55, 436 (1997); J.M. Tavares, M.M. Telo da Gama, P.I.C. Teixeira, J.-J. Weis, M.J.P. Nijmeijer, Phys. Rev. E, **Vol.** 52, 1915 (1995)

[41] B. Groh, S. Dietrich, Phys. Rev. Lett., **Vol.** 72, 2422 (1994); B. Groh, S. Dietrich, in *New Approaches to Problems in Liquid State Theory* (Eds. C. Caccamo, J.-P. Hansen, and G. Stell, Nato Science Series, Kluwer, Dordrecht, 1999)

[42] E. Waisman, Mol. Phys., **Vol.** 25, 45 (1973)

[43] N. F. Carnahan, K.E. Starling, J. Chem. Phys., **Vol.** 51, 635 (1969)

[44] J. S. Høye, G. Stell, E. Waisman, Mol. Phys., **Vol.** 32, 209 (1976)

[45] J. S. Høye, J. L. Lebowitz, G. Stell, J. Chem. Phys., **Vol.** 61, 3253 (1974), G. Stell, S. F. Sun, J. Chem. Phys., **Vol.** 63, 5333 (1975), J. S. Høye, G. Stell, J. Chem. Phys., **Vol.** 67, 524 (1977), G. Stell, J.-J. Weis, Phys. Rev. A, **Vol.** 16, 757 (1977)

[46] Y. Rosenfeld, N. W. Ashcroft, Phys. Rev. A, **Vol.** 20, 1208 (1970)

[47] F. J. Rogers, D. A. Young, Phys. Rev. A, **Vol.** 30, 999 (1984)

[48] G. Zerah, J. P. Hansen, J. Chem. Phys., **Vol.** 84, 2336 (1985)

[49] C. Caccamo, G. Pellicane, D. Costa, D. Pini, G. Stell, Phys. Rev. E, **Vol.** 60, 5533 (1999)

[50] C. Caccamo, P. V. Giaquinta, G. Giunta, J. Phys. Condens. Matter, **Vol.** 5, B75 (1993), C. Caccamo, Phys. Rev. B, **Vol.** 51, 3387 (1995), C. Caccamo, G. Giunta, G. Malescio, Mol. Phys., **Vol.** 84, 125 (1995)

[51] J. S. Høye, G. Stell, J. Chem. Phys., **Vol.** 67, 439 (1977)

[52] J. S. Høye, G. Stell, Mol. Phys., **Vol.** 52, 1071 (1984)

[53] J. S. Høye, G. Stell, Int. J. Thermophys., **Vol.** 6, 561 (1985)

[54] D. Pini, G. Stell, R. Dickman, Phys. Rev. E, **Vol.** 57, 2862 (1998)

[55] A. Borge, J. S. Høye, J. Chem. Phys. **Vol.** 108, 4516 (1997)

[56] M. E. Fisher, Rev. Mod. Phys. **Vol.** 70, 653 (1998)

[57] J. S. Høye, D. Pini, G. Stell, Physica A, **Vol.** 279, 213 (2000)

[58] D. Pini, G. Stell, J. S. Høye, Int. J. Thermophys., **Vol.**19 , 1029 (1998)

[59] D. Pini, G. Stell, N. B. Wilding, Mol. Phys., **Vol.** 95, 483 (1998)

[60] D. Pini, G. Stell, N. B. Wilding, J. Chem. Phys., **Vol.** 115, 2702 (2001)

[61] D. Pini, Ge Jalin, A. Parola, L. Reatto (submitted to Chem. Phys. Lett.)

[62] L. Verlet, J.-J. Weis, Phys. Rev. A, **Vol.** 5, 939 (1971)

[63] J. S. Høye, G. Stell, Mol. Phys., **Vol.** 52, 1057 (1984)

[64] J. S. Høye, G. Stell, Physica A, **Vol.** 244, 176 (1997), J. S. Høye, G. Stell, Physica A, **Vol.** 247, 497 (1997)

[65] J. S. Høye, A. Borge, J. Chem. Phys. **Vol.** 108, 8830 (1998)

[66] N. U. Andresen, A. Borge, J. S. Høye, J. Chem. Phys. **Vol.** 115, 9165 (2001)

[67] E. Kierlik, M. L. Rosinberg, G. Tarjus, J. Stat. Phys., **Vol.** 89, 215 (1997); *ibid* **Vol.** 94, 805 (1999); *ibid* **Vol.** 100, 423 (2000)

[68] S. Grollau, E. Kierlik, M. L. Rosinberg, G. Tarjus, Phys. Rev. E, **Vol.** 63, 41111 (2001)

[69] S. Grollau, M. L. Rosinberg, G. Tarjus, Physica A, **Vol.** 296, 460 (2001)

[70] A. Dickman, G. Stell (submitted to Mol. Phys.)

[71] J. S. Høye, G. Stell, Mol. Phys., **Vol.** 32, 195 (1976)

[72] C. Jedrezejek, G. A. Mansoori, Acta Phys. Pol. A, **Vol.** 57, 107 (1980), S. M. Foiles, N. W. Ashcroft, Phys. Rev. A, **Vol.** 24, 424 (1981), J. Konior, C. Jedrezejek, Mol. Phys. 63,**Vol.** 63, 655 (1988), E. N. Rudisill, P. T. Cummings, Mol. Phys.,**Vol.** 68, 629 (1989)

[73] M. Wertheim, in "The Equilibrium Theory of Classical Fluids" (eds. H. Frisch, J. Lebowitz), Frontiers in physics, Benjamin, (New York, 1964)

[74] R. J. Baxter, Aust. J. Phys., **Vol.** 21, 563 (1968)

[75] E. Arrieta, C. Jedrzejek, K. N. Marsh, J. Chem. Phys., **Vol.** 95, 6806 (1991)

[76] G. Pastore, Mol. Phys., **Vol.** 55, 187 (1988)

[77] W. F. Ames,*Numerical Methods for Partial Differential Equations* (New York: Academic Press, 1977)

[78] A. Cheng, M. L. Klein, Phys. Rev. B, **Vol.** 45, 1889 (1992)

[79] L. A. Girifalco, J. Phys. Chem., **Vol.** 95, 5370 (1992), **Vol.** 96, 858 (1992)

[80] M. H. J. Hagen, E. J Meijer, G. C. A. M Mooij, D. Frenkel, H. N. W. Lekkerkerker, Nature (London), **Vol.** 365, 425 (1993)

[81] N. W. Ashcroft, Nature (London), **Vol.** 365, 387 (1993)

[82] E. Lomba, N. G. Almarza, J. Chem. Phys., **Vol.** 100, 8367 (1994)

[83] C. F. Tejero, A. Daanoun, H. N. W. Lekkerkerker, M. Baus, Phys. Rev. Lett., **Vol.** 73, 752 (1994)

[84] A. Cheng, M. L. Klein, C. Caccamo, Phys. Rev. Lett., **Vol.** 71, 1200 (1993)

[85] L. Mederos, G. Navascues, Phys. Rev. B, **Vol.** 50, 1301 (1994)

[86] C. Caccamo, Phys. Rev. B, **Vol.** 51, 3387 (1995)

[87] M. Tau, A. Parola, D. Pini, L. Reatto, Phys. Rev. E, **Vol.** 52, 2644 (1995)

[88] C. Caccamo, D. Costa, A. Fucile, J. Chem. Phys., **Vol.** 106, 255 (1997)

[89] M. Hasegawa, K. Ohno, J. Chem. Phys., **Vol.** 111, 5955 (1999), **Vol.** 113, 4315 (2000)

[90] A. L. C. Ferreira, J. M. Pacheco, J. P. Prates-Ramalho, J. Chem. Phys., **Vol.** 113, 738 (2000)

[91] M. C. Abramo, C. Caccamo, D. Costa, G. Pellicane, Europhys. Lett., **Vol.** 54, 468 (2001)

[92] V. I. Zubov, Molec. Mater., **Vol.** 13, 385 (2000)

[93] P. V. Giaquinta, G. Giunta, Physica (Amsterdam), **Vol.** 187A, 145 (1992), P. V. Giaquinta, G. Giunta, S. P. Giarritta, Phys. Rev. A, **Vol.** 45, 6966 (1992)

[94] J. W. Perram, Mol. Phys., **Vol.** 30, 1505 (1975)

[95] C. F. Tejero, M. Baus, Phys. Rev. E, **Vol.** 57, 4821 (1998)

[96] J. Hafner, *From Hamiltonians to Phase Diagrams* (Berlin: Springer, 1987)

[97] G. Stell, M. Hemmer, J. Chem. Phys., **Vol.** 56, 4274 (1972)

[98] L. Blum, J. S. Høye, J. Stat. Phys., **Vol.** 19, 317 (1978)

[99] C. Caccamo, D. Costa, G. Pellicane, J. Chem. Phys., **Vol.** 109, 4498 (1998)

[100] R. J. Baxter, J. Chem. Phys., **Vol.** 52, 4559 (1970)

[101] E. Arrieta, C. Jedrzejek, K. N. Marsh, J. Chem. Phys., **Vol.** 86, 3607 (1987)

[102] C. Caccamo, G. Giunta, C. Hoheisel, Phys. Lett. A, **Vol.** 158, 325 (1991), C. Caccamo, G. Giunta, Mol. Phys., **Vol.** 78, 83 (1993)

[103] S. J. Gregg and K. S. W. Sing, *Adsorption, Surface Area and Porosity* (London: Academic Press, 1982)

[104] F. Brochard and P.G. de Gennes, J. Phys. (Paris) Lett., **Vol.** 44, 785 (1983)

[105] E. Pitard, M. L. Rosinberg, G. Stell, and G. Tarjus, Phys. Rev. Lett., **Vol.** 74, 4361 (1995)

[106] L. Monette, A. Liu, and G. S. Grest, Phys. Rev. A, **Vol.** 46, 7664 (1992)

[107] R. Evans, J. Phys.: Condens. Matter, **Vol.** 2, 8989 (1990)

[108] J. A. Given, Phys. Rev. A **Vol.** 45, 816 (1992)

[109] J. A. Given, J. Chem. Phys., **Vol.** 96, 2287 (1992)

[110] M. L. Rosinberg, G. Tarjus, and G. Stell, J. Chem. Phys., **Vol.** 100, 5172 (1995)

[111] E. Kierlik, M. L. Rosinberg, G. Tarjus, and P. Monson, J. Chem. Phys., **Vol.** 103, 4256 (1995)

[112] L. A. Fanti, E. D. Glandt, and W. G. Madden, J. Chem. Phys., **Vol.** 93, 5945 (1990)

[113] E. Lomba, J. A. Given, G. Stell, J. J. Weis, and D. Levesque, Phys. Rev. E, **Vol.** 48, 233 (1993)

[114] A. Meroni, D. Levesque, and J. J. Weis, J. Chem. Phys., **Vol.** 105, 1101 (1996)

[115] C. Vega, R. D. Kaminsky, and P. A. Monson, J. Chem. Phys., **Vol.** 99, 3003 (1993)

[116] K. S. Page and P. A. Monson, Phys. Rev. E, **Vol.** 54, R29 (1996)

[117] R. D. Kaminisky and P. A. Monson, Phys. Rev. E54, R29 (1996) Phys., **Vol.** 95, 2936 (1991)

[118] D. M. Ford and E. D. Glandt, J. Chem. Phys., **Vol.** 100, 2391 (1994)

[119] M. Álvarez, D. Levesque, and J.-J. Weis, Phys. Rev. E **60**, 5495 (1999)

[120] B. Hribar, O. Pizio, A. Trokhymchuk, and V. Vlachy, J. Chem. Phys., **Vol.** 109, 2480 (1998)

[121] M. J. Fernaud, E. Lomba, and J.-J. Weis, Phys. Rev. E, **Vol.** 64, 051501 (2001)

[122] E. Paschinger and G. Kahl, Phys. Rev. E **Vol.** 61, 5320 (2000)

[123] E. Paschinger, D. Levesque, Gerhard Kahl, and J.-J. Weis, Europhys. Lett., **Vol.** 55, 178- 183, (2001)

[124] G. Kahl, E. Schöll-Paschinger, A. Lang, Monatshefte für Chemie **Vol.** 132, 1413-1432 (2001)

[125] M.J. Gillan, Mol. Phys. **Vol.** 38, 1781 (1979).

[126] S. Labik, A. Malijevsky, and P. Vonka, Mol. Phys. **Vol.** 56, 709 (1985).

[127] N.B. Wilding, Phys. Rev. Lett. **Vol.** 78, 1488 (1997); Phys. Rev. E **Vol.** 55, 6624 (1997)

Acknowledgements

Curriculum Vitae

Personal Data

Name:	Elisabeth Maria Schöll-Paschinger
Date and place of birth:	29. Juli 1974, Wien (Austria)
Nationality:	Austrian
Marital status:	married with Dipl.-Ing. Joachim Schöll
Private address:	Bürgerspitalgasse 29/24
	A-1060 Wien

Education & Studies

1980 - 1984	Primary school Mater Salvatoris, Wien
1984 - 1992	Gymnasium Mater Salvatoris, Wien
1992 - 1999	Studies in Technical Physics, Technische Universität Wien Diploma thesis: 'Structural and Thermodynamic Properties of Fluids in Porous Media' (supervisor: Dr. G. Kahl)
1994 -	Studies in Technical Mathematics, Technische Universität Wien
1999 -	Ph.D. student at the Institut für Theoretische Physik, Technische Universität Wien